

Modular, Polymeric Development Platform for Microfluidic Applications
Design, Fabrication, Testing and Examples

Zur Erlangung des akademischen Grades eines
Doktors der Ingenieurwissenschaften

an der Fakultät für Maschinenbau der
Universität Karlsruhe

vorgelegte
Dissertation

von
Master of Science Proyag Datta
aus Baton Rouge

Tag der mündlichen Prüfung: 6. Juni 2007

Hauptreferent: Prof. Dr. V. Saile
Korreferent: Prof. Dr. J. Goettert

Acknowledgements

First and foremost I would like to thank Dr. Jost Göttert for his mentoring, guidance and support which went much above and beyond what is expected from a PhD advisor. I would like to thank Prof. Volker Saile and Dr. Mathias Heckeke who provided essential feedback and helped streamline my work.

This thesis is on the topic of system integration and any such effort is result of teamwork. Jens Hammacher, Sitanshu Gurung, and Christian Raschke made contributions to various portions of the theoretical and experimental work. Fabrication of molds, machines and mechanical fixtures were critical for my work. I'd like to thank Jason Guy who micro-milled my 3-D designs and models into brass mold inserts. I'd also like to thank George Gascon who machined my macro fixtures and parts.

I would like to acknowledge the Bio-MEMS and microfluidics community in general as this work has been influenced by the existing prior art in the field and it is my hope that my work will likewise influence future development. The applications that were implemented as part of this work were based on the ideas and expertise of collaborators from various disciplines of science. I would like to acknowledge Ramanuj Lahiri, Feng Xu, Mark Pease, Svetlana Zinoveva and Henry Bellamy for using my system platform for their applications and as a result providing me with valuable data and feedback on improving the platform.

My work could not have been accomplished without the help and support from my co-workers at CAMD and the infrastructure provided by the facility.

Last but not the least; I would like to thank my parents and my wife Shreya for the love and encouragement.

Abstract

Biological-Microelectromechanical Systems (Bio-MEMS) devices and Lab-on-chip or μ -Total Analysis Systems (μ TAS) have the potential to provide attractive solutions for a variety of sensing and diagnostic needs in life-science, medical and environmental monitoring applications. Since its initial steps in the early 1990 significant research has been carried out to develop simple microfluidic components such as mixers, splitters and valves all the way to complex systems such as blood analysis devices and capillary electrophoresis systems that enter the market in a first generation of products. While there exist stand-alone, very sophisticated solutions for specific tasks the general use of microfluidic solutions in many science and engineering areas is not fully established due to a lack of easy access to the technology and convenience of operation. In order to fully explore the potential of Bio-MEMS and μ TAS solutions for a broader user community the equivalent to what the printed circuit board is for microelectronics application is needed in microfluidics - a user-friendly, standardized microfluidic development platform.

The focus of this thesis is the design, fabrication and test of a microfluidic development platform that can take over the role of a printed circuit board for microfluidic applications. The designed platform is modular in nature with individual polymer modules vertically stacked together to form the complete system. Each module may contain multi-domain components such as microfluidic elements, optical waveguides, electronic wiring, magnetic parts, and biological surfaces. The system addresses macro-micro and micro-micro interconnection issues and provides the user with a flexible, modular and easy to use experimental setup that provides a frame work of basic functions and also a high degree of flexibility to meet the specific user demands.

The individual polymer modules are fabricated by hot embossing. A methodology for rapidly optimizing the embossing process for a given mold design and material was developed. Studies were conducted to evaluate the influence of process parameters on the dimensional variation in the molded parts. Innovative methods were developed to subsequently align, seal, assemble and interconnect the modules to each other and to the outside world. Repeatable alignment to better than 100 μ m was achieved using a passive alignment technique. The microfluidic structures can either be sealed temporarily using a silicone gasket or permanently using thermal bonding depending on the user requirements.

The potential of the microfluidic development platform was verified in a number of customer-driven experiments including cell culture for Hansen's disease studies, development of giant magnetoresistive (GMR) based bio sensor, optical interrogation of DNA, magnetic separation of paramagnetic microbeads, microreactor for wet-chemical synthesis of magnetic nanoparticles including in-situ EXAFS analysis, and a crystal growth test chip for protein crystallography experiments.

Zusammenfassung

Biological-Microelectromechanical Systems (Bio-MEMS) und Lab-on-Chip oder μ -Total Analysis Systems (μ TAS) eröffnen neue und attraktive mikrotechnische Lösungen für Sensor- und Analyseanwendungen in verschiedenen Bereichen einschließlich Medizintechnik, Umwelttechnik und den Biowissenschaften. Umfangreiche Forschungs- und Entwicklungsarbeiten sind seit den ersten Anfängen um 1990 durchgeführt worden und haben Ergebnisse geliefert, die von einfachen Strukturen wie Mixern, Verzweigern oder Ventilen und Pumpen bis hin zu komplexen Systemen wie Blutanalysechips und kapillarelektrophoretischen Trennsystemen reichen und von denen einige vor der Markteinführung stehen. Obwohl es bereits eine Vielzahl von sehr ausgeklügelten Systemlösungen für spezielle Analyseaufgaben gibt, steckt die umfangreiche Nutzung mikrofluidischer Analysechips für viele wissenschaftliche und technische Anwendungsbereiche noch in den Kinderschuhen, da mikrotechnische Lösungen immer noch schwer zugänglich und bedienbar sind. Um BioMEMS und μ TAS Systeme für einen größeren Anwenderkreis zur Verfügung zu stellen, wie es beispielsweise für den Bereich der Mikroelektronik durch das Printed Circuit Board erreicht ist, muss eine analoge mikrofluidische Entwicklungsplattform bereitgestellt werden, die den Ansprüchen hinsichtlich Benutzer- und Bedienungsfreundlichkeit genügt und dabei gleichzeitig maximale Flexibilität für die unterschiedlichen Ideen und Herausforderungen anbietet.

Die Untersuchungen, die im Rahmen dieser Doktorarbeit durchgeführt wurden, konzentrieren sich auf das Design und die Herstellung sowie verschiedene Funktionstests einer mikrofluidischen Entwicklungsplattform, die die Rolle eines printed circuit board für mikrofluidische Anwendungen übernehmen soll. Das Herzstück der modular ausgelegten Plattform ist eine vertikale Anordnung mikrofluidischer Chips, die den kompletten Fluidtransport regelt. Die einzelnen Module können neben den mikrofluidischen Elementen auch weitere Funktionselemente integrieren wie beispielsweise optische Wellenleiter, elektrische Leiterbahnen, magnetische Filter und bioaktivierte Oberflächen.

Die Plattform berücksichtigt die Makro-Mikro Schnittstellen und ermöglicht somit die bequeme und einfache Nutzung des Aufbaus. Standardisierte Mikro-Mikro Schnittstellen erlauben eine flexible Verwendung unterschiedlicher Chips und damit eine optimale Nutzerfreundlichkeit.

Die einzelnen Polymerchips werden durch Heissprägen hergestellt. Es wurde ein optimiertes Fertigungsverfahren etabliert, welches eine schnelle Prozessoptimierung für unterschiedliche Chipdesigns und Abformmaterialien erlaubt. Die im vertikalen Aufbau zusammengefügte Chips werden mittels V-Gruben, die Teil des standardisierten Chipdesigns sind, und entsprechenden Passstiften passiv zueinander justiert mit einer Genauigkeit von besser als $100\mu\text{m}$ für eine Chip Standardgröße von $25\text{mm} \times 75\text{mm}$. Dazu war es notwendig, umfangreiche Parameterstudien durchzuführen und die Einflüsse verschiedener Prozessgrößen auf die lateralen Chipabmessungen zu bestimmen.

Verschiedene Methoden zum Verdeckeln und Verbinden der einzelnen Chips werden erprobt und erlauben sowohl die vorübergehende Deckelung mit Hilfe einer Silikondichtung als auch die permanente Deckelung mittels eines thermischen Verschweissprozesses.

Neben den grundlegenden Entwicklungsarbeiten wurden die Einsatzmöglichkeiten der mikrofluidischen Plattform anhand einer Vielzahl von anwendungsspezifischen Lösungen, die für verschiedene Kollaborationspartner gefertigt wurden, getestet. Diese Beispiele befassten sich mit Experimenten für Zellkulturen zur Untersuchung der Hansen Krankheit, systematischen Untersuchungen zur Entwicklung eines GMR (giant magnetoresistive) Biosensors, der optischen Auslesung von fluoreszierenden DNA Proben, der magnetischen Trennung von paramagnetischen Bead-Lösungen, *in-situ* EXAFS-(Extended X-ray Absorption Finestructure) Untersuchungen an magnetischen Nanoteilchen, die mit Hilfe von Mikroreaktoren in einer nasschemischen Reaktion hergestellt wurden, und der Erzeugung von Kristallen für Untersuchungen mittels Proteinkristallographie.

Contents

1. Introduction	1
2. Background	5
2.1. Microfluidic / Bio-MEMS Systems	6
2.2. Challenges of Microfluidic Development and Packaging	9
2.3. Microfluidic Systems and Solutions	15
2.4. Functional Specifications for a Modular Platform	21
3. From Chips to Modular Systems	24
3.1. 3-D Microfluidic Platform and Modular Concept	24
3.2. Assembling the Development Platform	32
3.2.1. Alignment of Chip Stack	32
3.2.2. Sealing	39
3.3. Process Model for Project Management	50
4. Polymer Micromolding	55
4.1. Hot Embossing	57
4.2. Challenges in Polymer Micromolding	58
4.3. Optimization of Hot Embossing Parameters	59
4.3.1. Experimental Method	61
4.3.2. Materials and Results	66
4.4. Dimensional Variation in Embossed Parts	69
4.5. Hot Embossing- A Viable Technology for Mass Production	76
5. Fabrication Processes for 3-D Module	79
5.1. Mold insert Fabrication and Molding	80

5.2. Post Processing of Molded Parts	85
5.2.1. Machining and Cleaning	85
5.2.2. Electronic Interconnect Creation	87
5.2.3. Metrology and Inspection	93
6. Application Demonstrators	95
6.1. Cell Growth Device	95
6.2. Protein Crystallization Platform	98
6.3. Giant Magneto-Resistive Sensor(GMR) based Bio-Detection	101
6.4. Nanoparticle Reactor for X-ray Analysis	108
6.5. Embedded optical Waveguide for Fluorescence Excitation	112
7. Conclusion	118
8. References	121
Appendix A : Passive Alignment using elastic averaging	i
Appendix B : Calculation of Alignment Accuracy	vi
Appendix C : Experimental and simulation details for soft gasket sealing layer between two microfluidic chips	viii
Appendix D : Evaluation of clamping force applied via screw torque	x
Appendix E : Interactional Effects of Hot Embossing Parameters	xi

1. Introduction

Microfabricated devices play a significant role in our modern lives. Micro-Electromechanical Systems (MEMS) or Microsystems Technology (MST) based components are seen in a variety of products that improve our quality of life, such as car airbag sensors, digital projection systems, ink-jet printers, and in health care devices such as blood analyzer [1]. These advanced devices demonstrate significant benefits over conventional devices because of their high functionality and reliability combined with reduced size, weight, cost and energy consumption.

Based on their fabrication methodology, MEMS components may be broadly classified into monolithic and hybrid. The DLP® (Digital Light Processing) chip fabricated by Texas Instruments¹ is an example of a monolithic device where an extremely complex system is built on one single substrate by putting it through a series of well controlled microfabrication processing steps. Hybrid components on the other hand consist of parts that are fabricated separately and then assembled together to form the functional device. In the field of microfabricated fluidic devices for biological applications (Bio-MEMS), a hybrid fabrication methodology is typically preferred to easily accommodate the addition of biological functionality.

Microfluidic Bio-MEMS devices are a subset of the field of MEMS focusing on the analysis of biological samples using miniaturized fluidic components. Microfluidics can be used to drastically reduce the size scale of biological and chemical systems such as diagnostic tools for medicine, platforms for high throughput drug screening, sensors for environmental monitoring, and reactors for scalable production of chemical and bio-chemical products [2]. A typical biological process involves multiple steps such as sample preparation, separation, amplification, reaction, detection, analysis etc. The components required for each individual step are complicated and the development of the whole device is typically accompanied by significant research in order to achieve the desired performance. In addition, integration of

¹ <http://www.dlp.com/>

these individually developed components is often cumbersome and contributes significantly to the overall cost.

Material selection is another important factor in Bio-MEMS applications because biological and chemical reactivity (or the lack of it) determines the suitability of a particular material. Polymers have replaced glass in a number of macro scale biological applications such as 96-well plates, pipettes and microcentrifuge tubes. Polymers are low in cost and hence it is economically viable to make disposable components avoiding cross-contamination. Polymers also exhibit properties (e.g. surface modification for improved cell adhesion) that can be used beneficially when handling biological elements. Hence they are the material of choice for a large number of Bio-MEMS applications.

Considerable research has been carried out towards developing distinct components for specific functions relevant to a biological process such as fluid pumping, mixing and separation. Furthermore, dedicated microfluidic based cell lysis devices [3], Polymerase Chain Reaction (PCR) devices [4], separation technology [5] and detection and analysis devices [6] have been developed utilizing the advantages of microfluidics for specific tasks. The nascent field of Bio-MEMS has combined the knowledge from different domains to spawn many unique devices such as micropumps and microvalves [7, 8], cellular growth and observation platforms [9], capacitive and resistive sensors and optical detectors [6]. Research and technology development towards manufacturing these “Lab-on-Chip” components has seen very significant efforts and in a lot of cases the capabilities of microfabrication technology exceed current needs and are pushing new frontiers in the fields of biology and life sciences.

Today, some stand-alone microtechnology based systems are available to carry out blood glucose measurements for diabetics (Accu-chek® [10]), point-of-care blood chemistry measurements (I-STAT® [11]) and genetic analysis experiments (GeneChip® Instrument System [12]). These are examples of application specific systems that are the product of many years of focused research and development.

While the component level technology and the fabrication processes associated with polymer microfluidics are fairly mature, the packaging², assembly and system development aspects of microfluidic devices have seen lesser research and development efforts. Often, the advantages of micro scale devices are rapidly overshadowed if the interaction between the micro and macro world is cumbersome. Sample, reagents and buffers have to transition from the macro world into the micro analysis chip. Interactions and interconnections between the different domains (fluidics, electronics, optics and biology) essential for a complete microfluidic system have typically been carried out on an ad hoc basis. As a result, system development needs a lot of time, effort and money, and the final engineered device is often an isolated dedicated solution. However, no general development approach exists and every new system development effort has to be started from scratch.

Attempts have been made to simplify the microfluidics integration and development process. Companies like ThinXXS³ and Microfluidic ChipShop⁴ have developed some component level polymeric 'labware' that makes it convenient to carry out microfluidic experiments, and Upchurch Scientific⁵ markets connectors and manifolds capable of easily interconnecting and handling micro volumes of fluid. On the other hand companies like Agilent offer specialized solutions and products that use customized approaches to packaging and interconnection with many years of research and development. These examples illustrate a gap between the component level technology and a dedicated microfluidic system – namely a development platform that can be used to investigate complex multi-domain systems involving microfluidics, electronics, optics and biology. This platform serves as a prototyping, small scale experimental setup speeding up the process of product development. Such a platform will allow researchers to carry out experiments and build application specific devices without having to develop each and every component. Existing components and modules could be reused in different

² Packaging for the course of this work is defined as any auxiliary manufacturing activity beyond the basic component fabrication that is necessary to make that component usable in conjunction with other components.

³ <http://www.thinxxs.com/>

⁴ <http://www.microfluidic-chipshop.com/>

⁵ <http://www.upchurch.com/>

applications much like in the field of electronics. The platform would shorten development times of new Bio-MEMS devices and result in faster growth of market opportunities in many areas.

The goal of this thesis is designing and building a standardized development platform for microfluidic and Bio-MEMS applications. The platform addresses the packaging and interconnection issues associated with developing a complete solution for a process flow for life science applications which typically involves a number of sub-steps and is best distributed onto several interconnected chips. Fluidic interconnect formation on the macro-micro level and on the micro-micro level is a common factor in any microfluidic system as is proper sealing of the individual microfluidic components. These aspects have been addressed in detail, along with the general methods of fabrication, alignment and mechanical assembly of the system. The chips which form the functional modules are fabricated by hot embossing, which is a polymer molding process that is ideal for prototype fabrication and small scale production since it carries low overheads and the turnaround time is short. Protocols were developed to quickly evaluate ideal hot embossing parameters for a given mold insert and polymer material. Systematic studies were also carried out to predict the dimensional variation in the molded parts as a function of molding parameters.

During the course of this work, the system development platform was used as a tool for preliminary investigation in a number of diverse applications including cell culture for Hansen's disease studies, chemiluminescence experiments, giant magnetoresistive (GMR) sensor based bio-detection development, optical interrogation of DNA, magnetic separation of paramagnetic microbeads, a microreactor for X-ray absorption spectroscopy of nanoparticles and as a platform for protein crystallography experiments. These examples illustrate that the goal of this work to develop a user friendly platform for polymer based microfluidics that allows the user to integrate microfluidic components with electronics, biology and optics was successful achieved. They also indicate opportunities for further expansion that will be discussed at the conclusion of the thesis.

2. Background

Similar to the miniaturized devices in other fields of science and technology, Bio-MEMS⁶ and microfluidic⁷ devices have significant advantages, over large scale devices in terms of performance and cost including-

1. Enhanced Speed, Parallel Processing and Automation – The smaller an object or a system is, the lower its inertia and hence the faster it responds. Therefore, microdevice based analytical systems produce results much quicker than conventional systems [6]. Microfluidics also opens the doors for automation and parallel processing of the same sample or multiple samples on a single chip, providing better data and more reliable results.

2. Low reagent consumption – Consumption of reagents is much less in a microdevice when compared to conventional systems [2]. This is a significant advantage as some reagents used for biological analysis can be prohibitively expensive, costing hundreds of dollars for a few microliters.

3. Sensitivity – Scaling laws of microsystems [13] show that smaller devices can produce responses exponentially faster and better signal-to-noise ratios. This means that microdevices will be capable of detecting and analyzing smaller volumes and lower concentration samples than conventional large scale devices.

4. Portability – For example, handheld Point-of-Care devices manufactured by I-Stat®[14] are capable of carrying out real time analysis at the patient's bedside instead of using a conventional pathology lab.

5. Low cost –With maturity of the technology, mass production of bio-analytical devices will ultimately lead to low cost and disposable products that will enable consumers to better monitor their health.

⁶ Bio-MEMS is defined as a MEMS solution for a biology or life sciences problem, typically involving microfluidics and other associated components such as pumps, valves, electronics etc.

⁷ Microfluidics is a field of microtechnology that involves handling very small volumes (micro, nano and picoliters) of fluid. Popular applications for microfluidics include inkjet print heads and Bio-MEMS devices.

Though there are many benefits of microfluidics, the field is experiencing the usual hurdles faced by any new and disruptive technology⁸. This section discusses current state of the art in microfluidics and the issues of packaging, assembly and system development in microfluidics as they are relevant for this thesis.

2.1. Microfluidic / Bio-MEMS Systems

In the past, we have seen silicon based electronic microdevices revolutionize our lives. Low cost commercially available electronic systems have touched every aspect of our existence. They enhance productivity (computers), entertain us (televisions, music players), provide health care (pacemakers), improve communication (cell phones) and even ensure our safety (motion sensors, alarms). Apart from the fundamental advances in the core technology of semiconductor fabrication, the success of microelectronics was made possible due to robust electronics packaging and assembly technologies that were developed in parallel. Component level packaging protects the delicate silicon chips and creates an independent module that can be integrated into a larger system. System level assembly and packaging which is enabled by multi-layered printed circuit boards and advanced interconnection technology (e.g. Flip-chip bonding, Ball Grid Arrays) forms the working system by integrating numerous individual components. Electronics packaging and assembly is a multi-billion dollar industry and it also happens to add significantly to the cost of the final product. The standardized packaging of electronic components creates rugged stand alone modules which anyone can use to build their own specific device.

The first set of microfluidic structures were also fabricated in silicon [15-17] as the technology of silicon bulk micromachining was easily adapted for structural microfabrication. Subsequently, glass was the material of choice for microfluidics [18, 19] because it was optically clear and historically has been the material of choice for macro scale biological labware (e.g. test tubes, microscope slides).

⁸ Technological advancement can be incremental or disruptive. A disruptive technology is totally different from the predominant existing technology which it replaces. E.g. Digital photography replacing film photography

With the advancement in polymer technology, polymers were seen as the material of choice for microfluidic structures because of lower cost, easier manufacturing processes, and the unique properties that could be engineered into the polymer material itself for added functionality. The lower cost of polymer parts makes it viable to fabricate disposable devices which are necessary to avoid contamination in biological applications. Predominant technologies for polymer fluidics microfabrication include hot embossing [20-23], injection molding [20, 24] and combinations of lithography and casting processes [25].

Today, we see a similar scale of interest and growth in the fields of Bio-MEMS, microfluidics, nanotechnology and bioinformatics as microelectronics had experienced in its nascent years. Miniaturization in fluidics will provide many advantages identical to those experienced by miniaturization of electronic devices. Electronic devices like computers are faster, smaller, and cheaper and use less power than those available 10 years ago. Microdevice based biological systems are beginning to demonstrate similar advantages over existing, conventional solutions, for example the handheld blood chemistry analyzer developed by I-Stat[®] [11] and the table-top automated electrophoresis system made by Affymetrix[®] [12].

Microfluidics has other unique advantages making it a core technology for biology and life science applications. Biological interactions inherently occur on the micro scale. As shown in Figure 2.1, the size scale ranges from around 10 microns for cells and single celled organisms down to 10 nanometers for macro molecules such as DNA. Since the scale of biological elements is similar to the size scale of the microdevice, some unique opportunities are generated, such as cell level and even molecular level interactions that were impossible before the advent of microdevices. Until recently, experiments have been largely based on statistical analysis of the behavior of a population of subjects that were too small to analyze individually. Now this paradigm is changing with the advent of micro and nano scale devices that allow experiments and observations on individual cells [9], single strands of DNA [26], and protein molecules. The ability to create structures on the micro and nano scale also creates the possibility of mimicking surface characteristics of naturally occurring

structures. This is advantageous in fields like artificial tissue culture as textured scaffolding can be designed and fabricated for the growth of tissue [27] and eventually whole organs. All these events and interactions occur on the micro/nano scale. However the human interface with these microdevices cannot be achieved directly on such a small scale. In order to leverage the advantage of the micro scale environment in the world of biology, it is necessary to have a convenient macro-micro interface such that biologists can use their macro-scale tools to interact with the micro world.

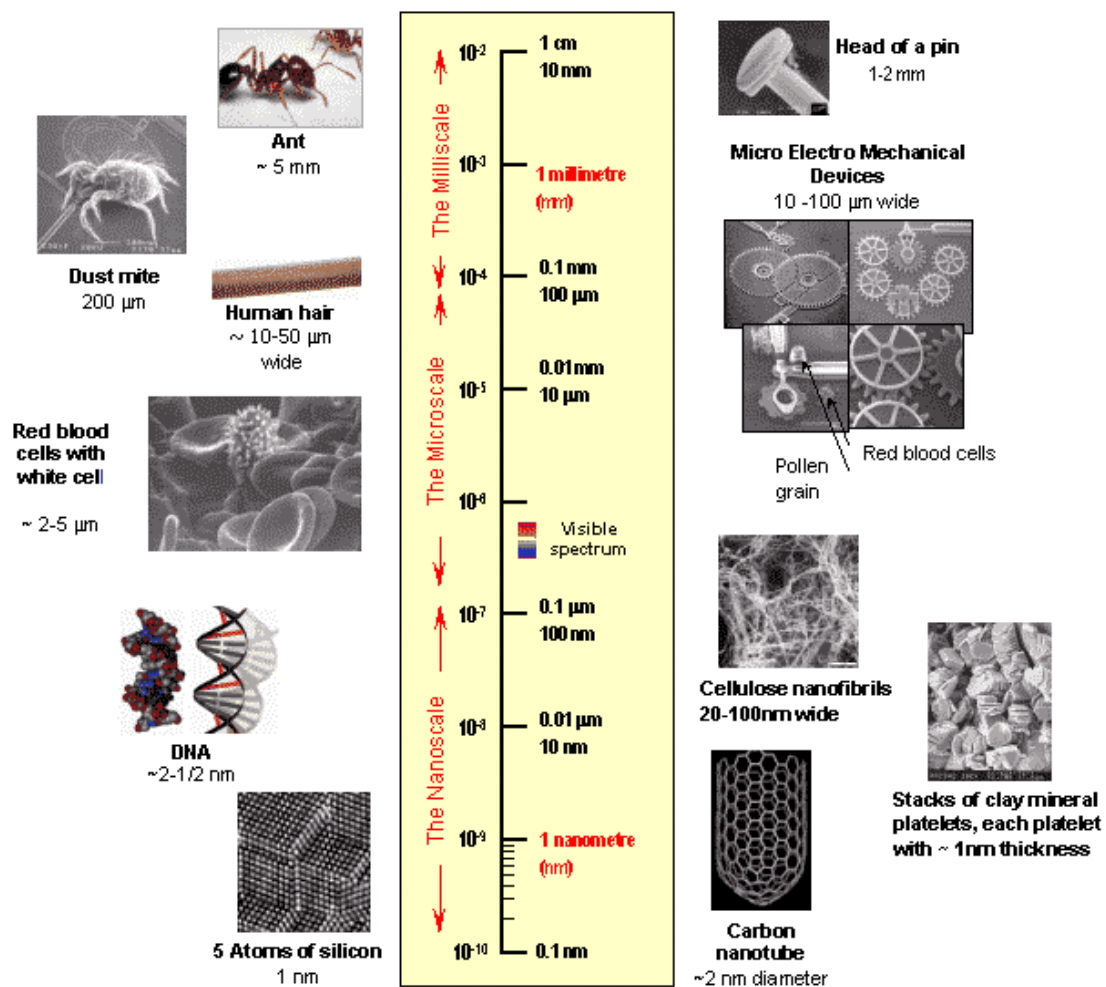


Figure 2.1: Illustration of size scale (Source: <http://www.sustainpack.com/nanotechnology.html>).

The other feature which makes microfluidics and biology natural partners is the fact that most biological interactions occur in an aqueous environment. Hence

microfluidic devices provide the ideal environment for analyzing or sensing biological species. This concept is well accepted in academia and documented by the large and growing number of publications and conferences dedicated to microfluidics and lab-on-a-chip solutions⁹. We are now also seeing a number of commercial products that showcase the successful transition of Bio-MEMS devices from research laboratories to the private sector.

Nanotechnology, a field which is considered the most significant disruptive technology of current times is also closely tied to applications involving microfluidics and Bio-MEMS. Microfluidics provides a means of handling, interacting with and utilizing nanometer scale entities such as carbon nanotubes and nanoparticles. Microfluidic devices have been used to fabricate nanoparticles [28] and apply nanoparticles for tagging and separation of biological elements [29]. Carbon nanotubes inside microfluidic channels have been used as sensor elements capable of detecting very low concentration samples [30]. Thus microfluidics is a stepping stone and an enabling technology for a number of nanotechnology applications.

But for microfluidics development to progress rapidly, the packaging, assembly and prototyping infrastructure have to be developed in parallel with the fundamental technologies to provide a seamless, user friendly and standard library of modules that serve as components in larger systems.

2.2. Challenges of Microfluidic Development and Packaging

Packaging involves the concepts of enclosing, connecting and integrating a component into a sub-system or a sub-system into a higher system. In the case of microelectronics, Rao R.Tummala in his book, Fundamentals of Microsystems Packaging [31] defines packaging as “the bridge that interconnects the ICs and other components into a system level board to form electronic components”. Packaging a component has three fundamental functions-

⁹ A publication search on Engineering Village (<http://www.engineeringvillage.org/>) for ‘microfluidics’ yields 5869 results. A journal titled “Lab on a Chip” is published by RSC Publishing (<http://www.rsc.org/>) that is dedicated to academic publications on miniaturization for chemistry, biology & bioengineering applications.

1. Connect it to the external environment so that it can receive input and deliver output.
2. Protect it from the undesirable elements of the external environment such as heat, dust, moisture and mechanical shock.
3. Provide optimal conditions for the component to function efficiently. This function may involve many aspects ranging from thermal management to minimizing electromagnetic interference or maintaining precision alignment.

Microfluidic packaging is a nascent field but it is gaining importance as microfluidic devices are becoming a commercial reality. It presents the same challenges that are seen in electronics packaging with the added complexity of multi-domain ¹⁰ integration, coupled with the need to interact with and maintain compatibility to existing laboratory equipment. Figure 2.2 illustrates the role of microfluidic packaging. Individual components from various technological domains such as optics, fluidics, electronics and biology are interfaced and interconnected to make a module. Many such modules may be combined and used in conjunction with existing macro scale laboratory equipment to form a functional microfluidic system. Thus hierarchically, a **component** is defined as an individual entity like a mixer structure, a silicon chip or microspotted biological molecule. These components combine to form a **module** which is capable of performing sub-tasks and has limited functionality by itself. A number of such modules may be combined to perform a sequence of sub-tasks to create a microfluidic **system**.

The fabrication technologies for microfluidics often involve aggressive chemicals and/or high temperatures and these harsh processes are usually incompatible with active biological elements. These factors imply that the packaging, assembly and interconnection issues faced are more complex than those in the field of microelectronics which deals primarily with conductive interconnects.

Whether the component or device is microelectronics or microfluidics, packaging is a crucial and challenging aspect of fabricating a robust and commercially viable

¹⁰ Devices may contain elements of technology from different fields like mechanical engineering, electronics, optics, biology, chemistry and so on. These multiple domains come together during the packaging process.

product. For rapid development, standardized test platforms are an essential technology. Since it is necessary to generate awareness about a technology and lead it to gain wider acceptance, making microfluidic development platforms and standard experimental setups available to the public at a low cost is a step towards achieving this goal.

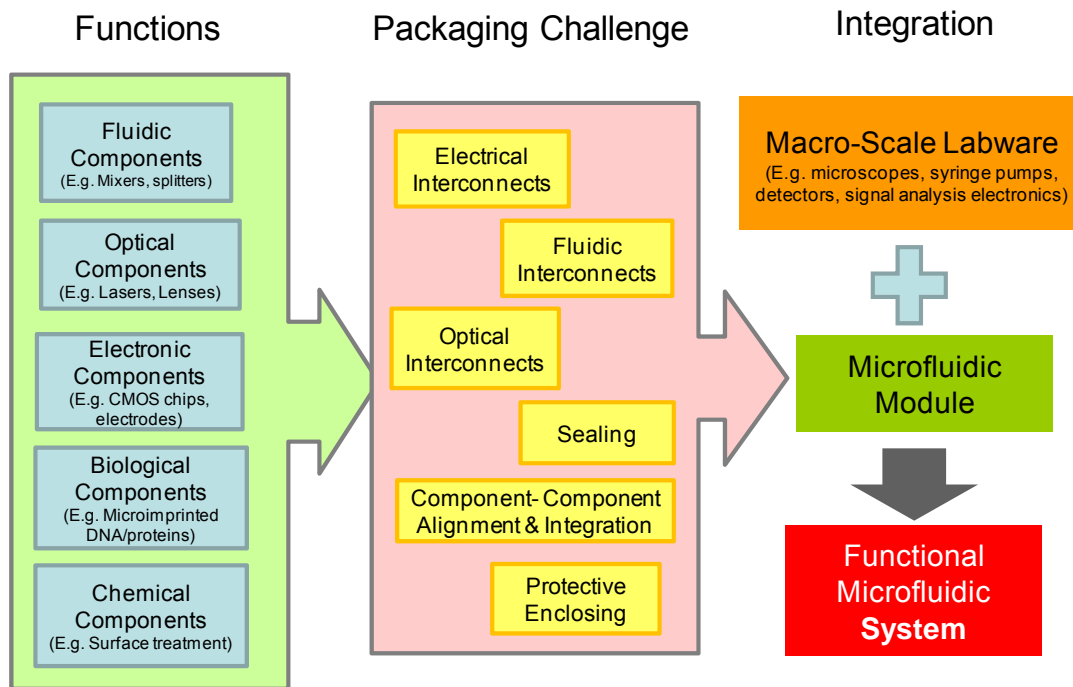


Figure 2.2: Schematic illustrating the role of microfluidic packaging in integrating individual components towards forming a functional system.

At this point in time there are no well-defined and standard modules in microfluidics like the diode, transistor or integrated circuit chip in electronics. Every microfluidic application uses uniquely designed and fabricated components. The presence of multiple domains also pushes the need for customized solutions for each and every application. Thus, though many individual solutions using similar approaches exist, there is no common platform that will benefit the broader user community. The absence of standardization or off the shelf components leads to a long and expensive development path for any microfluidic device that can only be pursued by commercial interests with substantial financial backing. If the existing similar microfluidic solutions were developed using a well defined structure into

standard modules, there would not be any need to redesign identical components for every new application.

In microfluidics, there is no equivalent to the breadboard or printed circuit boards (Figure 2.3) seen in electronics that will allow users to plug individual microfluidic modules together to form a working system for experiments and in fact no generally accepted standard methods or formats exist which enable easy connection or assembly of microfluidic components. The product of microfluidics research is closely tied in with biology and any research involving biology is statistical in nature, requiring a number of samples to be run in parallel in any single experiment. This is evidenced by the presence of standard laboratory formats such as the 96-well plate (Figure 2.4). Hence, standardization at this stage is essential in order to produce consistent hardware to biologists.

Developing a user friendly, plug & play breadboard like microfluidic platform for users to experiment with, and making such a platform available to educational institutions will introduce microfluidic technology to the future generations at an early age, leading to wider acceptance of the technology. It can function as a common development platform, into which researchers can plug in their own customized module with minimal effort to carry out experiments (Figure 2.5a). It also has the possibility of being accepted as a standardized platform for researchers, eliminating the need for developing new experimental setups for every single application. Once a library of modules for performing different functions is established, then users may pick parts straight out of this library to perform certain functions much like it is in the electronics industry today, where a user can build a very complex system by picking parts from a commercial catalog.

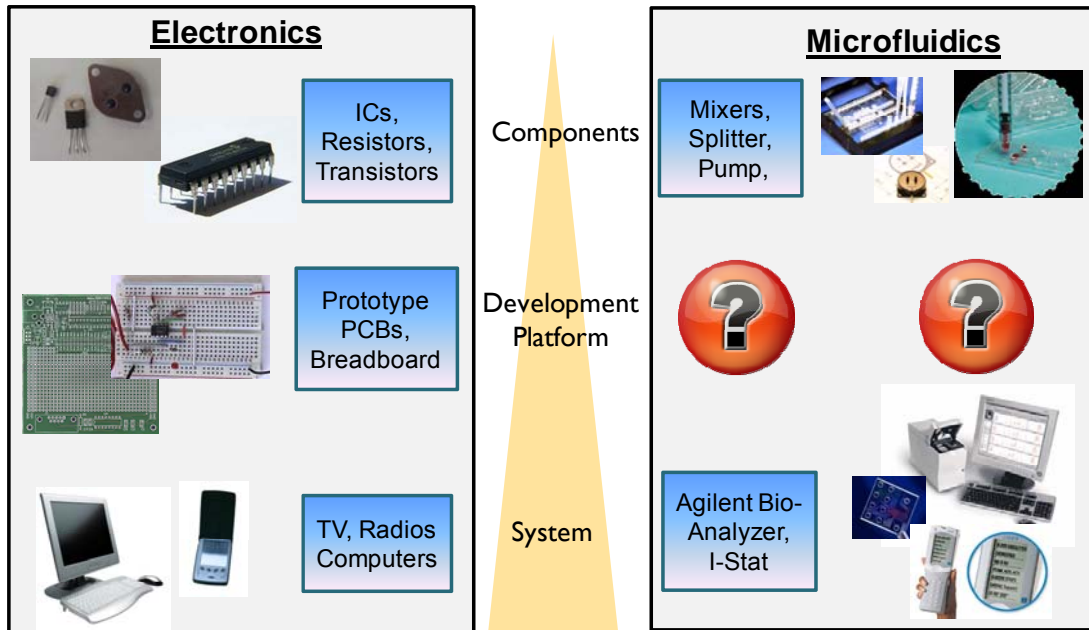


Figure 2.3: Schematic illustrating the analogies between microelectronics and microfluidics and highlighting the absence of a breadboard-like development platform in the field of microfluidics.

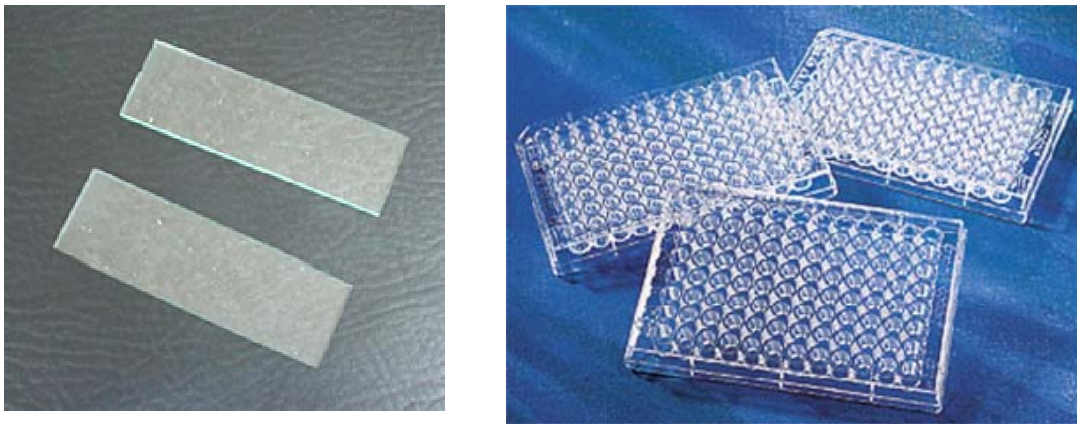


Figure 2.4: Experimental hardware commonly used in biology - a microscope slide (Left, Source: www.laboratory-supply.com/slides.html) and a 96-well plate (Right, Source: www.htslabs.com/).

Standardization of methods and formats for development of applications is not only helpful, but is essential because of the complexity of analyzing biological entities using microfluidic, microelectronic, micro-optic and other microtechnology based solutions. The need for quick, broad screening of biofunctional surfaces, samples, and processes, is a motivation to create a flexible development platform

that enables simultaneous construction and analysis of biological samples using a microfluidic configuration that also mirrors the microfluidic setup of final applications.

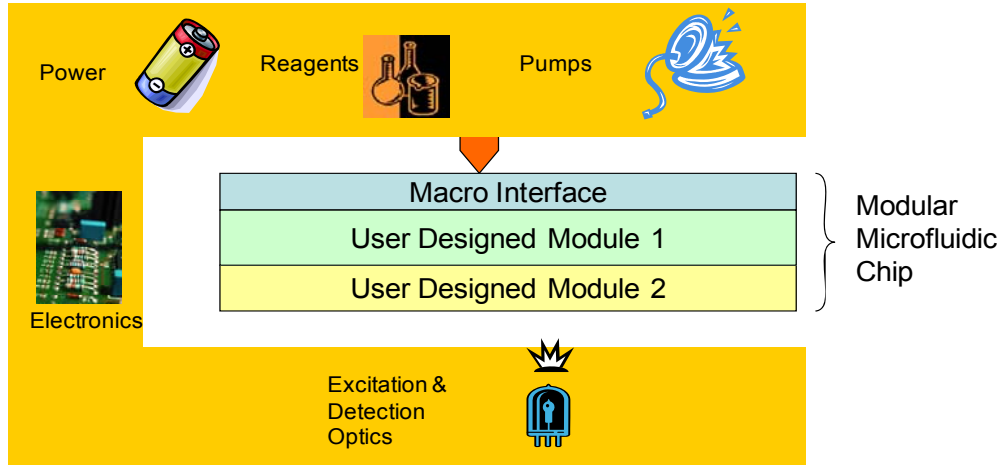


Figure 2.5a: Schematic of a microfluidic test platform where user defined microfluidic chips are integrated into an existing infrastructures that handles all the auxiliary requirements for the application.

Figure 2.5b illustrates an example of how a biological analysis protocol may be broken down and executed by individual modules, each module being responsible for specific operations. The modules consist of a number of components that may be produced by different fabrication processes and then assembled together during a packaging process. Such an approach is conceptually defined as a modular development platform.

As this was an effort to develop a general purpose microfluidic development platform, it was mandatory to understand the existing industrial and academic solutions and problems. A literature study was carried out to document the state of the art commercially available microfluidic solutions as well as the ongoing research efforts to further push Bio-MEMS technology. This information was used as a technical guideline for the modular development platform investigated in this thesis.

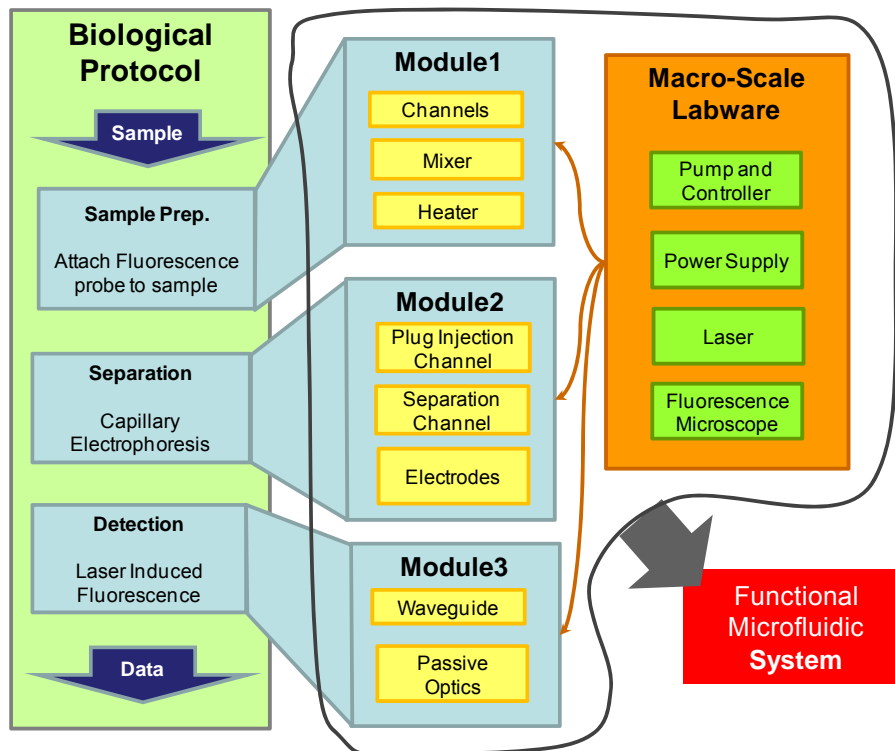


Figure 2.5b: Schematic illustrating an example of how a biological analysis protocol may be broken down into modules based on function. Each module performs a limited function but when multiple modules are combined, it forms the complete system allowing complex analysis.

2.3. Microfluidic Systems and Solutions

An internet search on Engineering Village¹¹ (an academic publication search engine) for the term “microfluidic” brings up 5741 records for publications between the years 1990 and 2007. This illustrates the vast amount of research that has been done in this field. Review articles by Gravesen et al [32], Reyes et al [2], Erickson et al [33] and Morgensen et al [6] provide a comprehensive overview of the field of microfluidics, applications and the fabrication technologies. Works cited in these reviews address the integration of microfluidics with optics, electrodes, heaters, pumps, valves, CMOS electronics and biological entities such as DNA and whole cells. A wide range of applications are discussed, including PCR devices, electrophoresis based separation devices, and fluorescence and conductivity based measurement devices to only mention a few. A number of interconnection technologies for microfluidics have been presented in academic publications [24, 34-

¹¹ <http://www.engineeringvillage2.org/>

37] and a review of interconnection philosophies is presented by Fredrickson et al [38]. All the discussed systems use various formats, integration and interconnection methodologies. A common set of standards and a well defined library of formats and technologies are lacking.

Microfluidic systems technology for biological and medical analysis and sensing are at a point where commercial products based on the technology are making their appearance on the market. In a majority of the cases, companies have a unique technology or competence that is applicable to a niche segment in the field of microfluidics as discussed in the following examples.

Analytical laboratory systems from **Affymetrix**[®] (<http://www.affymetrix.com>) provide glass microfluidic chip based electrophoresis systems for DNA, RNA and protein separation. They are the most established in the market, in this field, because the company provides a complete solution package - the computer controlled automated system and consumables for the system that includes reagents and disposable chips. Micro scale liquid chromatography is the niche application of the company **Nanostream**[®] (<http://www.nanostream.com/>). Micro Parallel Liquid Chromatography (μ PLC) is carried out on a 24 column cartridge that works with their tabletop systems. The 24 columns allow parallel processing of samples, speeding up the analysis time. It is available in different design formats and with different solid phases for specific applications. Affymetrix[®] and Nanostream[®] are examples companies manufacturing highly specialized proprietary systems, designed and fabricated to perform a dedicated analysis task.

Fluigent[®] (<http://www.fluigent.com/>) specializes in precision flow control technology for microfluidics and Lab-on-chip devices that would replace conventional pumping devices such as peristaltic or syringe pumps. They are also in the process of commercializing a specialized capillary based DNA separation process.



Figure 2.6a: Fluigent MFCS-8C flow controller (Left) uses air pressure to drive liquids and is capable of flow rates ranging from less than a nanoliter per minute up to hundreds of microliters per minute. Schematic (Right) shows the setup using such a system (Source: Fluigent’s website).

Concept to Volume (C2V) (<http://www.c2v.nl/>) is a Netherlands based company that has a wide range of products and services listed on their website. However, of special interest with reference to the scope of this work is the “microDELTA™” concept that looks at an electronics-like assembly and packaging solution for microfluidic components along with electronic components. **Microfluidic Chipshop**® (<http://www.microfluidic-chipshop.com/>) is based in Jena, Germany. Their base technology is polymer microfluidic chip and polymer micro-titerplate fabrication. Some standard chips are available from their catalog but Microfluidic ChipShop® also carries out custom fabrication of specific designs in silicon, polymer, glass, and ceramics. **ThinXXS**® (<http://www.thinxxs.com/>) is marketing a microfluidics development kit that uses injection molded polymer microfluidic slides which are laid side by side and interconnected using parallel microfluidic bridges. The slides have ports on them for connectors and the bridges to plug into. ThinXXS® also has a micro pump module with a footprint identical to that of a microscope slide to allow easy fluid handling. The kit is capable of combining up to 4 chips side-by-side to perform more complex functions. Both, Microfluidic Chipshop® and ThinXXS® are examples of user driven module development efforts. The side-by-side chip layout adopted by ThinXXS® while convenient to use, incorporates significant fluidic dead volume between the chips. A standard method of integrating non fluidic components like electronic pathways would also benefit the functionality of this kit.

Micalyne[®] (<http://www.micalyne.com/>) has a MEMS foundry infrastructure that provides development and fabrication services to customers. Apart from that, their microfluidic product line consists of a laser induced fluorescence (LIF) system which uses glass microfluidic chips. These chips are available in standard as well as customer specific designs, taking full advantage of Micalyne's microfabrication expertise and capabilities. Capillary electrophoresis is the method used for separating the samples and the system includes a high voltage power supply for driving the electrophoresis.

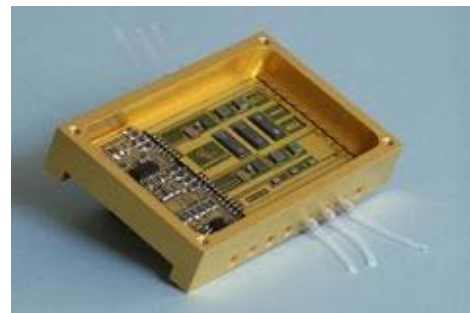
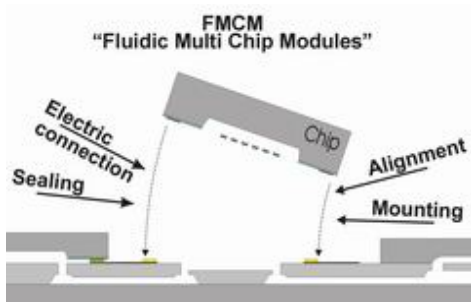


Figure 2.6b: Schematic (Left) of microDELTA™ platform for interconnection of fluidic modules into a multi-chip-module system and integration with electronics (Right).

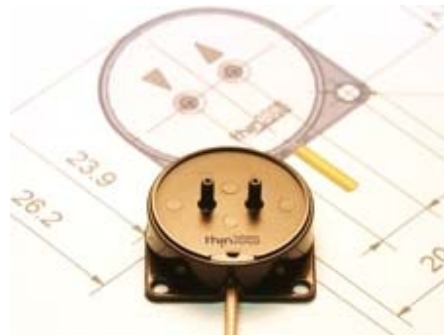
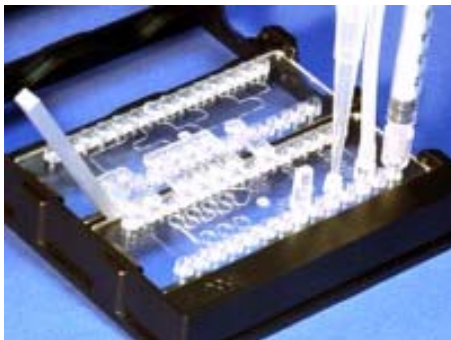


Figure 2.6c: ThinXXS microfluidic construction kit with adjacently laid out individual slides connected by bridge (Source: ThinXXS website).

Figure 2.6d: Piezo actuated diaphragm micro-pump from ThinXXS (Source: ThinXXS website).

Cascade Microtech[®] (<http://www.cascademicrotech.com/>) has been in the business of building electronic probe stations for testing semiconductor products at various stages of fabrication. They have adapted their probe station technology to test microfluidic chips by adding the technology to make temporary fluidic

connections to these chips. **Gyro**[®] (<http://www.gyros.com/>) has combined the 'Lab-on-CD' [39] microfluidics with an automated test platform to provide a powerful parallel processing system for protein quantification and drug discovery applications. The system uses centrifugal forces to move liquid from one point to another on the Bioaffy[®] CD, and has an integrated Laser Induced Fluorescence (LIF) [6] based measurement system to read fluorescent markers in the processed fluids.

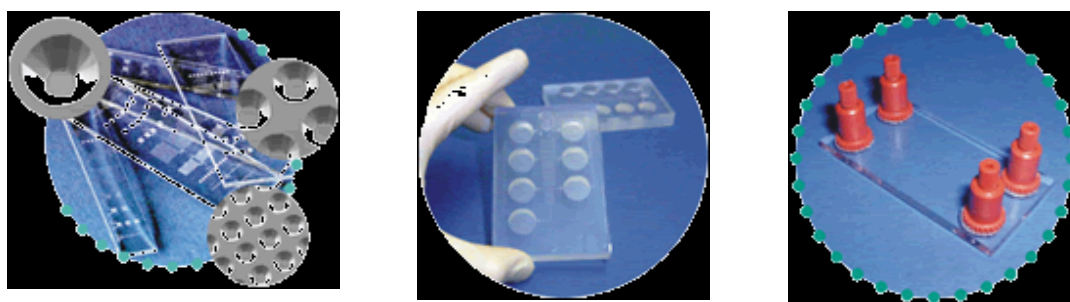


Figure 2.6e: Molded polymer microfluidic chips and titerplates offered by Microfluidic ChipShop[®] (Source: Microfluidic Chipshop website).



Figure 2.6f: Microfluidic probe station by Cascade Microtech, with electrofluidic dispensing microport (Inset) (Source: Cascade Microtech website).

Among the companies researched, **Micronics**[®] (<http://www.micronics.net/>) was the only company which has commercialized a biological/chemical development platform in the form of its disposable Active[™] Lab Cards which in conjunction with

Micronics' microFlow™ System to control fluid flow, lets users develop assays and explore new chemistries using reduced volumes of sample and reagent. Both, Gyro® and Micronics® provide conceptually similar test platforms which consist of an instrument and a disposable polymer part that can be designed for specific applications. However, neither system is truly a flexible development platform because the disposable components are prefabricated and hence the user cannot make changes without going through a complete design and fabrication cycle.



Figure 2.6g: Gyros Bioaffy® CD microlab (Left) and Gyrolab® Workstation LIF (Right) for automated protein quantification for drug discovery applications. (Source: Gyros website).

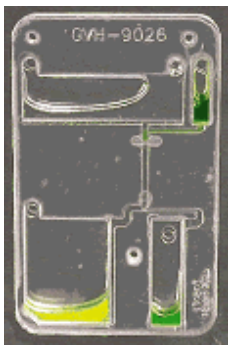


Figure 2.6h: The H-Filter® Access™ Lab Card.



Figure 2.6i: The microFlow™ system consisting of an array of precision syringe pumps for controlling fluid flow in the lab card (Source: Micronics website).

After reviewing the academic literature and commercial systems available in the market, it was found that there are numerous products at the component level and module level. There are also a few examples of specialized systems that address specific applications but a simple, robust, flexible and yet somewhat standardized user friendly microfluidic development platform for microfluidic applications is missing. Most available systems and devices addressed specific niches, but the generic system that would take biological labware to the next level is yet to be developed.

2.4. Functional Specifications for a Modular Platform

As illustrated in section 2.3 a wide range of microfluidic applications and technology solutions already exist. Hence the modular development platform should be flexible and capable of integrating different technological solutions and functional domains. The microfluidic platform should be capable of connecting to standard macro instruments such as syringe pumps or optical microscopes, thus including the pre-existing, conventional labware into the portfolio of operations. Since this is a platform that is meant to be used by researchers from all disciplines, simple assembly, disassembly and handling were some of the key design criteria. For biological applications, open access to the surface of the fluidic channels is an important feature as that allows the user to carry out surface modification of the fluidic path or attach biological elements to it using techniques such as microspotting. However, for the microfluidics to function, fluidic pathways have to be sealed. In order to satisfy both requirements and provide a flexible development platform, the ability to temporarily seal and open microfluidic chip was considered a necessary design criteria. A summary of the functional design criteria is presented in Table 2.1 and used throughout this thesis as a design guideline. Developing a complete system requires a whole spectrum of technologies. For a microfluidic system, fabrication of polymer chips, sealing them, interconnecting and assembling them are technologies relevant to every application. Since this was an effort to develop a general purpose system, efforts were focused on a few selected areas so as to have the broadest impact on many different applications (Figure 2.7).

Aspect	Criteria
Ease of Use	Familiar format for biologists. Simple assembly - that a technician can perform in <5 minutes without need for microscope.
Modularity	Platform will be modularized such that individual modules can be redesigned, reused and interchanged without affecting the rest of the assembly.
Compatibility	Must be compatible with existing lab equipment.
Materials	Modules may be fabricated from any kind of polymer but should be capable of integrating glass and silicon components too.
Cost	Minimal cost to allow the parts of system to be disposable if the application so requires.
Flexibility	The interfaces between the macro-micro world must be flexible to allow different types of connections to be designed in and modules should be capable of accommodating a wide range of designs.
Multi-Domain	Capable of integrating electronics, optics, biology, magnetic with the microfluidics.
Fabrication	Scalable fabrication process where prototype to small scale production will not require significant change in fabrication process or substantial development time.
Turnaround	The fabrication process should be capable of going from a design to a finished part in 2-3 weeks keeping with the spirit of rapid prototyping.

Table 2.1: Summary of functional design criteria for microfluidic development platform.

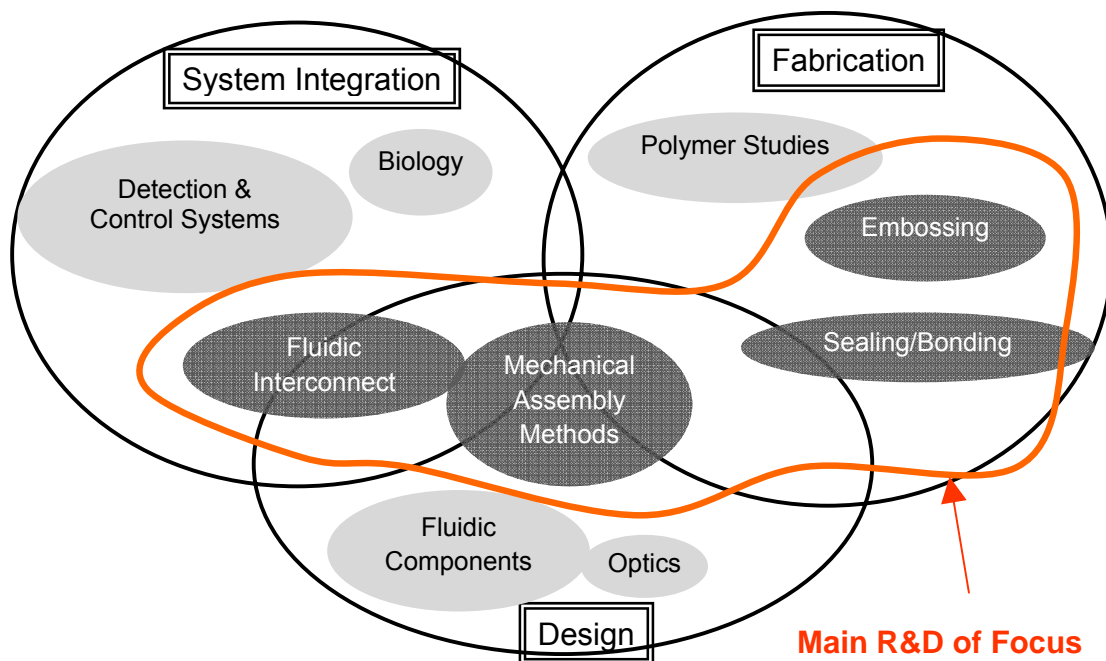


Figure 2.7: Venn diagram illustrating the broad research areas and the areas of focus.

This system platform enables a user to develop, test and optimize a working microfluidic device rapidly, because it addresses issues such as fluid delivery and control of operations that may not be the primary focus of the particular research being carried out, but are nevertheless necessary for an operational device. It effectively bridges the gap between the macro and micro world as it interfaces with existing standard laboratory equipment. A modular design philosophy ensures that the system is flexible and functional modules once developed can be reused easily for different applications. Both the design and the fabrication aspects of the system were conceived with the intention of easy transition to commercialization and mass production.

3. From Chips to Modular Systems

The overall efficacy and success of microfluidics is dependent not only of the micro scale components, but also on the ability to make it convenient to use with a high level of reliability. If considered analogous to microelectronics, the channels, mixers, splitters and other microfluidic elements, while a few orders of magnitude larger in size, are similar to the micro scale elements of an integrated circuit (IC) chip like transistors and resistors. Once packaged into the plastic or ceramic package we are so familiar with, the electronic chip becomes a functional module that can be used in different circuits as required. These functional modules become components of various working systems. The ability to design and fabricate various microfluidic components in the form of mixers, distributors, pumps, valves etc has been demonstrated in many academic publications (Section 2). However, to simplify and ultimately encourage application development efforts, modularizing these individual components in order to make them stand-alone units is crucial. With the microfluidic development platform, a step in that direction is taken.

The concept developed to transition from individually set up microfluidic chips and ad hoc interfaces towards a complete system development platform with standardized interconnects and well defined interfaces is discussed in detail in this section. Each component in the platform, its function and design are discussed along with some fundamental modeling used to better understand and optimize the particular function.

3.1. 3-D Microfluidic Platform and Modular Concept

At the heart of the development platform is a set of polymer microfluidic chips that are vertically stacked and interconnected. Each chip is designed to perform a specific function, thus making it an independent module. The modules combine in the vertical stack to form a complete functional system. This configuration ensures minimal dead volumes as the fluid moves from one functional module to the next through vias which is the shortest path possible. The modules may have an open microfluidic surface for dip chemistry or microspotting and covered only while

assembling in the system. The modules are joined using a combination of sealing technologies. Alignment between these modules is necessary for the vias between the modules to interconnect. Passive alignment between the modules of the stack was used to achieve this. The means of connecting macro fluidic and electronic input into the stack are handled by features designed into a platform on which the microfluidic stack sits. The platform interfaces with standard lab equipment such as syringes and pipettes and the format of the chip resembles that of a standard microscope slide, making it compatible with typical laboratory equipment (labware) such as microscopes.

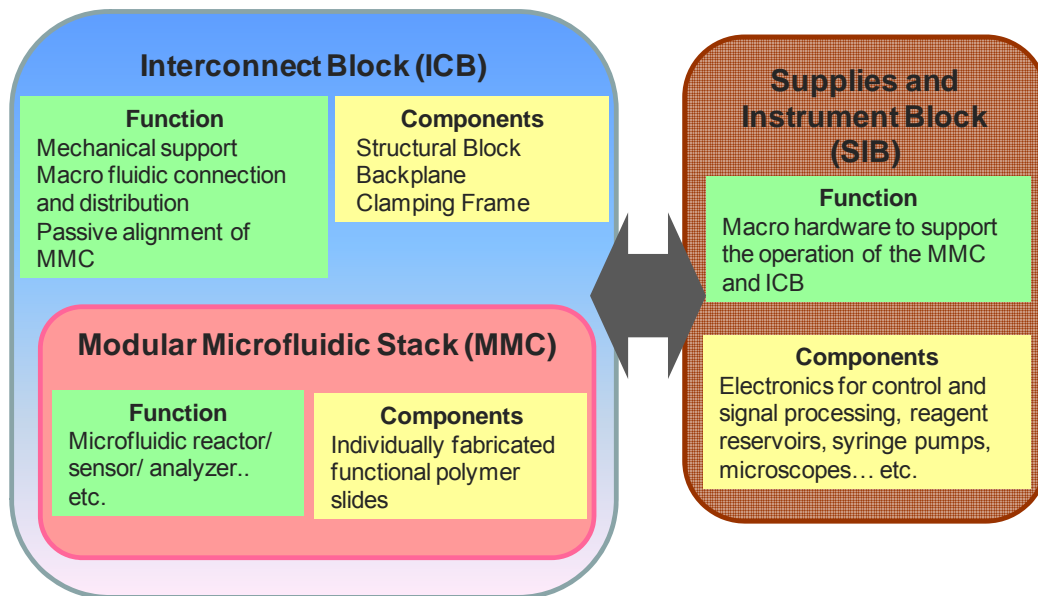


Figure 3.1: Schematic of the modular system architecture, illustrating the functional demarcation of the different parts.

The 3-D microfluidic development platform consists of 3 fundamental parts (Figure 3.1) –

- a. A Modular Microfluidic Chip (MMC) - This is a polymer part on which the actual reactions take place. It consists of a vertical stack of individual chips where each chip is associated with specific functions. The chips are designed and fabricated independently and then assembled and interconnected to form the MMC. The form factor for the MMC resembles a traditional microscope slide making it compatible with pre-existing labware. This chip was envisioned as a disposable part of the

system, if the application so requires. The first chip in the MMC is a common interconnect chip with fluidic ports, a port for an electrical connector and windows to verify the alignment accuracy of subsequent chips (Figure 3.2). Different user defined chips may be stacked onto this interconnect chip to form the MMC. All the chips must adhere to the basic format shown in Figure 3.2 but the fluidic region may be patterned as necessary for the application and customer requirements.

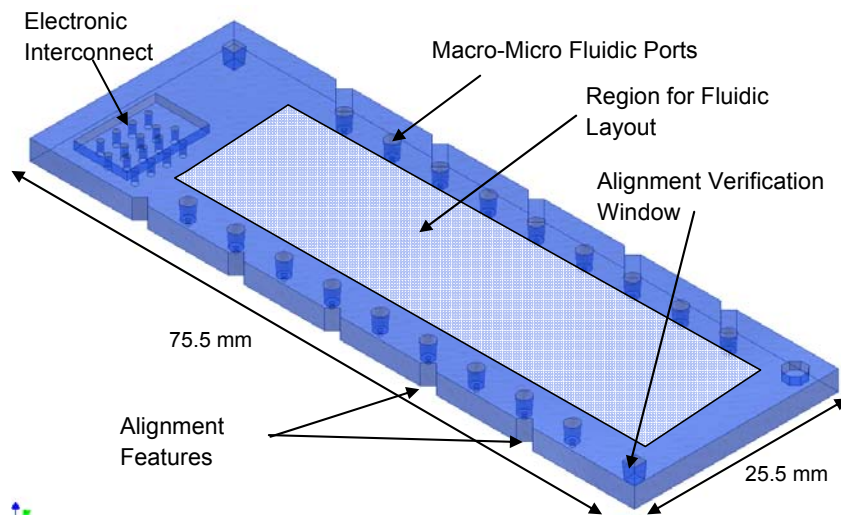


Figure 3.2: Schematic of interconnect chip that is the first chip in the MMC. It consists of fluidic ports, a port for an electrical connector and windows to verify the alignment accuracy of subsequent chips.

b. An Interconnect Block (ICB) – This unit is the framework in which the MMC is assembled and connected. It consists of three components (Fig. 3.3) – a structural block that is the interface to the macro world, a microfluidic backplane, and a mechanical clamping frame. The structural block is the macro-micro fluidic interface with ports on the side for syringes to plug in (Note: The port design can be modified to make it compatible with Luer fittings or any other commonly used macro connector). The structural block also provides the mechanical support for the system and serves as the bottom for the clamping frame to attach to. The clamping frame is designed to passively align the multiple chips of the MMC in the vertical direction and also create a temporary seal between them via the clamping force if applicable. It consists of ten steel dowel pins fitted into a plastic part. The dowel pins act as

alignment elements that mate with V-groove features on the MMC. The backplane in the ICB is the fluid distribution manifold between the inlets (Figure. 3.4) on the structural block and the MMC. The fluid distribution network on the backplane is custom fabricated based on the specific routing requirements. The alignment and the temporary sealing will be discussed in sections 3.1.1 and 3.1.2, respectively.

c. A Supplies and Instrument Block (SIB) –This consists of the instruments, and other macro scale lab equipment that supports the functioning of the microfluidic device. The SIB may consist of reagent supplies, pumps, microscopes, control electronics, signal processing units, data acquisition units, etc.

A solid model of the system development platform is shown in Figure 3.3. Fluid from the “outside world” enters through the structural block (ICB) via standard syringes. It is then routed by microchannels in the backplane to different nozzles. The nozzles on the backplane mate to ports on the interconnect chip of the MMC and through this network, fluid is delivered into the MMC (Figures 3.4a,b). This design minimizes dead volume in the whole fluidic circuit as the path from the syringe into the MMC is defined by bores in structural block and does not use any conventional connection tubes. An image of the assembled development platform is shown in Figure 3.5.

Separating the development platform into these 3 fundamental parts is beneficial in a number of ways. With this configuration, parts like the MMC can be treated like a ‘consumable’ and disposed after every experiment while the other parts are reused. The development timeline is also shortened because each of these parts can be developed and modified in parallel. So long as common interface rules guide the interaction between these parts, they can be modified as required and yet be put together to function as an integrated system. Figure 3.1 illustrates the components and architecture of the development platform. The MMC hosts the primary functions of fluid handling, mixing, reacting, separating and sensing, and consists of microstructured polymer chips. It is enclosed and supported by the ICB which provides macro-micro interconnection, alignment capability, fluidic distribution and

structural support to the MMC. The functioning of the ICB and MMC are supported by external equipment (SIB) as required for the particular application.

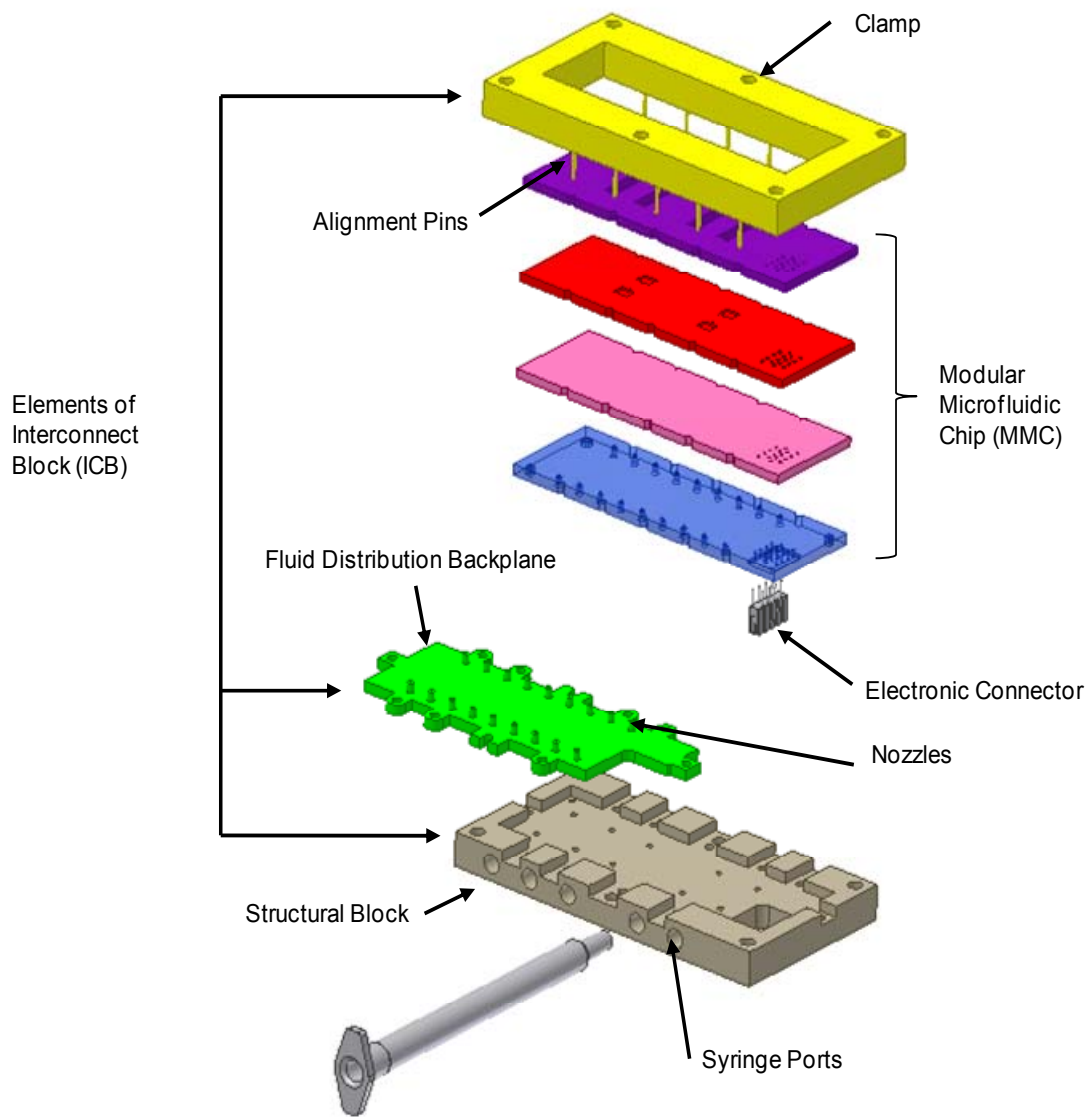


Figure 3.3: Solid model representation of the components of Interconnect Block

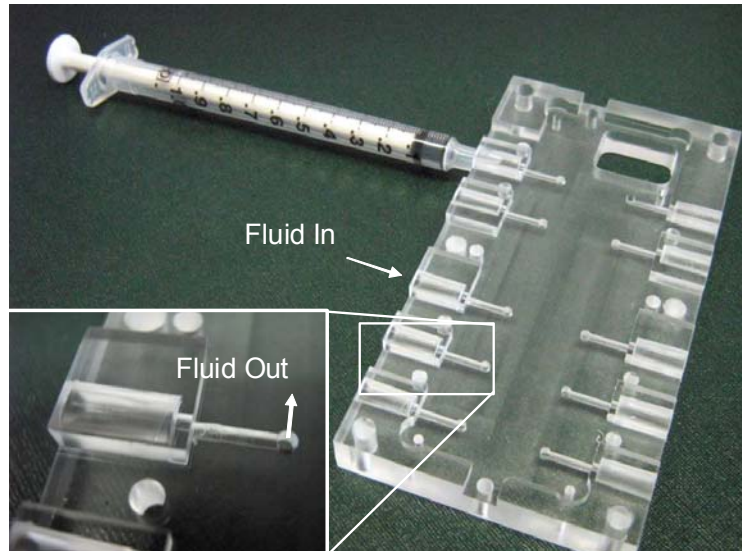


Figure 3.4a: Image of structural block with a connected syringe. Inset shows close up of fluid bore connecting syringe inlet to the backplane.

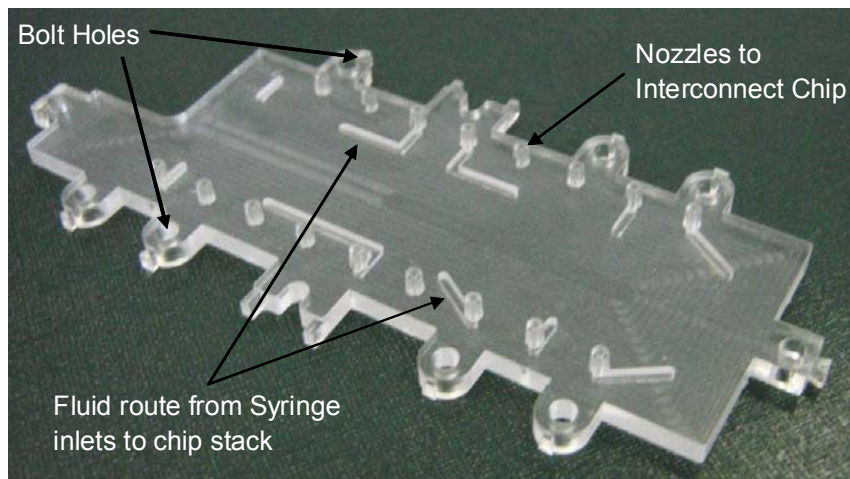


Figure 3.4b: Image of backplane that is responsible for routing fluid from the structural block to ports on the MMC.

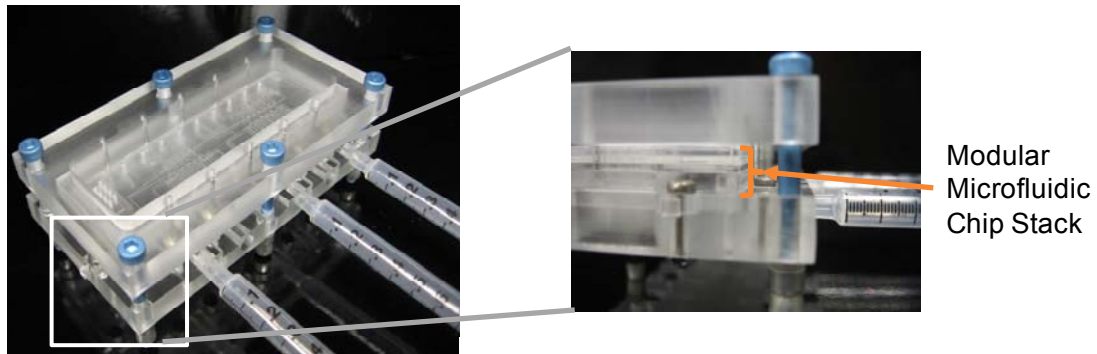


Figure 3.5: Image of the MMC assembled into the ICB and connected to syringes.

Flexible Operation of the Development Platform

The inherent modularity and flexibility in the design also offers many alternative ways of assembling and using the system. For example, the backplane and structural block may not be used altogether and molded nozzles can be connected directly into the ports. Sealing between the layers of the stack may also be achieved either in a temporary clamped mode or permanently sealed mode.

Individual nozzles (Figure. 3.6) for the microfluidic stack are useful when the design in question is simple and initial prototypes are being made where the fluid is driven from an external pump. So fluid can be driven into the microfluidic stack directly through a tube connected to these nozzles. When a more complicated fluidic network is desired, the backplane concept can be used, which effectively reduces total dead volume in the system and can conveniently handle and distribute multiple fluids simultaneously.

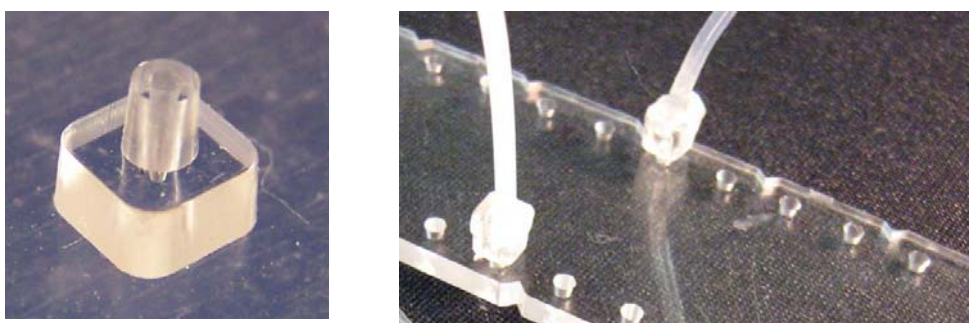


Figure 3.6: Molded single nozzle (Left) and molded nozzle connecting to fluidic chip.

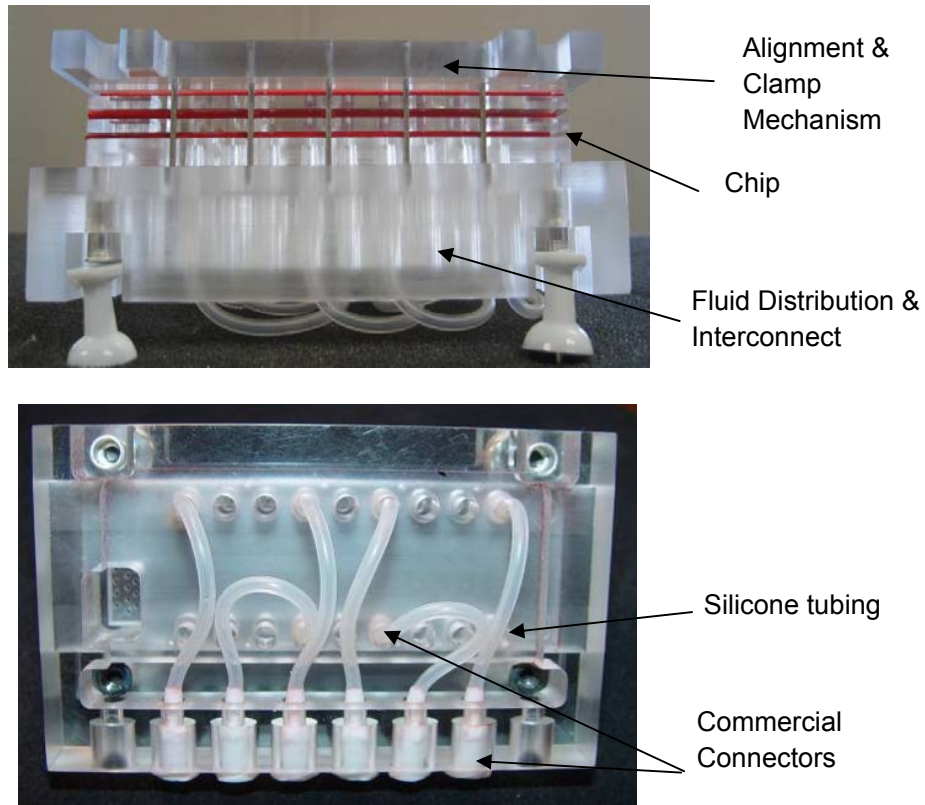


Figure 3.7: Design of Interconnect block (ICB) using commercial connectors and silicone tubing to deliver fluid into the microfluidic chip stack (MMC) useful for applications which do not tolerate any contamination of the fluidic pathways.

An alternate configuration of the system (Figure. 3.7) was also designed and fabricated in which the fluidic connections were made using individual silicone tubes and commercial connectors. Although this design entails larger dead volumes, it may be used in applications where contamination between subsequent experimental runs has to be avoided. For the contamination critical pathways, the silicon tubes may be replaced after each experiment.

These two examples demonstrate the potential and flexibility of the development platform where components can be modified as required by the application and yet seamlessly be assembled to work with the rest of the system.

3.2. Assembling the Development Platform

The aspects of flexible assembly and user friendly handling have been addressed with the mechanical clamping approach. This approach using passive alignment methodology between different chips of the MMC and systematic studies including simulation and experiments were conducted and will be described in the following sections.

3.2.1. Alignment of Chip Stack

As multiple layers are vertically stacked to form the complete microfluidics chip, precise alignment of the chips is necessary to ensure exact positioning of all fluidic interconnects. Failure to accurately align the chips to each other will lead to blockage of fluid flow from one layer to the next (Figure 3.8).

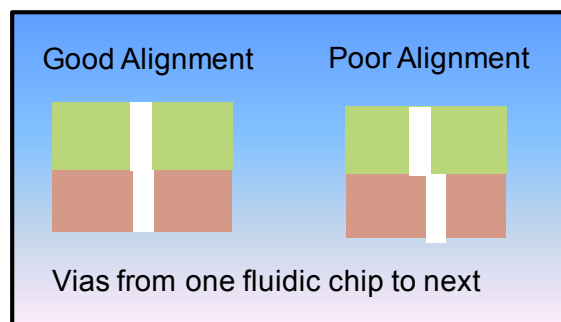


Figure 3.8: Schematic illustrating the effect of poor alignment of the microfluidic chip stack on connecting vias from one layer to the next.

Keeping with the spirit of versatility of the design philosophy, different layers of the chip with various designs should align with sufficient accuracy to form the final device. This poses a challenge, since post fabrication, some dimensional variation of the polymer part from the original design is always observed. These variations depend on part geometry and molding conditions. The geometry of the part is driven by design requirements and the molding conditions are driven by the goal of achieving a well formed, low stress part. Since these parameters cannot be optimized for minimum dimensional variation, the different layers of the modular chip stack exhibit different dimensional changes with respect to the original design. In

order to compensate for this inherent variation, an alignment method called elastic averaging [40] was chosen.

Concept of Elastic Averaging

Elastic averaging is an alignment technique in which a solid body is mechanically aligned to another by over-constraining them using a large number of fairly compliant members. The elastic properties of the material and the constraint structure cause deformations in each individual contact feature to average out over the sum of contact members throughout the solid body [40]. The repeatability and accuracy of an elastically averaged system can be as good as that of a kinematically constrained system. This method also has the advantage that the resultant assembly has higher stiffness and lower localized contact stresses. The repeatability of alignment is inversely proportional to the square root of the number 'n' of contact points [41]. The accuracy of an elastically averaged interface is on the order of square root of 'n' better than the accuracy of the contacting elements [42].

Molded polymer parts have dimensional variation from their original design. The total variation is the combination of errors accumulated from the mold insert fabrication process and the embossing process. The alignment members are V-grooves on the walls of the molded chips (Figure 3.9). Such an alignment feature design was chosen as it allowed the chips and the alignment markers to be formed monolithically from a single mold insert and molding process, thus minimizing the above mentioned errors. 1mm diameter steel dowel pins attached to the clamping fixture act as the secondary alignment feature. The dowel pins align into the crevices of the V-grooves (Figure 3.9). As the dowel pins are fixed into holes in a plastic fixture, it behaves like a cantilevered beam and exhibits a natural compliance. Because the contact locations in the V-groove are in a soft polymer, they also exhibit compliance.

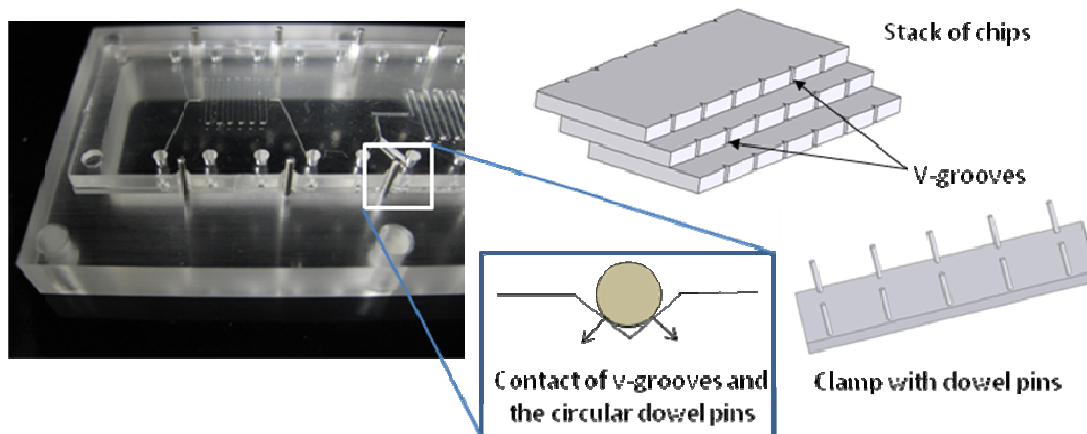


Figure 3.9: Elastic averaging based alignment with dowel pins and V-grooves used to align the chips assembled in the MMC.

A simple mathematical model was used to estimate the alignment accuracy of the chips using elastic averaging. The chips in the MMC were modeled with 2 springs at each contact point (Figure 3.10) where one spring represents the dowel pin and the other represents the compliance of the plastic due to contact stresses. The total stiffness of each contact is given by Eq. 3.1.

$$\frac{1}{k_{total}} = \frac{1}{k_{geom}} + \frac{1}{k_{hertz}} \quad (\text{Eq. 3.1})$$

where k_{geom} represents the stiffness of the dowel pin and k_{hertz} represents the stiffness due to the compliance of the plastic where the dowel pin makes contact with it (calculated based on Hertzian contact stresses).

Based on this, the stiffness matrices can be formed for each of the contacts. As all these contacts are part of one body, cross coupling effects are present between these contacts. The localized stiffness matrices can be combined to form a global matrix incorporating the cross coupling effects between the individual contacts.

$$\begin{bmatrix} F_1 \\ F_2 \\ \vdots \\ F_n \end{bmatrix} = \begin{bmatrix} k_1 & k_{12} & k_{13} & k_{14} \\ k_{12} & k_2 & k_{23} & k_{24} \\ k_{13} & k_{23} & \ddots & \vdots \\ k_{14} & k_{24} & \dots & k_n \end{bmatrix} \begin{bmatrix} x_1 \\ x_2 \\ \vdots \\ x_n \end{bmatrix} \quad (\text{Eq. 3.2})$$

Where

F_n = Force at contact n

x_n = Displacement at n

k_n = Stiffness at contact n

k_{nm} = Cross coupling effects between contacts n and m

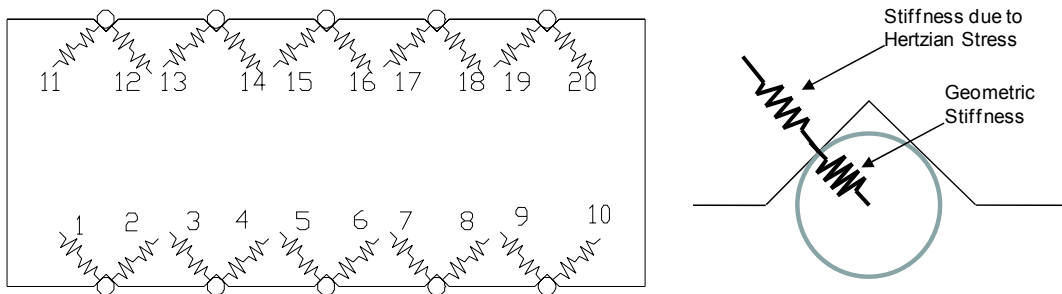


Figure 3.10: Schematic illustration of the polymer chip with 5 V-grooves on either side. The dowel pins are shown as circles making contact on the V-grooves. The first spring represents the geometric stiffness and the second one represents stiffness due to hertzian contact.

This model can be used to predict the overall alignment accuracy for given perturbations at the local contact sites. Random perturbations between $\pm 50 \mu\text{m}$ were applied at the local contact sites. The simulation was repeated 20 times with different sets of random numbers as perturbations. The resultant overall alignment accuracy was plotted for each of the simulation runs (Figure 3.11). Details of the stiffness calculations are summarized in Appendix A.

In order to experimentally verify alignment accuracy, markers were molded onto the chips and then their positions were measured after assembly. In order to simultaneously image alignment marks from both chips, two separate images were taken while keeping the setup stationary and only changing the focal plane of the microscope. The images were then overlaid using image processing software (Figure 3.12).

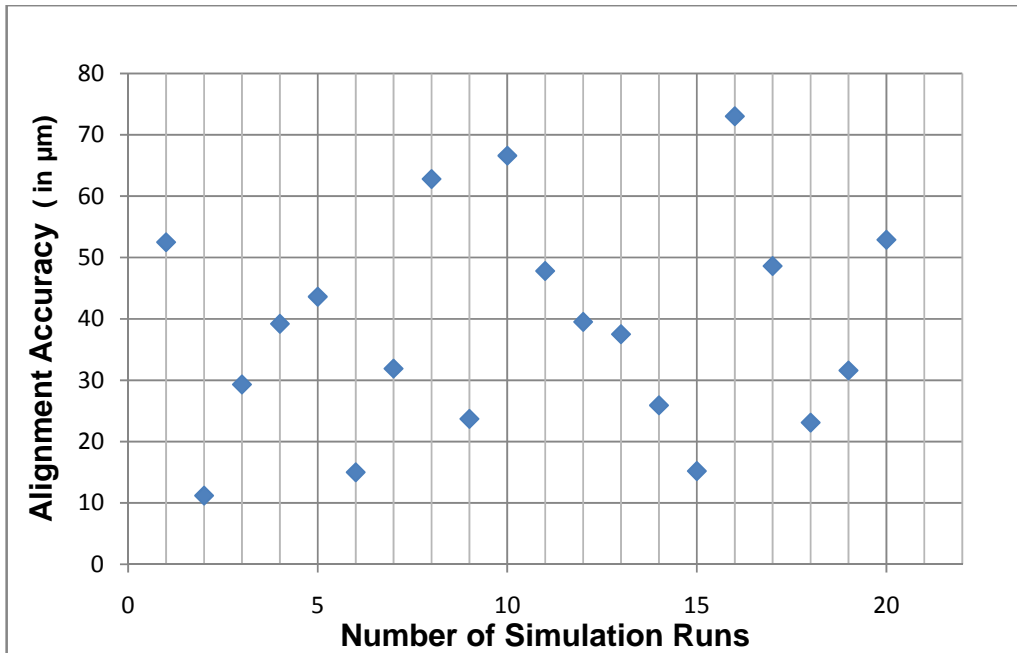


Figure 3.11: Simulation results for passive alignment of microfluidic chips. Random perturbations (within $\pm 50 \mu\text{m}$) at all the local contact sites were introduced and the overall alignment accuracy was plotted.

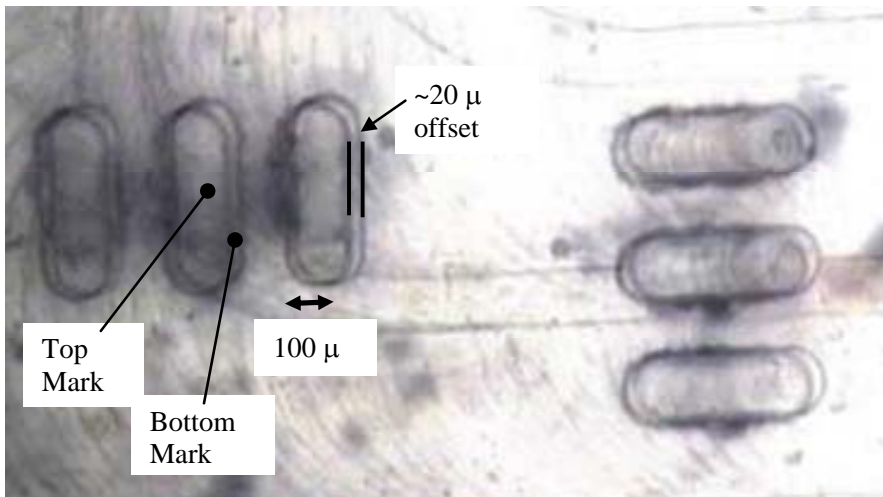


Figure 3.12: Image of overlaid alignment marks on 2 different layers of modular chip stack. It is observed that the alignment is better than 10 microns in the direction of the force, while in the lesser constrained direction, the alignment is not as accurate ($\sim 20 \mu\text{m}$).

To allow visual inspection through more than two chips, an alternative marker design using square windows was tested successfully. The squares are designed

such that the dimensions are smaller by 100 microns for each progressive layer of the microfluidic stack (Figure 3.13a). In order to accurately measure the chip alignment, the differential edge to edge measurement is used and the displacement of the center of one chip relative to the other can be calculated (Details discussed in Appendix B). If an approximate verification is desired, the user can also visually inspect to check if the squares lie within each other. If they do, the alignment accuracy is certainly better than 100 microns (Figure 3.13b).

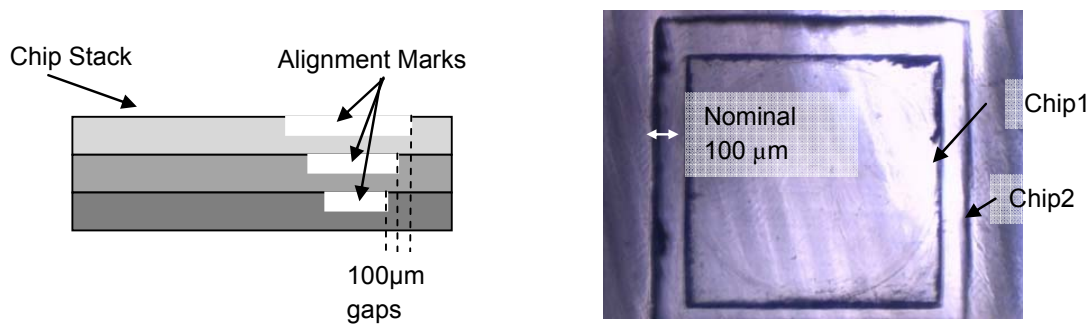


Figure 3.13a: Schematic illustrating the arrangement of alignment windows for easy verification

Figure 3.13b: Image of the alignment verification for 2 chips. Concentricity of squares is indication of good alignment.

Experimental verification of passive alignment using elastic averaging was performed with 3 different pairs of chips. The chip pairs were reassembled before each measurement and the alignment accuracy was measured as a function of alignment attempts as illustrated in Figure 3.14. Alignment accuracy was found to be consistently better than 100 microns and in best case scenarios was as good as 20 microns. Another set of experiments were conducted using different numbers of aligning pins to evaluate the accuracy as a function of the number of contact points. The results shown in Figure 3.15 illustrate the linear relationship between alignment accuracy and the square root of the number of contact points used for the alignment.

Based on this data, it can be concluded that microfluidic interconnection vias from one chip to the next will always align for fluid flow to occur so long as the diameters of the vias are 100 µm or larger.

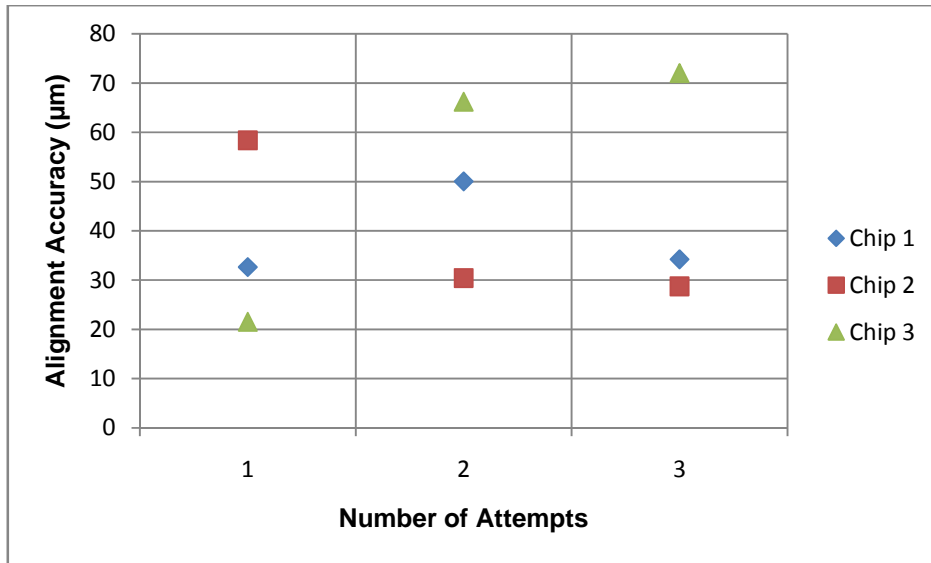


Figure 3.14: Resultant graph of the measured alignment accuracy for multiple passive assembly attempts, illustrating repeatable accuracy of better than 100 μm

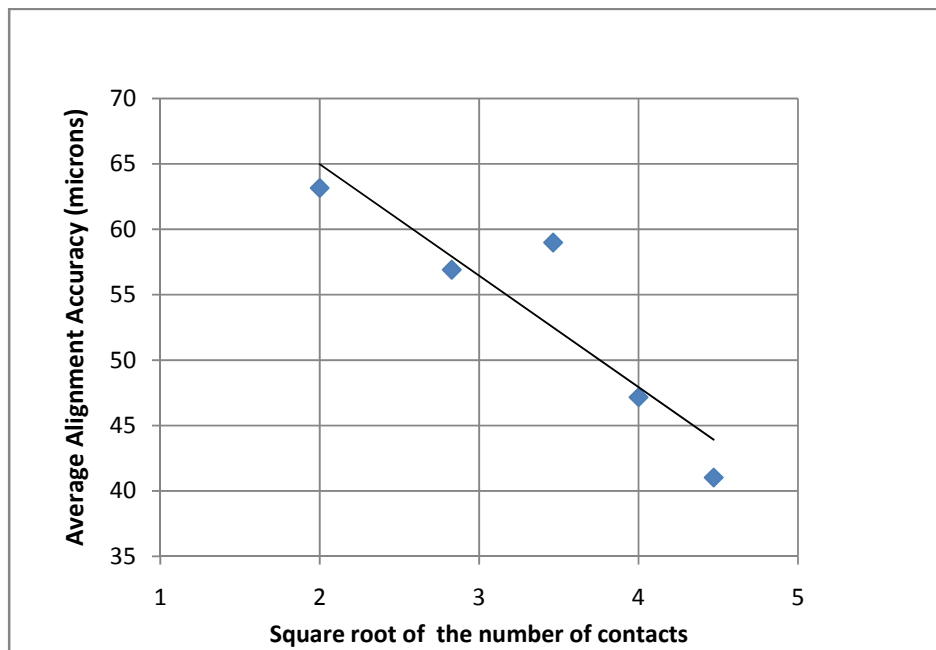


Figure 3.15: Measured effect of the number of aligning contact points (alignment pins) on alignment accuracy

3.2.2. Sealing

Sealing technology is a critical part of the system development and an in depth study of the various sealing technologies available was carried out. It was also realized that a single solution for all sealing requirements is not possible but that different sealing technologies need to be established to meet the varying demands. The birth of microfluidics was with structures fabricated from glass and silicon material and sealing was never a problematic issue because anodic bonding technology [75] and silicon fusion bonding were very well established methods of bonding these materials without deforming or destroying the microstructures. However, with polymers a variety of bonding technologies exist which have their distinct advantages and disadvantages, including surface modification using UV light [76], solvents [23], laser [77], ultrasonic energy [78], thermal compression, lamination [79] and adhesive/tape [80] technology.

Material considerations play a prime role in microfluidics for biological applications. Biological interactions with material drive the choice of polymer being used and indirectly influence the bonding technology too. It is desirable to limit the number of materials that come in contact with the fluid. Adhesive technology and solvent assisted bonding are both excellent bonding methods because they can be used with almost any kind of polymer. They form a gel-like layer at the bonding interface to create a bond. However, both these methods introduce a third material (solvent, adhesive) which may impact the interactions with the biology. If a liquid adhesive is being used, ensuring that the channel geometry does not get blocked by adhesive flowing into it is another challenging problem.

Laser bonding is a very attractive technology for polymer bonding and a line of commercial polymer laser bonding machines for microfluidic and other applications called Novolas™ are available from Leister® [81]. The technology relies on laser energy being absorbed by an opaque polymer and raising the temperature in a localized zone at the interface sufficiently to melt and fuse the two polymer materials. This necessitates that the top polymer layer be transparent so that the laser light can pass through it unimpeded. The bottom layer (or the surface of this

layer) has to be opaque or otherwise capable of absorbing the laser light at the interface. Typically, most transparent polymers do not absorb the wavelength of laser light (940nm) used for sealing applications. In order to seal two clear polymer materials, a light absorptive dye material has to be applied to the interface. This material called Clearweld™ (<http://www.clearweld.com/>) is available commercially and research is underway to incorporate it into polymers during the molding process.

Ultraviolet surface modification effectively lowers the glass transition point of a polymer at the surface so thermal compression bonding can be applied at much lower temperatures and pressures to effectively seal a microfluidic chip with minimal deformation of the structures [82].

For the flexible operation of the microfluidic stack the modules could be permanently or temporarily sealed using gaskets between the modules (Figure 3.16). In order to enable temporary gasket sealing, a customized gasket fabrication method was used. A direct thermal sealing process was chosen as an optimal solution for permanent sealing.

In both sealing methodologies, for a good seal, a controlled and uniform pressure has to be applied over the whole contact area. Irrespective of the method of sealing being used, the fundamental mechanism is that a soft layer at the interface of the two chips being bonded deforms to form the seal. In case of temporary sealing, the soft layer is a rubber gasket and in case of permanent bonding it is a layer of melted plastic. From the mechanical aspect the problem is that of application of uniform pressure over a fairly large area. The process methodology and parameters that were used for elastomeric gasket formation and direct thermal sealing are discussed in detail.

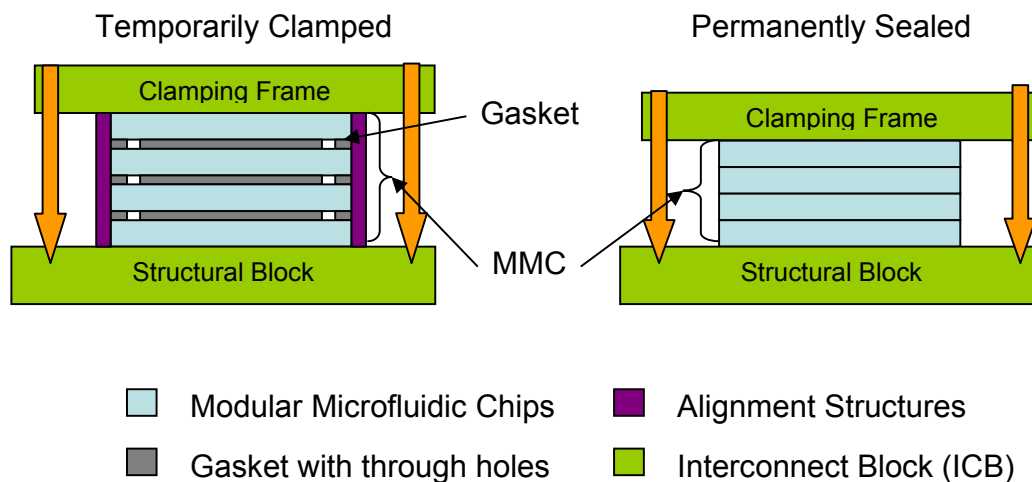


Figure 3.16: Schematic illustrating stack operation in temporarily clamped and permanently sealed mode.

Temporary Sealing

When building the microfluidic stack in temporarily clamped mode, the chips of the MMC exist as individual pieces that are assembled together into a stack and clamped down on the ICB. During the clamping process, the ICB ensures that the chips are automatically aligned to each other and temporary sealing is achieved by using gaskets between the different chips and applying sufficient clamping force (Figure. 3.16). The clamping force is applied by bolts which connect the clamping frame and the structural block (part of the ICB, see Figure 3.5).

The ability to temporarily assemble and seal microfluidic chips is a very attractive feature for biological applications because it provides an open faced chip that can be surface prepared like a standard microscope slide, for example, subjected to dip chemistry or microspotting prior to loading into the microfluidic stack. It also allows simple post processing of reaction products or in-depth analysis using a microscope or other analytical instruments. It provides the highest degree of flexibility; a user can pick different functional chips from a kit, assemble them together and have a complete working system ready on hand.

Different elastomeric materials were explored for forming the gasket using a casting process. A negative mold was formed first in plastic by micromilling; the

casting compound was then poured into this form and pressed with a glass plate (Figure 3.17). After curing the material for the required amount of time, the glass was removed and the formed flexible gasket was peeled manually off the form. The technique is commonly used for producing microstructures in PDMS, where the negative mold is typically formed by SU-8 lithography [25].

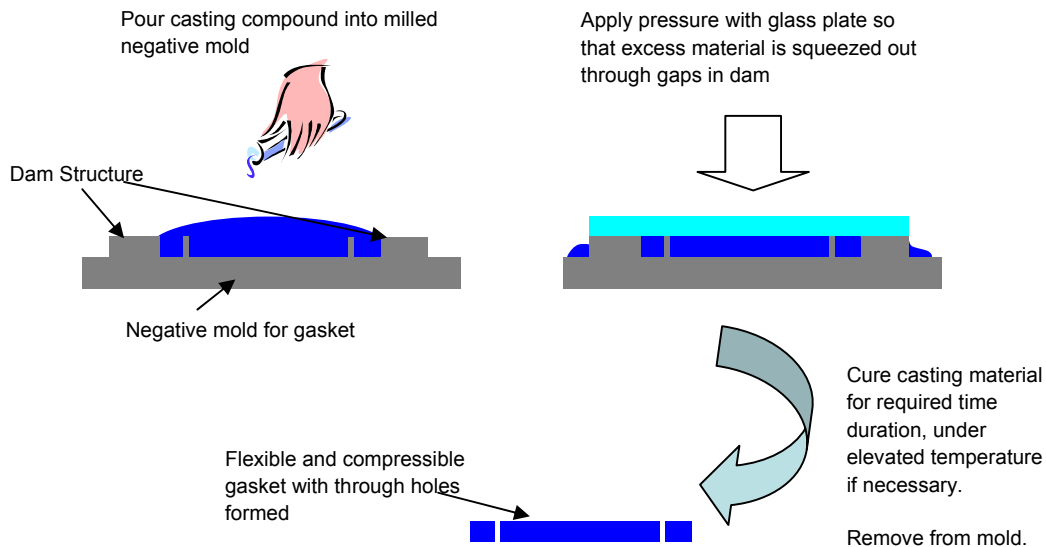


Figure 3.17: Schematic of gasket creation process.

The temporary sealing is dependent on the clamping force exerted by the bolts that are tightened manually. Due to the uncontrolled nature of the clamping force the repeatability of the assembled stack is not as good as that of a permanently sealed MMC. Thus, there is a limitation on the minimum feature and channel geometry that is allowable on the chips as the soft gasket material will deform and occlude small channels.

Gasket Compression Modeling

A better understanding of the gasket compression was necessary to ensure proper temporary sealing without excessive deformation of the gasket into channels and also to estimate the bulging behavior of the soft gasket material to occlude through holes (vias) for interconnection formed in it. Finite element modeling was

done to better understand the behavior of the gasket under compressive forces. The compressive modulus of the materials used to form gaskets was not readily available, hence the information was evaluated experimentally (Details in Appendix C). Since the region of interest in the gaskets was the interconnection vias, a cross sectional 2-D model was used for the simulations. The boundary conditions imposed on the model are shown schematically in Figure 3.18a.

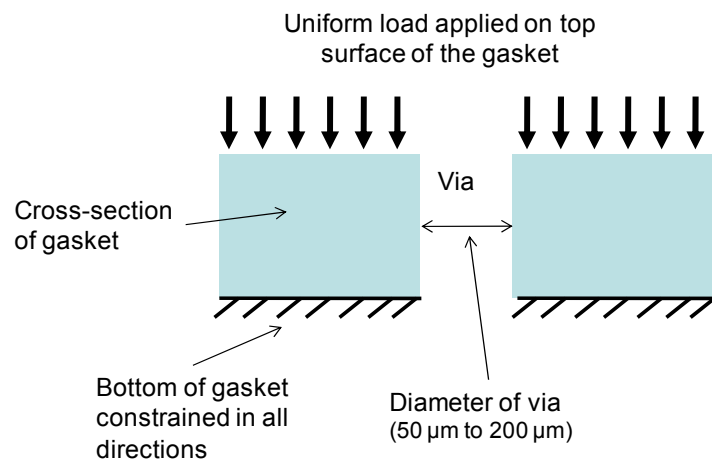


Figure 3.18a: Schematic illustration of the boundary conditions.

Figure 3.18b below shows the results from one of the 2-D simulation runs indicating the amount of closure of the through holes. Based on the simulation, it was seen that the closure of through holes in a compressible silicone elastomeric gasket is proportional to the amount of compression but independent of the thickness of the gasket (Figure 3.19).

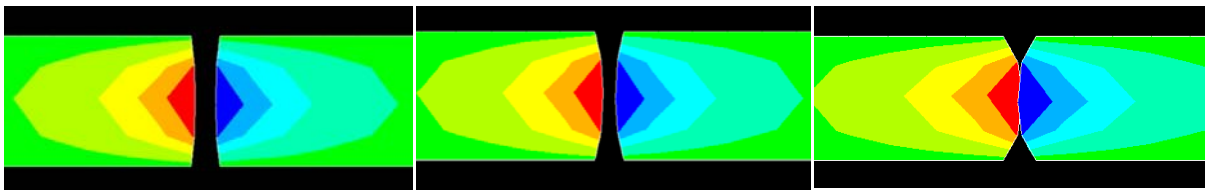


Figure 3.18b: Occlusion of gasket through holes with compression of gasket. A 100 μm dia hole in a 500 μm thick gasket as it is compressed 50, 100 and 200 μm (left to right).

It was seen that for holes 50 μm and larger, the extent of compression was equal to the diameter of the holes being occluded. Hence it can be concluded that for a gasket made from cast silicone material, if the diameter of a via is larger than the thickness of the gasket, the via will never be blocked due to deformation of the

material as the gasket is compressed. As a design rule, vias should not be made any smaller than the expected compression of a gasket necessary for good sealing.

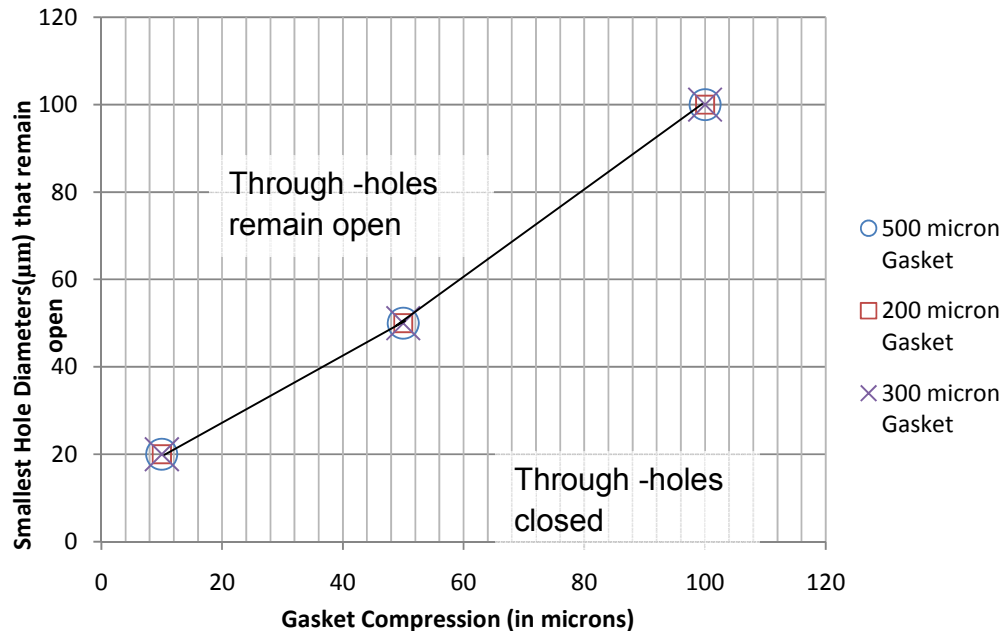


Figure 3.19: Graph indicating closure of gasket holes as a function of compression of a Silicone gasket for 3 different gasket thicknesses. This result was obtained from 2-D finite element simulations.

In spite of the limited applicability, ‘temporarily clamped’ mode of operation has significant advantages that make it ideal when size limitation and precise geometric control are not demanding. Soft gaskets for sealing were used successfully with channels down to 500 µm x 500 µm in cross section.

For microfluidic chips with smaller channels, a permanent sealing approach has to be adopted. In ‘permanently sealed’ mode, the chips of the MMC are irreversibly sealed together to form the MMC. Since the sealing process is well controlled, these chips can have much smaller features (channels as small as 50 µm x 50 µm were sealed and tested).

Permanent Thermal Sealing

Permanent sealing can be achieved using a number of methods. After a thorough literature review, solvent assisted bonding and direct thermal sealing were tested as the optimal methods for sealing the MMC.

During solvent assisted bonding, a thin layer of polymer surface is softened, that effectively acts as glue. After solvent treatment, the parts may be subjected to low temperature thermal compression sealing or only compression under ambient temperature conditions. Solvent assisted sealing can produce very good results with minimal deformation of channel geometry. Some efforts were made to carry out PMMA-PMMA sealing using iso-propyl alcohol (IPA) as a solvent. The mating faces of the parts to be sealed were sprayed with IPA, sandwiched and were passed through the heated rollers of a lamination machine (Model HRL 4200, Dry-Film Laminator by Think & Tinker, Ltd¹²). This resulted in good sealing in most regions of the chip. The channel dimensions of the chip were 200 x 500 μm and the laminator was set to a temperature of 80 $^{\circ}\text{C}$. The chip was sealed and then cross-sectioned to measure deformation. The images in Figure 3.20 show the part before and after sealing at the same magnification. As can be seen, the deformation is virtually negligible.

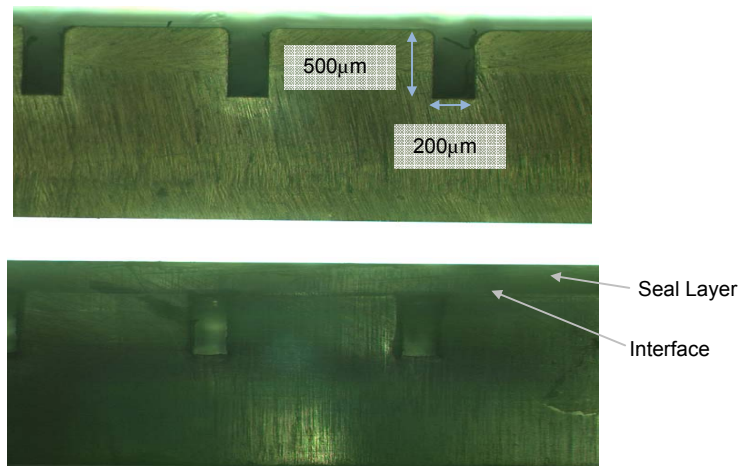


Figure 3.20: Cross sectional image microfluidic channels before (Top) and after (Bottom) sealing. As can be seen, the deformation of the channel geometry is negligible.

However sealing using this method proved somewhat inconsistent as can be seen in Figure 3.21. The IPA solvent distributed and wetted the surface in an uncontrolled fashion, thus producing irregular sealing. It can be seen in Figure 3.21 that the dye flowed through the channel may leak at points where the sealing

¹² <http://www.thinktink.com/>

irregularities intersect with channel geometry. Rapid and uncontrolled evaporation of the solvent (IPA) is believed to be the cause of this inconsistent sealing and as there is no method available to regulate the phenomenon, a non-solvent based direct thermal sealing was adopted as the most suitable and controllable method for permanent sealing.

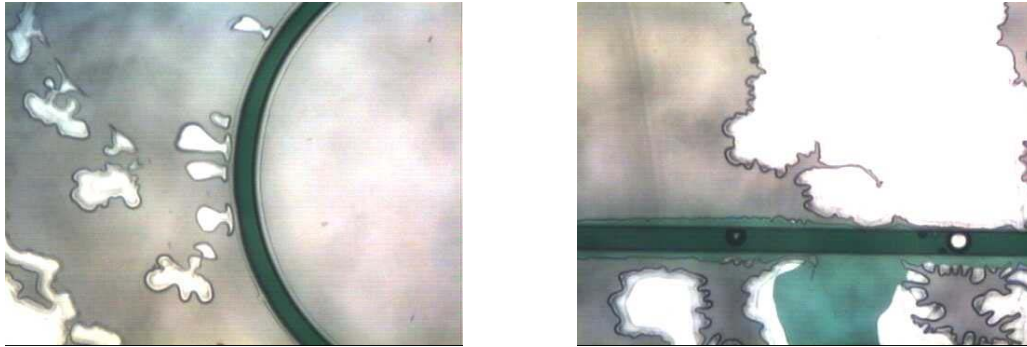


Figure 3.21: Irregularities in sealing observed during solvent assisted polymer sealing.

Sealing via direct thermal bonding can be carried out in any heated press and the Jenoptik HEX02 hot embossing machine can be used for the purpose. However, the technical drawback of using a press with fixed plates is illustrated in Figure 3.22a. There will always be an angle between the plates and the parts being sealed. If this angle exceeds the depth of the channels being sealed, it will either lead to improper sealing on one side of the chip or will lead to total blockage of the channel at the other end.

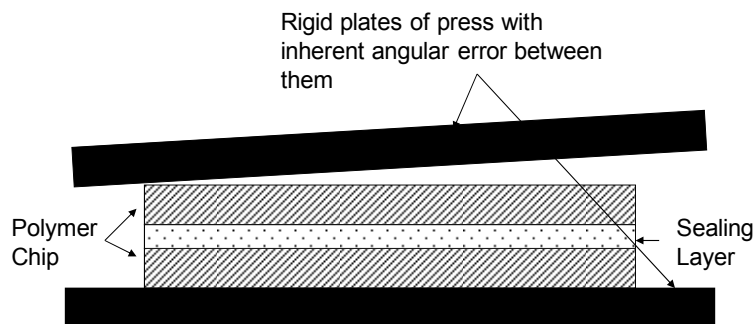


Figure 3.22a: Schematic illustrating problems of angular error associated with using a press with fixed pressure plates.

In order to overcome this problem, a spring-loaded fixture (Figure 3.22b) was used where the plates would conform to the chip surface and the springs would apply the sealing force. The force being applied was gauged from the deflection of the springs. This was a very attractive solution as the fixture was small and simple and could be placed directly in an oven to carry out sealing under well controlled temperature conditions. In order to better understand the mechanics of this simple fixture a finite element analysis (FEA) was carried out to evaluate the approximate deformation of the copper plates. The results from the FEA (Figure 3.23) show that the copper plate deflects up to 45 microns around the edges of the 1" x 3" chip that is being sealed under the 3.8 kgf bonding force being applied by each of the 6 springs. This was experimentally verified as non-uniform sealing in different areas of the chip was observed. Inconsistencies in the sealing result were also seen from run to run. A combination of deformation of the sealing plates and variations of the spring force were surmised to be the probable causes.

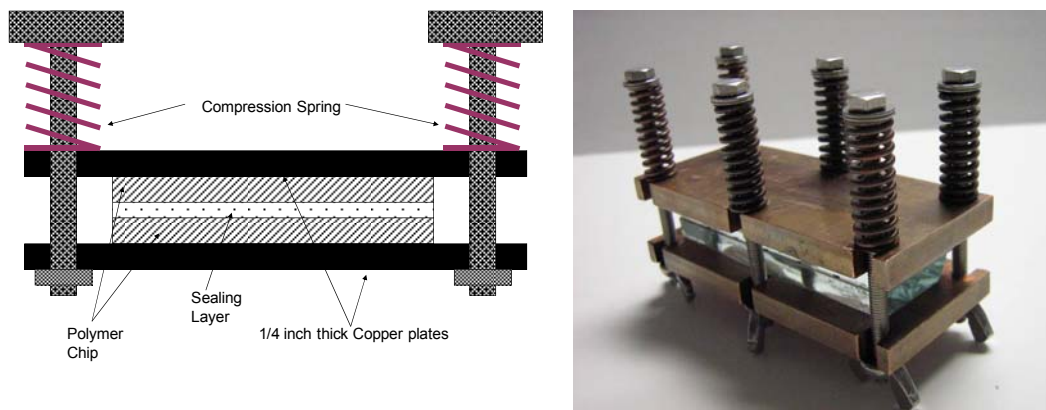


Figure 3.22b: Schematic illustrating a spring loading fixture used to compress and seal polymer microfluidic chips (left) and the actual fixture (right).

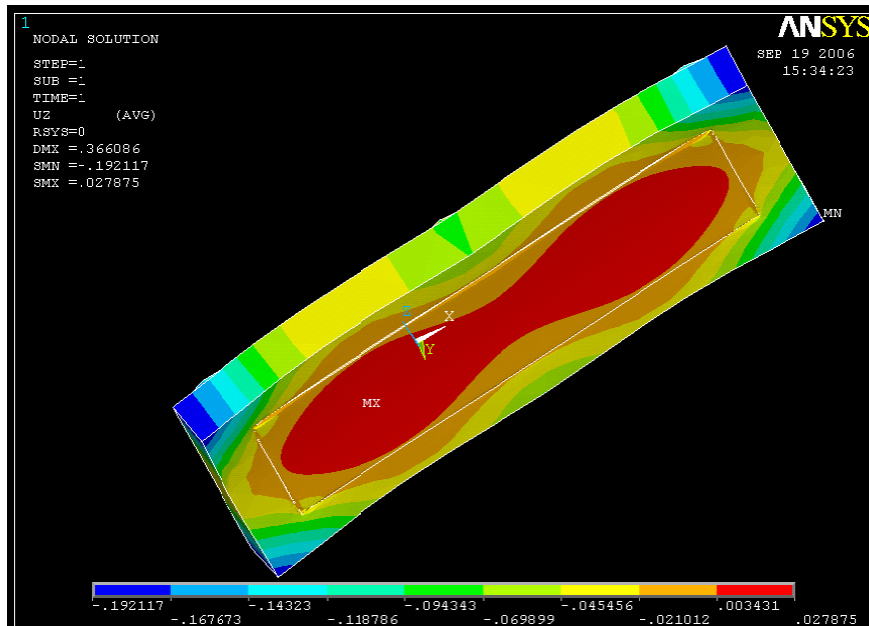


Figure 3.23: Image from FEA simulation of a flat copper plate used for sealing the microfluidic chips. Scale on the bottom represents the deflection in microns. As can be seen, within the central rectangle (which denotes the chip) there is a significant variation in deflection (Red region deforms 27 microns in one direction while the yellow region deforms up to 45 microns in the other direction).

The springs used for applying the clamping force were demonstrating plastic deformation over time which made them poor gauges of the force being applied. This unequal deformation automatically resulted in a non-uniform pressure distribution which resulted in poorly sealed chips. An effort was also made to correlate the applied force with the torque set on the bolts by using a calibrated torque wrench; however, that proved to be an inaccurate method as too many uncontrollable variables affect the relationship between the torque applied and the resultant preload (Appendix D). While the deflection of the clamping plates could be reduced by using a thicker and stiffer material, a qualitative method was necessary to quantify the pressure being applied in the sealing process.

In order to overcome these issues, a press was designed to replace the multiple springs with single point force application mechanism which tilts to adapt for non planar surfaces. The force is applied through a load cell in order to directly measure the force and pressure applied to the chip surface.

The mechanism of the press is shown in Figure 3.24. A ball joint is used to apply pressure on a rigid steel plate which allows the plate to tilt and align with the chip stack. The sealing equipment consists of a base and a movable cross-bar to adjust for different height ranges. The cross-bar is guided by two threaded guide columns and the height is fixed using nuts on the threaded columns. A pressure application head is attached to the cross-bar and is used to apply the compressive force to the polymer stack through the pressure plate. The motion of the pressure application head is kept vertical by 4 guide rods. The design of the pressure application head is shown as a schematic in Figure 3.24 (left). A load cell is integrated into the head to directly measure the force being applied to the stack. During the sealing process, the polymer will undergo some amount of deformation, as a result of which the sealing force would reduce significantly if it were not actively controlled. In order to avoid that, the force is applied through a high stiffness spring which will compensate the force for any reduction in thickness of the parts being sealed. At the tip of the pressure application head is a swivel head screw that allows the pressure plate to rotate and align to the surface to the parts being sealed. Thus any errors in parallelism of the parts are compensated by the swiveling motion of the pressure plate. The application of sealing pressure is controlled by the push screw that transmits the force through the spring, the load cell and the swivel head screw to the pressure plate.

The base plate has a central cavity to accommodate an insert plate which can either be a thick glass plate for infrared heating or may be replaced with a metal slab with integrated heater. The press was used successfully to seal the microfluidic chips and quantify the parameters needed for successful sealing. It was found that direct thermal bonding of PMMA sheets could be achieved at temperatures of 105 °C and 0.5 MPa without significant deformation of the channel geometry (Figure 3.25). Channels with cross sections down to 50 μm x 50 μm were sealed successfully.

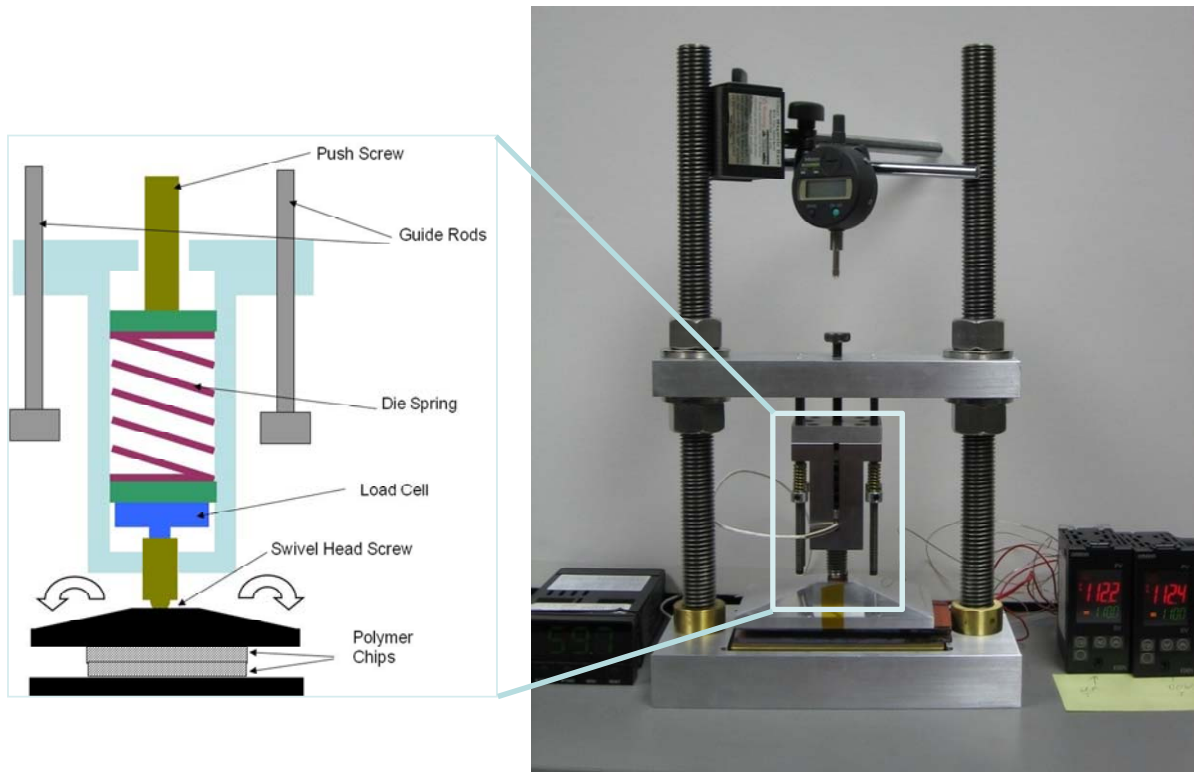


Figure 3.24: Image and internal schematic of press that was designed and built to improve and quantify the sealing process.

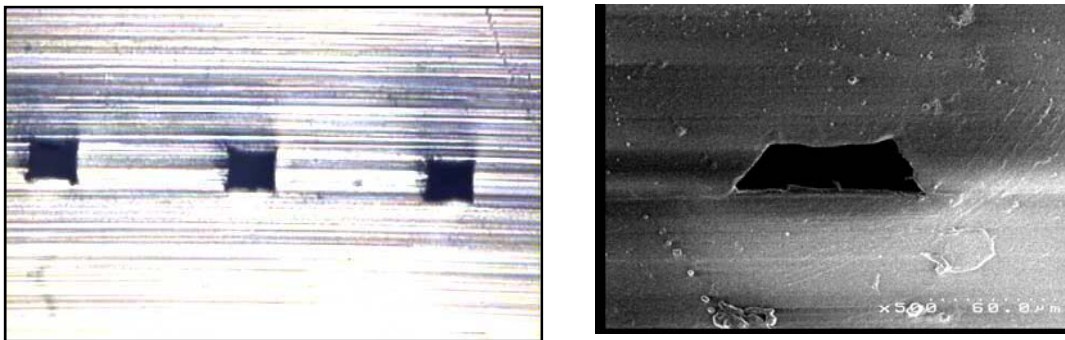


Figure 3.25: Cross section of thermally sealed microfluidic channels. All channels exhibit a good seal. $100\ \mu\text{m} \times 100\ \mu\text{m}$ channels (left) show minimal deformation, while $50\ \mu\text{m} \times 50\ \mu\text{m}$ channels (right) show some deformation.

3.3. Process Model for Project Management

The fluidic stack is a 'system solution' utilizing a variety of processes, materials, design rules and assembly and integration concepts. For any complex multi-

dimensional approach similar to this, it is of utmost importance to define boundary conditions which ensure good fabrication protocol and yet allow for flexible optimum designs. To achieve this, it is necessary to have a project plan in place reflecting the overall goal and also the path to get there.

Typically in an academic research environment, the process of deciding on and managing a project is done informally. The work done as part of this thesis involved significant multidisciplinary, applied research carried out in co-operation with internal and external partners/collaborators and quite often driven directly by a customer demand. The act of balancing a research effort with customer expectations of deliverables within time and cost constraints is a challenging task. It was felt that even in a research environment a well defined decision and process management flow was necessary [43] to maintain clarity and efficient communication. In order to achieve this, the process flow illustrated in Figure 3.23 was put in place.

First, the decision to pursue a research idea should be based on sound reasoning and thorough background research. Then the path taken to converting an idea into a working prototype or proof of concept device should be well thought out, keeping in mind the complexity of the project and the available resources and knowledge base. Defining tangible goals and interim milestones is also very important for effective project management.

This protocol was derived by using a combination of two well known process models followed in the software industry for project management– the Waterfall Model introduced by Dr. Winston W. Royce in 1970 and the Spiral Model introduced by Barry Boehm in 1988. The traditional Waterfall Model and Spiral Model are illustrated in Figure 3.26. The waterfall model is very rigid in structure and does not lend itself to adaptively making adjustments in the light of new information which is a common occurrence in research. The spiral model is more adaptive and suitable for projects that have a strong element of research induced uncertainty. However having the ability to easily redefine designs and requirements can often lead a project astray from its course. Combining these two models gives us the right element of rigidity and flexibility [44].

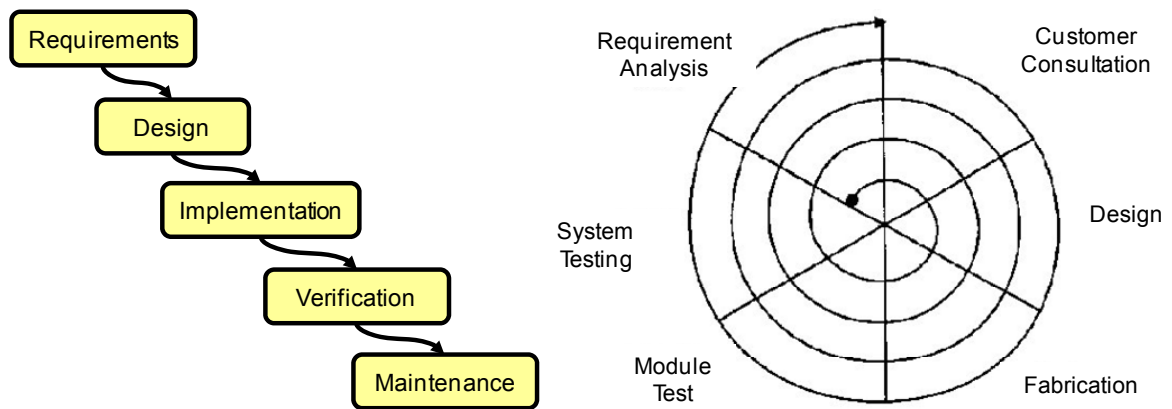


Figure 3.26: The waterfall process model (Left) and spiral process model (Right).

Development of the microfluidic stack followed the steps illustrated in the flowcharts in Figures 3.27. The flowcharts cover the process beginning with the decision on whether or not to pursue a project down to the actual execution and evaluation. It should be noted that information from every executed project contributes to ‘knowledge base’ which is an important goal for any research and development effort.

Decision points encountered at various points in the process flowchart serve as milestones and encourage communication, so serious problems are revealed early on in the project. The process flow for a project from initiation through execution and completion, when executed following clearly laid out steps, resulted in effective management and communication with team members and customers throughout its duration.

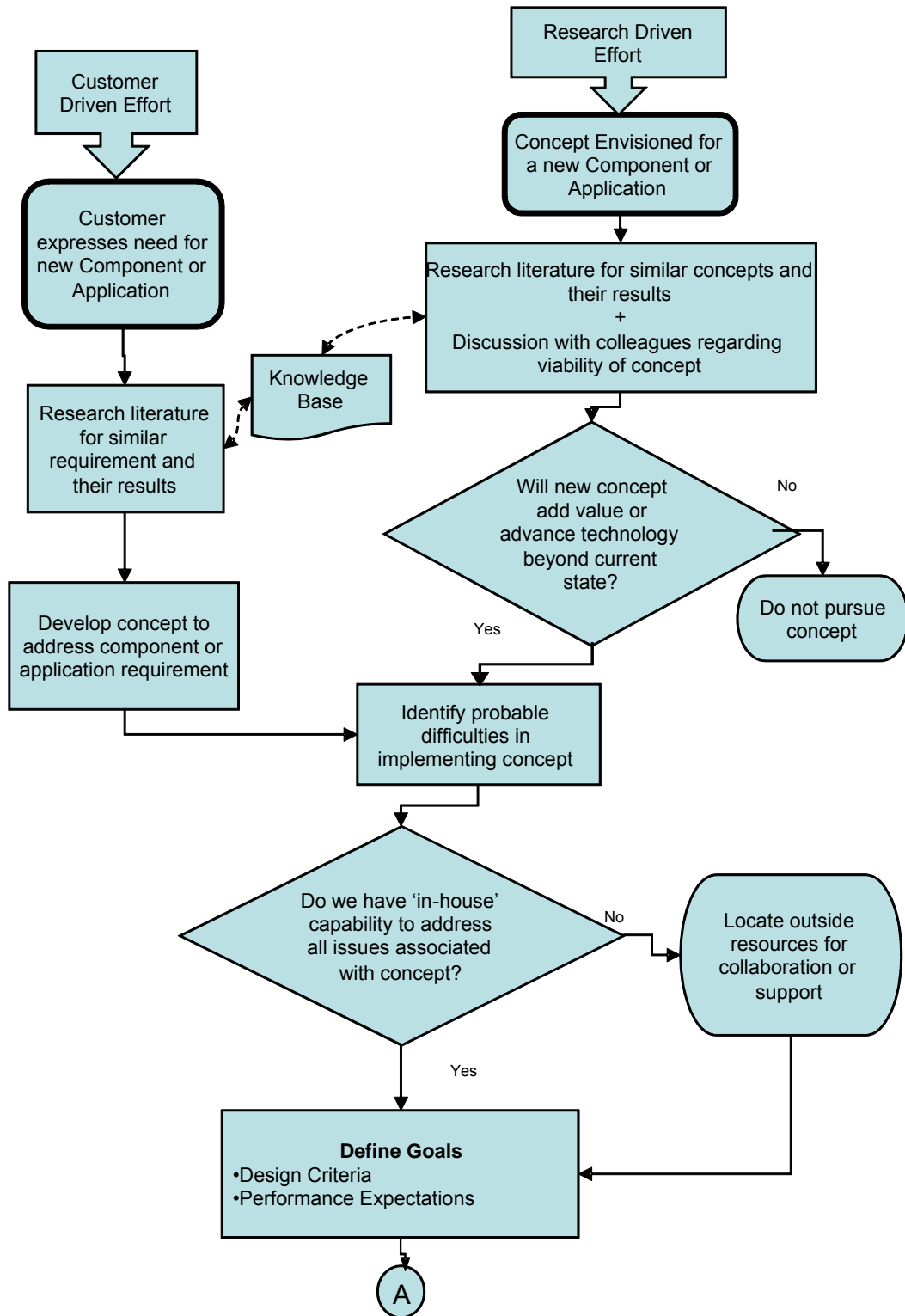


Figure 3.27a: Flowchart for project acceptance and execution process.

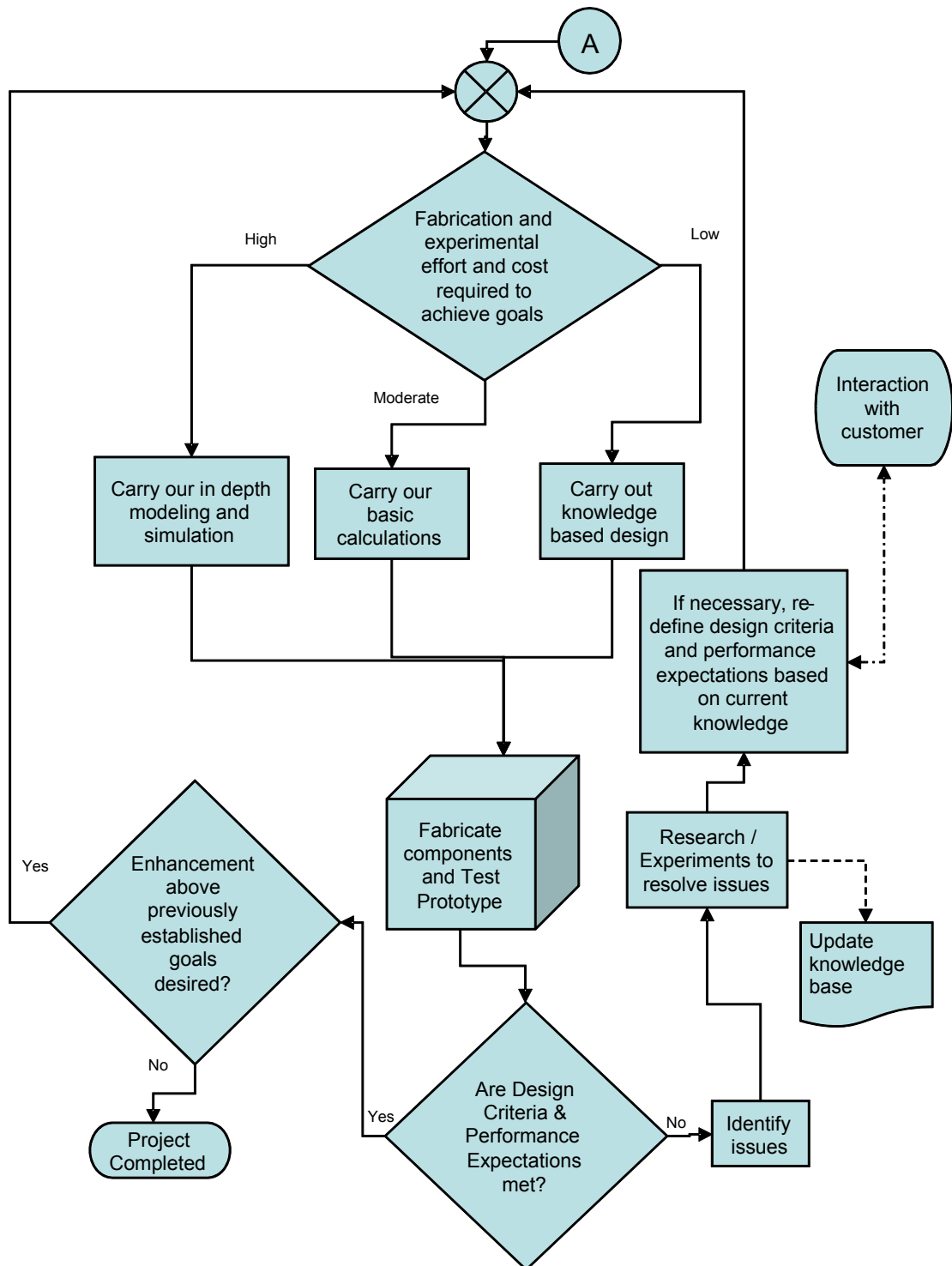


Figure 3.27b: Flowchart for project acceptance and execution process (contd.).

4. Polymer Micromolding

Plastics and polymers are found in diverse aspects of our lives ranging from food packaging to airplane components to artificial organs [45]. We also see polymers replacing silicon and glass in the world of MEMS fabrication [22, 23]. Polymers are becoming the material of choice for microfabrication applications because they hold the promise of low-cost, commercially mass produced parts combined with dedicated material properties. Of particular interest are biomedical and microfluidic application where disposable chips for one time use are important and rely on low cost, high volume production in suitable polymer materials [46].

Polymers can be broadly classified into categories of thermoplastic or thermosetting. Thermosetting polymers are usually formed by reaction molding, i.e. the polymerization reaction is carried out inside a cavity that has the shape of the desired polymer part. Thermoset plastics have very specific applications, examples of which include vulcanized rubber used in automobile tires and bakelite which is fire resistant and is used for electrical insulation.

The scope of this work is limited to thermoplastic polymers which are the more commonly used category of polymers for replication applications. At low temperatures, the material behaves like an elastic solid. As the temperature is raised beyond the glass transition temperature (T_g), they rapidly lose elasticity passing through various phases of softening (Figure 4.1). Converting bulk thermoplastic polymers into a desired shape or form is typically done by a molding process, during which the material is subjected to elevated temperatures and pressures to change its shape. Upon cooling the polymer hardens and regains its original strength but now formed into the desired shape of the molding tool. A variety of molding methods exist for forming polymers and some of the popular ones are injection molding, extrusion, blow molding and hot embossing [47]. Thermoplastic polymers may be amorphous or crystalline in nature and most polymers contain a mixture of crystalline and amorphous components. The dominant characteristic (crystalline or amorphous) determines the behavior of the polymer [48]. The change a polymer undergoes in response to elevated temperatures, illustrated in Figure 4.1, shows

that crystalline polymers do not go through the gradual softening like amorphous polymers, but show a much sharper transition from solid to liquid. This makes crystalline polymers more challenging for molding processes such as hot embossing which rely on controlled flow to achieve complete mold filling.

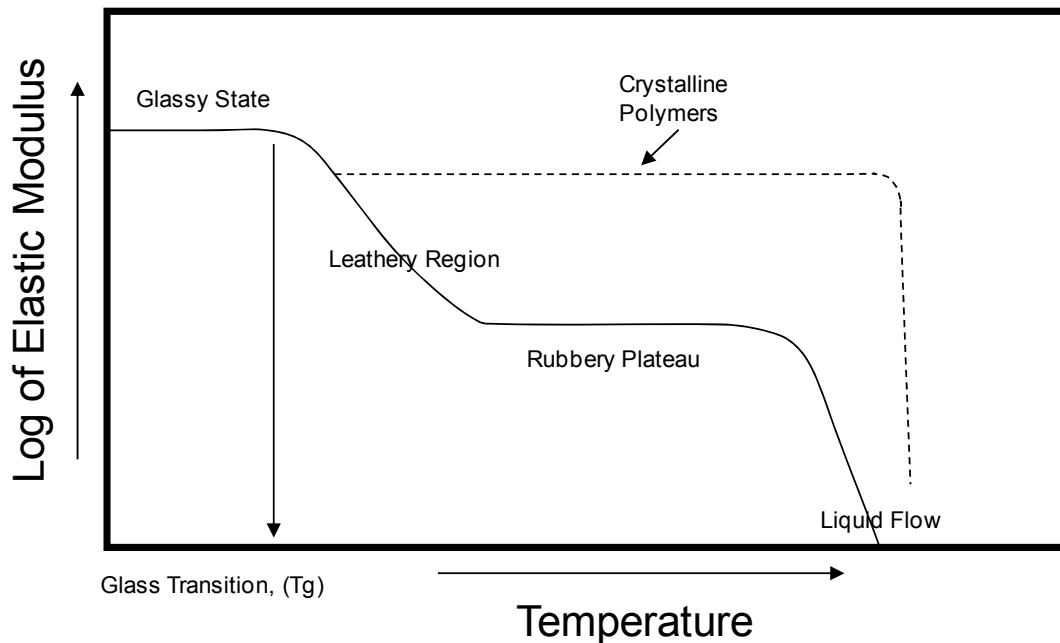


Figure 4.1: Graph illustrating reduction of elastic modulus of polymers with increasing temperature [48, 49].

The primary criteria for selecting a polymer for Bio-MEMS application is the biocompatibility of the polymer. Other considerations include optical clarity and thermal properties. Polymethylmethacrylate (PMMA), Polycarbonate (PC), Polypropylene (PP), Polystyrene (PS) and Cyclo-Olefin Copolymers (COC) are some of the commonly used polymers in Bio-MEMS fabrication.

PMMA and COC have excellent optical transmission and hence are preferred in applications requiring fluorescence or optical imaging. PC is thermally stable up to 120°C and is used extensively for high temperature applications like Polymerase Chain Reaction (PCR) [50], where the temperature has to be raised to 96°C. Most macro scale polymer labware like 96-well plates and cell culture dishes are made from polystyrene and hence it is a familiar material for biologists.

4.1. Hot Embossing

As mentioned earlier, a variety of technologies exist for thermally forming thermoplastic polymers into a desired shape. Of these, injection molding [51, 52] and hot embossing [21-23, 53] are two technologies that are most relevant to microfabrication. Hot embossing produces high accuracy, low stress parts and the mold design and process development are simpler and faster compared to injection molding. These characteristics make hot embossing the ideal choice for rapid prototyping and for applications where small batches of parts are desired. As rapid prototyping with a short turnaround time was one of the design criteria for the microfluidic system development platform, polymer molding by hot embossing was the primary method used for fabricating the microfluidic chips.

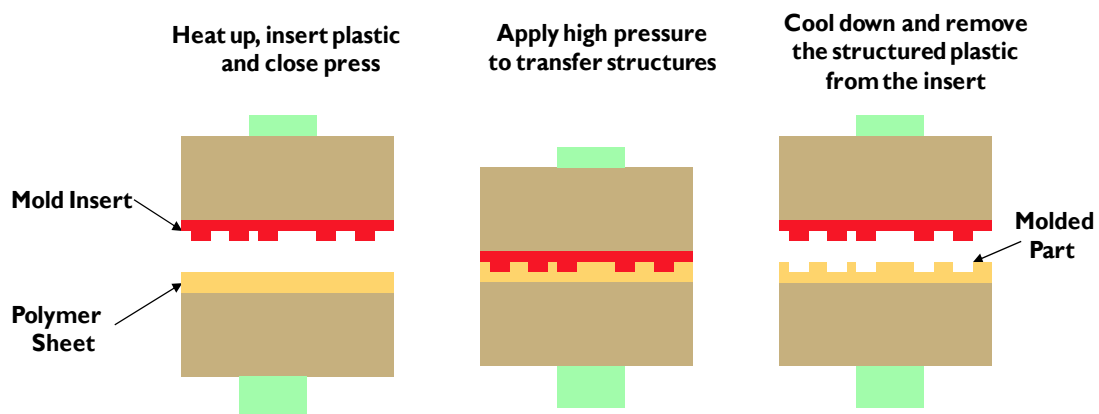


Figure 4.2: Schematic of hot embossing process.

The hot embossing process consists of using a temperature controlled press to transfer a pattern from a metal template (mold) to a polymer sheet (Figure 4.2). During the course of this work, all hot embossing activities were carried out on a Jenoptik Mikrotechnik [54] HEX02 machine (Figure 4.3). It is designed specifically for molding high aspect ratio micro and nano structures in polymers. The machine is capable of precisely controlling the pressing motion (1 μm resolution), temperature uniformity ($\pm 2^\circ\text{C}$ over a 100 mm dia. molding area), and is equipped with advanced demolding capabilities. Micro-molding is done under vacuum to keep air from being trapped in the microstructures which would result in poor mold filling and voids in the molded part. The machine allows continuous control and measurement of all the

above parameters during the molding process, thus resulting in a high degree of repeatability between process runs. Details of the mold fabrication process and the equipment are discussed in Sections 5.1.

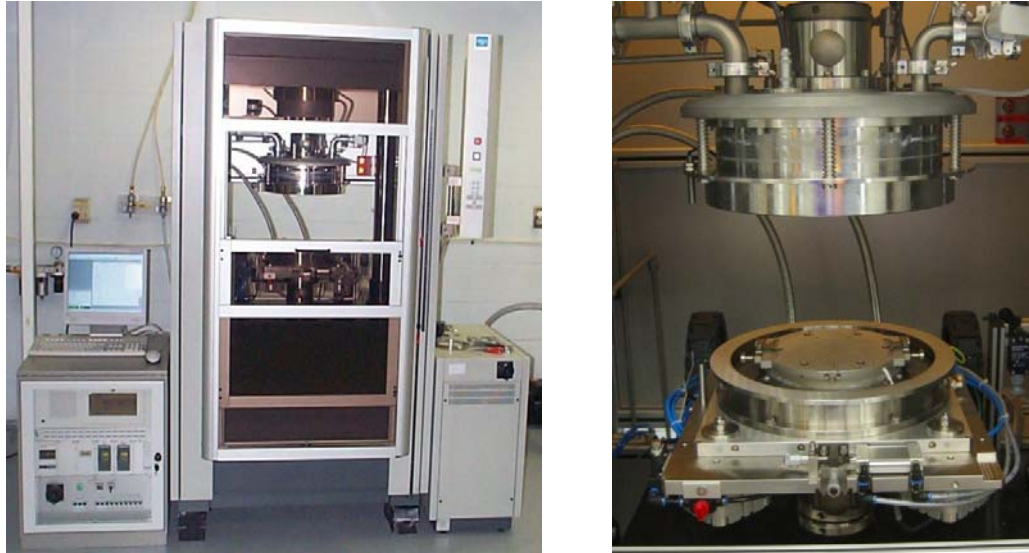


Figure 4.3: The Jenoptik[®] HEX02 hot embossing machine used to mold microstructured parts from polymer sheets.

4.2. Challenges in Polymer Micro-molding

The technology associated with molding large components is fairly well known. Typically, an isothermal molding process can be used for molding macro structures or low aspect ratio microstructures such as compact disks in which a polymer melt is pressed against a mold insert that is kept at a fixed temperature below the T_g of the polymer [20]. However, for micro structures, the large surface to mass ratio requires a variotherm process where the mold insert temperature is raised above T_g to ensure sufficient flow and proper insert filling [55]. Consequently the temperature of the mold insert undergoes thermal cycling, increasing the overall processing time significantly (typically 10-15 minutes). During molding and demolding microstructures, the process parameters have to be controlled very actively to ensure the best results.

Though the process parameters are dependent on the material being molded, precise characterization of material properties for molding purposes is not a practical

approach as batch to batch variations and environmental factors like moisture uptake alter the properties of the material. Other factors which add to inconsistencies in molding parameters are the combined effect of machine, fixture and mold insert setup. When embossing microstructures using the HEX02 molding machine there are interactions across many orders of magnitude. A heated press capable of generating 300kN of force is fitted with a mold insert that weighs 1 – 2 kilograms with microstructures which weigh less than a few micrograms. So while the region of interest is a few micrometers in size, process control can be exercised only on the macro scale. The methodology of attachment of the mold insert or placement of polymer substrate is another critical factor in enabling proper molding and any changes may result in significant process variations and embossing results.

4.3. Optimization of Hot Embossing Parameters

In order to achieve the best polymer filling of the insert and to avoid damage to the mold insert, polymer coming in contact with the microstructures must be raised to temperatures beyond the glass transition temperature of the polymer so that it is rubbery and during demolding the temperature must be lowered sufficiently to increase structural strength of the newly formed polymer microstructures [56, 57].

As mentioned in the last section, micro-molding is a thermo-mechanical process in which the bulk properties of the polymer material, mold insert and fixture have a dominant influence on the molding cycle parameters. The schematic in Figure 4.4 shows the typical setup of the embossing equipment. As can be seen, the mold temperature sensor is located approximately 20mm (varies from 17mm to 22mm depending on mold insert thickness) from the mold-polymer interface and the bottom substrate temperature sensor is located approximately 7mm (varies from 6mm to 11mm depending on polymer sheet thickness) from the mold-polymer interface where the actual molding is occurring. Therefore the sensors do not measure the actual molding temperature at the interface where the process control is required. This also makes the temperature reading dependent on the bulk properties of the mold insert, polymer material and the fixture method. It is also observed that

polymers of the same type exhibit slightly different glass transition behavior during embossing due to -

- Manufacturing process variations and additives
- Storage conditions such as moisture uptake
- Differences in thickness of the material being molded

Since the actual temperature and pressure at the polymer-mold interface cannot be measured precisely, an indirect experimental method using the existing control parameters was developed to easily derive the optimal molding conditions [58]. The method is using a 'dummy' mold insert with bulk properties and fixturing method identical to the actual mold insert, so that the delicate microstructured mold insert is kept safe from damage while the bulk thermo-mechanical behavior of the micromolding setup is replicated and used for determining the correct process parameters.

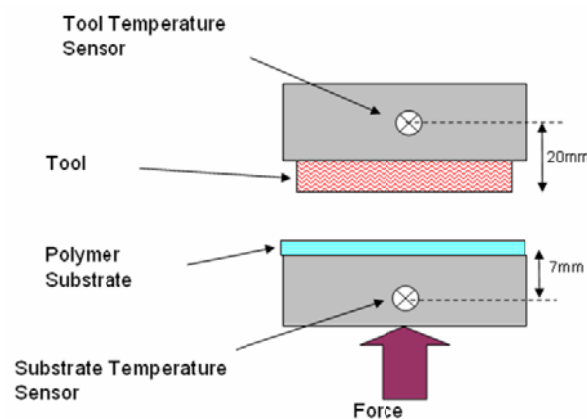


Figure 4.4: Schematic of hot embossing setup within the HEX02 machine.

Using this approach the correct range of processing parameters can be determined with only a few experiments. The procedure enables rapid development of the molding process and provides a good understanding and control of the cumulative behavior of the molding machine, mold insert and material.

4.3.1. Experimental Method

The experimental scope here is limited to molding of polymer features in the 10–500 μm regimes. For features in this size range, properties exhibited by the polymer are identical to the bulk properties of the material. High quality transfer of a pattern into polymer sheets is contingent on choosing the correct set of embossing parameters. The most significant process related parameters are the following:

- Molding temperature (maximum temperature applied during the embossing process).
- Molding force (maximum force applied during the embossing process).
- Molding rate (rate of displacement of the molding tool during the compression stage of molding).
- Hold time (time duration for which the Molding Force and temperature are held during embossing).
- Demolding temperature (temperature at which the demolding process is initiated).
- Demolding rate (rate of displacement of the molding tool during the mold separation stage).

While all the parameters affect the quality of molding, the molding temperature and force are the two primary significant variables. Choice of optimal force and temperature during molding ensures complete mold filling without excessive thermal or mechanical load on the mold insert or part, thus resulting in high quality parts and longer mold insert lifetime. Also, the force and temperature variables cannot be addressed individually as the glass transition temperature of a polymer varies as a function of the pressure being applied to it (Figure. 4.9). The graph in Figure 4.5 illustrates the changing parameters during the molding process. Every event occurring during the molding cycle is shown on the graph –

- Chamber Close – the molding chamber closes and is evacuated.
- Mold polymer contact - the mold slowly moves towards the polymer till it is in contact. No pressure is applied till the Molding Temperature is reached.

- Molding- once molding temperature is reached the insert presses into the polymer till a set force is reached.
- Hold time- time duration for which the polymer is held under molding pressure to achieve good mold fill.
- Cooling & Demolding – the mold temperature is reduced to below T_g and the mold and polymer are separated.
- Chamber Open – the molding chamber is opened to initial position and the molded part can be removed.

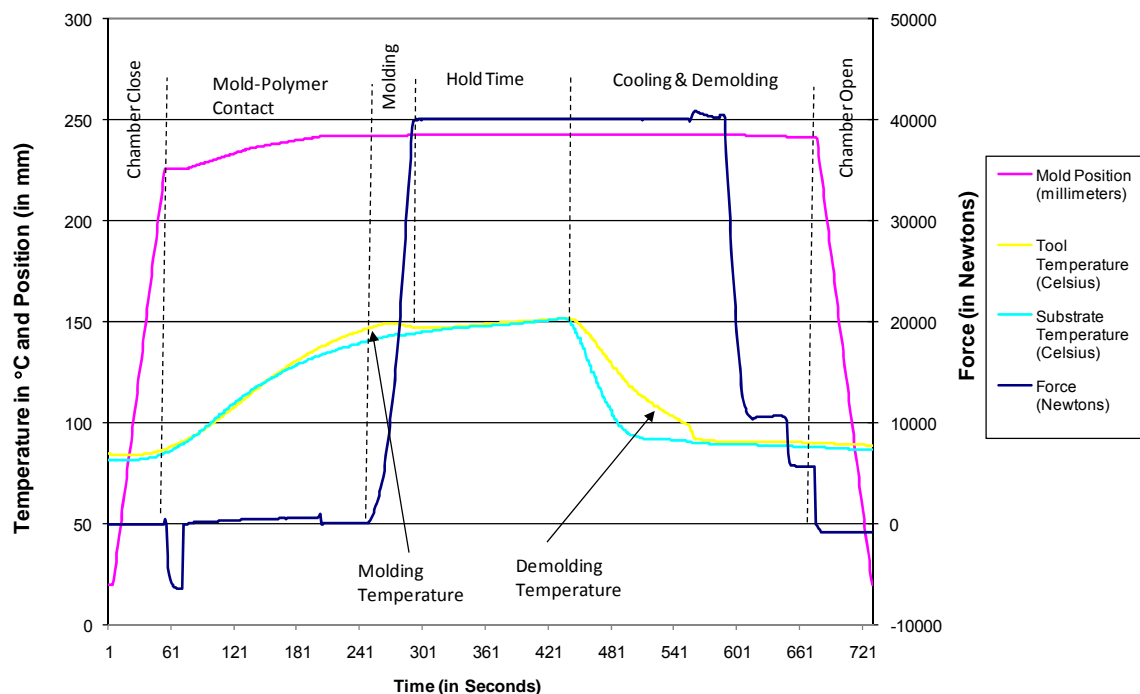


Figure 4.5: Graph of data captured by the Jenoptik HEX02 molding machine during a typical PMMA molding run. The events occurring during the molding process are marked on the graph.

The initial molding test was done with a ‘dummy’ mold insert resembling the actual mold insert’s bulk properties such as thermal conduction, heat capacity and thermal expansion, but without any delicate microstructures. Data from this experiment narrowed down the parameters to a range where the actual insert could be used with minimum development time and risk of damage.

Initially, the 'dummy' mold insert was brought in contact with the polymer material being tested and a constant force was applied. It should be noted that dynamically measuring the true pressure seen by the microstructures on the mold insert is impossible as the area of contact between the polymer and the mold face is constantly changing as the polymer softens and begins to conform to the mold insert surface. What is, however, being measured by a load cell in the molding machine is the total force seen by the polymer and the mold, and this may be used to calculate the approximate pressure. With the constant force being applied, temperature of the mold insert was then increased to well beyond the known glass transition temperature of the material.

The HEX02 data acquisition system continuously measures the temperatures and relative position of the insert and polymer during the molding cycle (Figure 4.5) and this data was plotted in a Displacement versus Temperature graph as shown in Figure 4.6. This representation provides a good insight into the occurrences taking place within the enclosed vacuum chamber. In the region marked $T \ll T_g$, the curve slopes downwards because the expansion of the material and machine column displaces the force unit in the negative direction. The curve levels out in the region marked $T \sim T_g$, and starts rising as the polymer begins to soften and conform to the mold insert face. When $T > T_g$ the curve starts sloping upwards as polymer loses viscosity and is beginning to flow, filling the insert cavities. This is the ideal zone for embossing the polymer since the polymer is sufficiently viscous to flow, but does not flow too freely yet. When $T \gg T_g$ (the curve is seen sloping up sharply) the polymer is very soft and quasi liquid and tends to flow out in all directions.

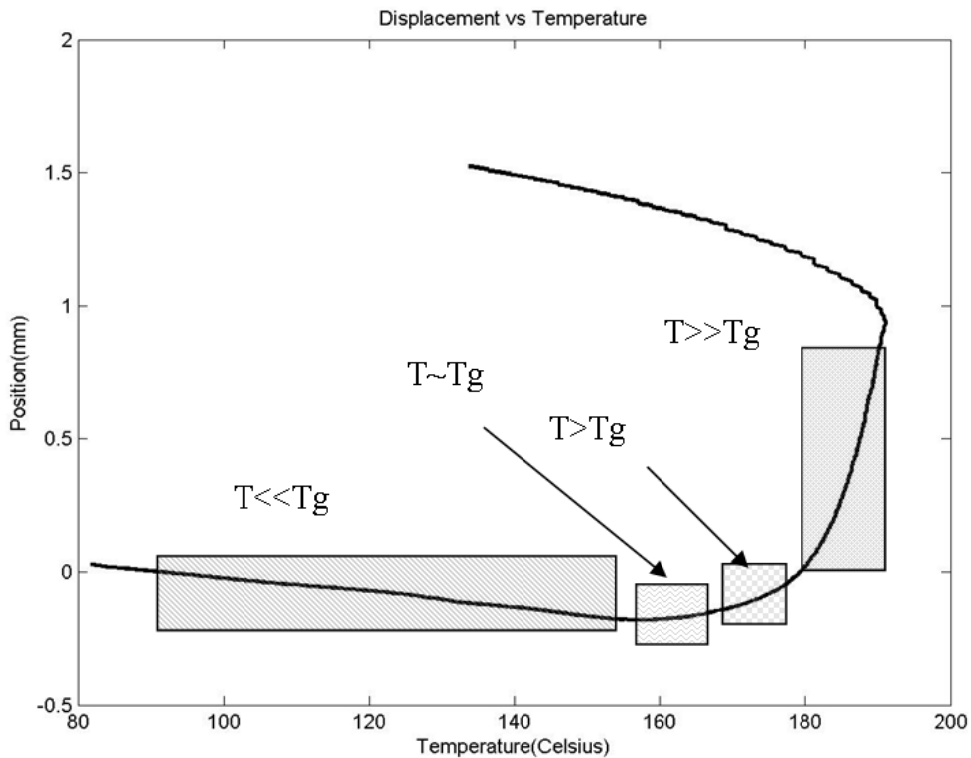


Figure 4.6: Displacement as a function of temperature with different states of the polymer material.

At this point the polymer flows too freely and embossing in this zone yields poor results. Beyond that point, as the mold is cooled, displacement due to contraction of the machine column is registered by the sensors.

Figure 4.7 illustrates the method used to define the best embossing temperature for a preset force. The zone formed by extending the two straight line regions of the graph marks off a section on the displacement-temperature curve. This is the region in which the polymer may be molded. A good starting point for the optimal conditions is the corresponding temperature at the midpoint of the curve section. In a small interval around this temperature (typically $\pm 3^\circ\text{C}$, ideal zone) fine-tuning of the parameters yields best molding results. In the course of this experiment, the dummy tool was a 10 cm \varnothing brass insert that had radial holes drilled on its surface. The micro mold insert that was used to verify the results was an identical micromachined brass disk with smallest cross structures of 50 μm line width.

The process flow used to arrive at the optimal hot embossing process conditions using the force-temperature graphs is as follows –

1. Determine approximate T_g from data sheets and manufacturer information.
2. Run Embossing test using dummy mold insert, ramping temperature from 10 °C below the T_g (from data sheet) up to 80°C beyond T_g .
3. Interpret Force-Temperature graph to evaluate ideal molding conditions (as shown in Figure 4.7).

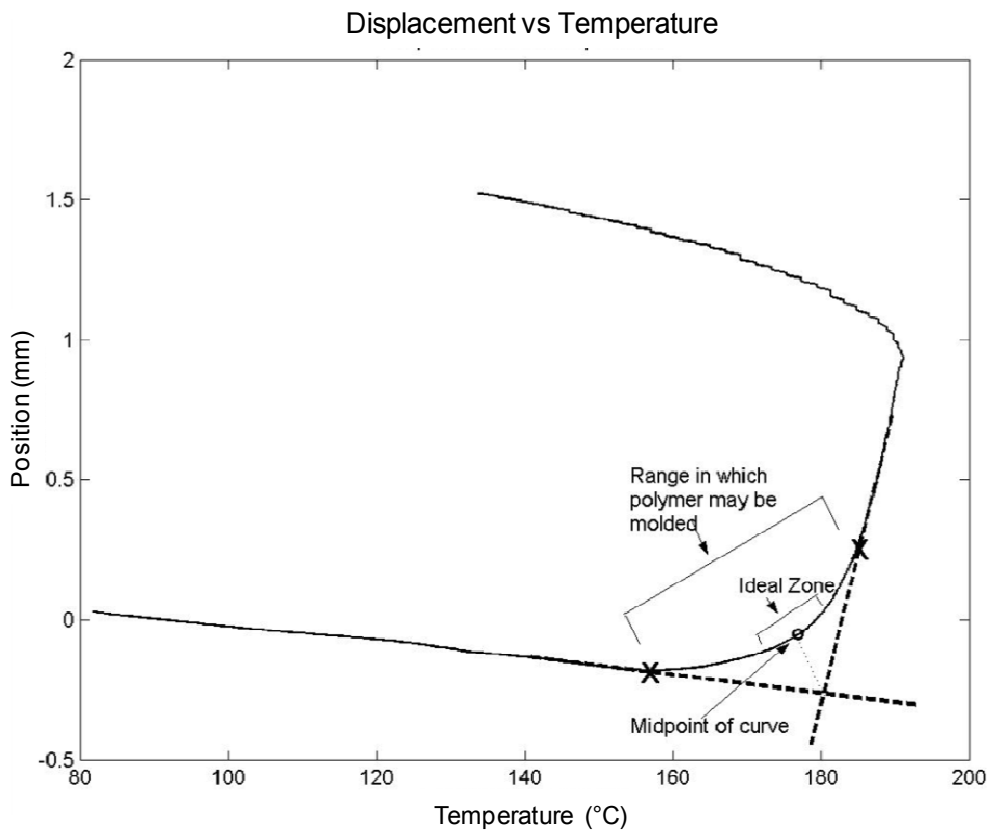


Figure 4.7: Derivation of ideal embossing zone from displacement-temperature graph

4.3.2. Materials and Results

Polymers are finding application in a multitude of MEMS applications in the fields of biology, medicine and chemistry to name a few [59]. PMMA is the most commonly used polymer for molding applications because of its biological compatibility, its optical properties, and ease of molding. Thus, being a commonly molded material, the molding conditions for PMMA are well documented [60, 61]. However, there are a number of other polymers such as Polycarbonate and Polypropylene that have properties making it desirable for specific applications [62, 63]. The previously described methodology has been used to successfully determine the ideal embossing conditions for PMMA, Polycarbonate and Polypropylene.

From a number of systematic material and process parameter studies conducted, the following two illustrate the value of this method. In the first set, commercially available 3/16" thick PMMA sheet material (Atofina, Plexiglas®) was used in the molding experiment at different molding forces. It has been observed qualitatively that molding PMMA under high forces were producing parts with high internal stresses. So in order to explore most gentle molding conditions at lower forces, experiments were run with different molding forces. In general, the higher the force the lower the embossing temperature could be. This is evident from the graph in Figure 4.8. As the molding force is increased, the ideal molding temperature becomes lower.

Figure 4.8 shows the displacement of the embossing piston as a function of increasing temperature for molding forces ranging from 2 – 10 kN. A region near the bottom indicates the temperature at which the polymer begins to soften and hence is the ideal point to commence molding. Based on information from Figure 4.7, experiments were carried out with the actual mold insert, demonstrating the value of this information. Figure 4.9 shows a series of pictures of microstructures taken after molding experiments have been carried out at a fixed force (5 KN) and slightly different temperatures. The corresponding point on the displacement versus temperature graph is also shown indicating that optimum parameters are related to

the region $T > T_g$ as predicted. The completely formed polymer structures indicate the optimized molding conditions.

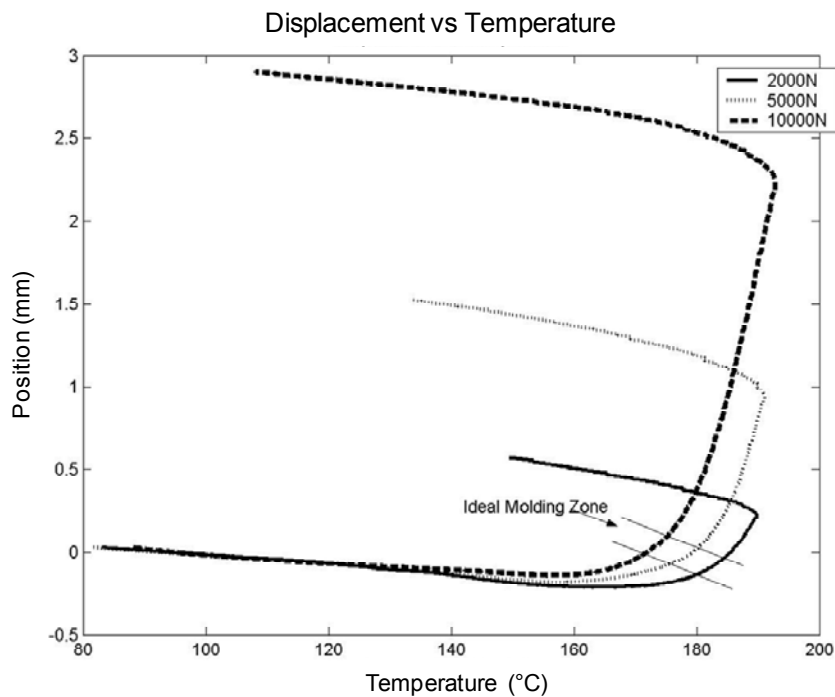


Figure 4.8: Displacement as a function of temperature for PMMA samples molded with different forces.

Other sheet materials from Polypropylene and Polycarbonate were investigated in order to identify best molding conditions. The displacement versus temperature graphs for these materials as well as PMMA are shown in Figure 4.10 for a fixed molding force of 10kN. The best molding temperature ranges can be inferred from the plot and are 175°C for PP, 185°C for PC and 172°C for PMMA. Another interesting observation is associated with the steepness of the slope at higher temperatures. While PC and PMMA show a similar, relatively slow increase allowing for some process tolerance for the optimum molding temperature and holding time, the polypropylene curve is very steep beyond the softening point. This indicates that this material loses viscosity very rapidly due to melting of the crystalline regions, thus making it challenging to pattern by hot embossing.

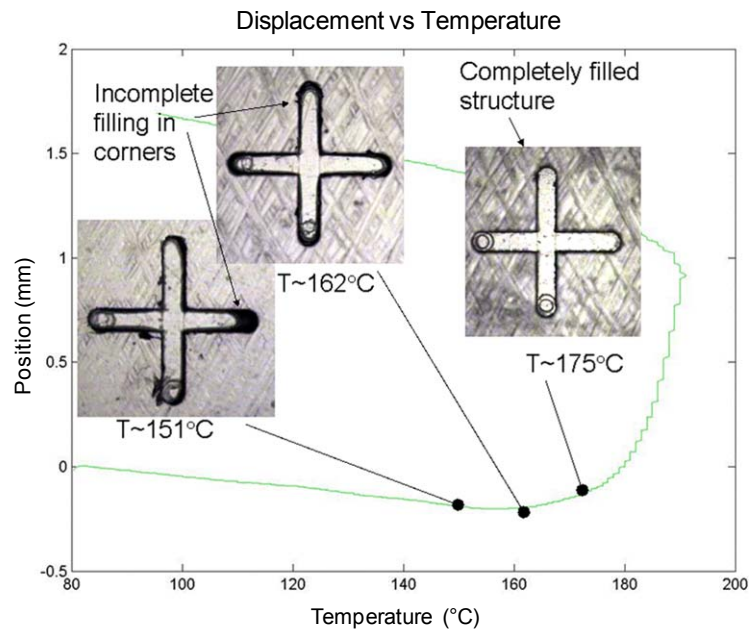


Figure 4.9: PMMA microstructure embossed under various conditions of temperature with a force of 5 kN; Width of the cross-bar pattern is 50 μ m.

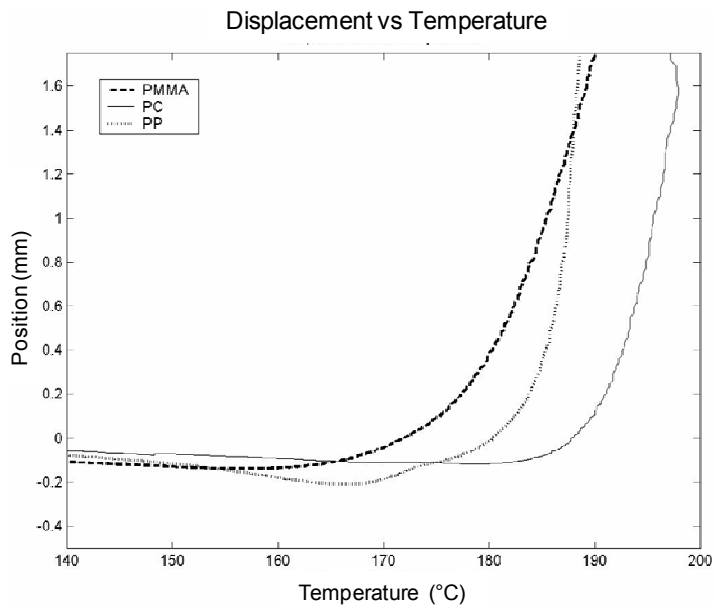


Figure 4.10: Displacement as a function of temperature comparing the behavior of 3 different polymers.

4.4. Dimensional Variation in Embossed Parts

Polymers typically have a higher coefficient of thermal expansion (CTE) compared to metals and ceramics¹³. Since molds are typically made from metal or silicon, this leads to significant difference in dimensions of a molded part from the dimensions of the mold. The change in dimensions is dependent on the geometry being embossed and on the process parameters being used during molding. An understanding of the influence of processing parameters on dimensional change enables more accurate part design and dimensional control which is relevant for passive alignment. It was therefore necessary to conduct a design of experiment (DOE) study to understand the influence of molding parameters on the dimensional variation.

The DOE study was formulated for a full factorial set of experiments to evaluate the influence of the most significant processing parameters and the results were compared with a simplified 2-D theoretical model.

During a typical embossing process, the mold insert is heated to about 30 °C above the glass transition temperature (T_g) of the polymer and pressed into the polymer. The polymer deforms to conform to the topography of the mold face. The mold insert and molded polymer are then cooled down to below the T_g of the polymer and then the mold is separated from the polymer. Thermal effects seen during the process can be separated into 4 phases.

1. Independent expansion of mold and polymer before pressing.
2. Thermal and stress effects during pressing.
3. Contraction and stress effects during cool down before demolding.
4. Independent contraction and stress effects of mold and polymer after separation.

The dimensional changes due to thermal effects in each of these stages can be modeled mathematically.

¹³ Typical Co-efficient of Thermal Expansion of Brass - 19.1 $\mu\text{m}/\text{m}\cdot^\circ\text{C}$, Nickel - 13.1 $\mu\text{m}/\text{m}\cdot^\circ\text{C}$, PMMA - 60 to 130 $\mu\text{m}/\text{m}\cdot^\circ\text{C}$, PC - 32 to 120 $\mu\text{m}/\text{m}\cdot^\circ\text{C}$, PP- 25 to 185 $\mu\text{m}/\text{m}\cdot^\circ\text{C}$

Phase 1 - This phase is modeled as a simple linear expansion phenomenon. Both the mold insert and polymer expand as the temperature is raised from room temperature to molding temperature. Dimensional distortions during this phase are very large as the temperature step is the greatest of all the phases. A mold insert fabricated at room temperature will show dimensional changes that increase radially outward from the center at elevated temperatures.

Phase 2 - During this phase, the temperature change is marginal and the polymer behaves like a highly viscous liquid that fills the mold cavities. The top layers of the polymer come in intimate contact with the mold insert face and conform to its topography. The lower layers of the polymer, however, do not undergo much change except for some compression. The temperature at which this phase occurs contributes to the amount of stress that is generated in the molded material.

Phase 3 - Through this phase, the polymer is reverting back to a solid and both the mold and the polymer are undergoing contraction as the temperature is lowered. Since the CTE of a polymer is typically higher than that of the mold insert, they shrink at different rates generating shear forces on the polymer and mold insert microstructure interface. Thus the structures are liable to bend and break under these shear forces especially when high aspect ratio features are being molded [64]. The demolding process has to tread a fine line that makes use of the elastic nature of the polymer at elevated temperatures to take up some of the shear stresses without plastic deformation. Correct choice of demolding temperature is crucial as an error on the high side and demolding when the plastic is too soft would result in plastic deformation of the molded microstructures. Demolding at too low a temperature would generate very high shear forces that will cause breakage, either of the polymer microstructures or of the structures on the mold insert, whichever is weaker.

Phase 4 - Once separated, the mold and the molded part are free to undergo contraction at their own rates. The final dimensions are reached as the polymer cools down to room temperature.

Based on this behavior, a simple mathematic model was defined to calculate the dimensional deformation due to thermal expansion and contraction of the mold and mold insert. The results from this serve as an approximate comparison for the experimental results described subsequently.

The CTE of the mold insert and polymer are defined as α_m and α_p , respectively. 'c' represents the mold and 'd' the polymer and the dimension of any structure on the on the mold or polymer can be chosen (Figure 4.11)

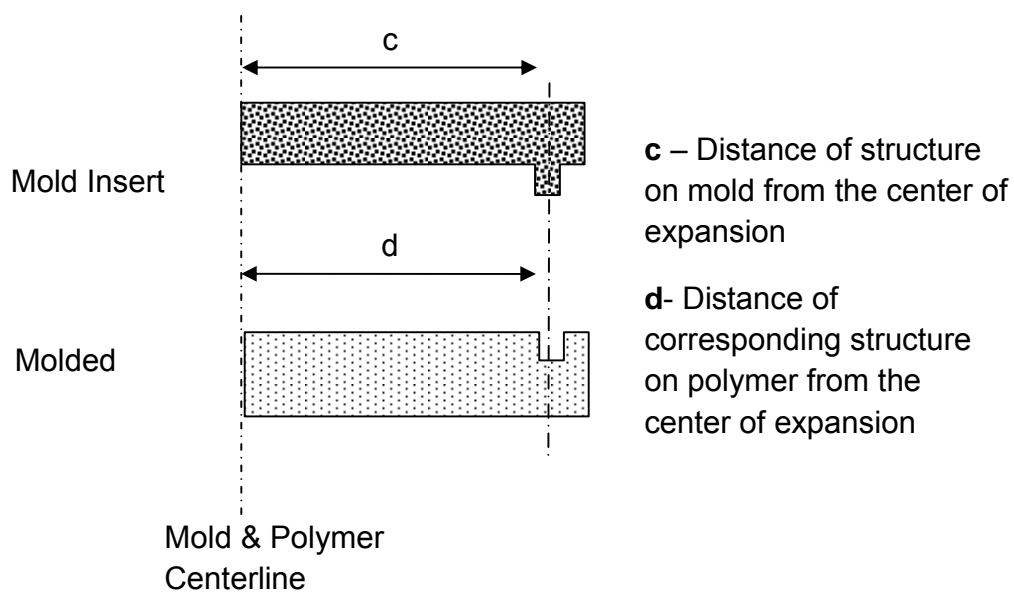


Figure 4.11: Graphical illustration of dimensions used for the mathematical model

Since this simplified model is linear, location of the structure on the mold face will not make any difference. So for a given change of temperature from $T_{initial}$ to T_{final} ,

$$c_{final} = \alpha_m c_{initial} (T_{final} - T_{initial}) + c_{initial} \quad \text{Eq 4.1}$$

$$d_{final} = \alpha_p d_{initial} (T_{final} - T_{initial}) + d_{initial} \quad \text{Eq 4.2}$$

Equations 4.1 and 4.2 give the dimensional change of the mold and the polymer, respectively.

In Phase 1 as the mold and polymer heat up to the molding temperature without interaction with each other, the dimensions are given by-

$$c_{molding} = \alpha_m c_{room} (T_{molding} - T_{room}) + c_{room} \quad \text{Eq 4.3}$$

$$d_{molding} = \alpha_p d_{room} (T_{molding} - T_{room}) + d_{room} \quad \text{Eq 4.4}$$

During Phase 2, the polymer in contact with the mold is in a semi-fluid state and is taking the form of the mold. In Phase 3 as the mold and polymer cool down to demolding temperature, they do so together and the dimensions of the polymer are largely driven by the mold.

Dimension of the mold at demolding temperature T_{demold} is given by-

$$d_{demold} = c_{demold} = \alpha_m c_{demold} (T_{demold} - T_{molding}) + c_{molding} \quad \text{Eq 4.5}$$

which is also equal to the dimension of the polymer at this point

As the mold and polymer cool down to room temperature in Phase 4, they contract at different rates. The final dimension of the polymer is given by

$$d_{room} = \alpha_p d_{demold} (T_{room} - T_{demold}) + d_{demold} \quad \text{Eq 4.6}$$

Based on this, the anticipated final dimensions of the molded part were calculated and compared with the experimental results (Figure 4.14).

For the experimental study, MiniTAB® Release 14 Statistical Software [65] was used to formulate and analyze the DOE study. A full factorial experiment was set up to mold PMMA by varying 5 molding parameters, yielding 32 different sets of molding conditions. The process parameters that were varied are molding temperature, demolding temperature, wait time, force and the thickness of polymer being molded.

A brass mold insert with raised rectangular posts 1mm tall and 1mm x 1mm in dimension were structured radially on the mold insert. Cross fiducials were placed

radially at gaps of 10mm, with the width of the cross being 250 μm (Figure 4.12). After molding according to the defined parameters, the dimensions of the gap between these structures on the molded PMMA parts and the same dimensions on the mold insert were measured at room temperature. The difference in dimensions between the mold insert and the molded parts was calculated to yield the actual variation of the molded polymer part from the brass mold. Measurements were carried out on a Nikon M-22U Measuroscope equipped with QC5200 edge detection and measurement software from Metronics® [66]. The combined error (human and machine) of measurement was verified to be within ± 2 microns using a length standard.

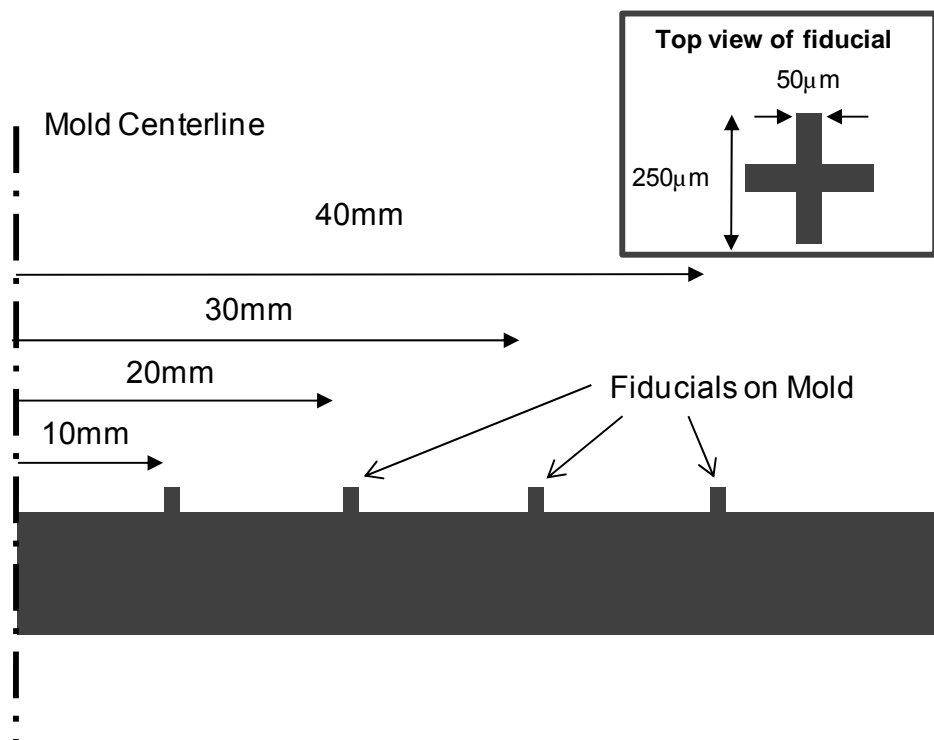


Figure 4.12: Schematic of mold insert for evaluating expansion of polymer parts as a function of processing parameters.

The experiment yielded 128 data points and MiniTAB® was used to analyze the data and plot the results (Figure 4.13). These plots indicate the dimensional changes as a function of the processing parameters - Molding Temperature, Demolding temperature, Wait Time and Force. It also shows the influence of the thickness of the material being embossed and the distance of the structures from the center of the mold. It should be noted that these graphs show the relative change in dimension compared to the brass mold insert.

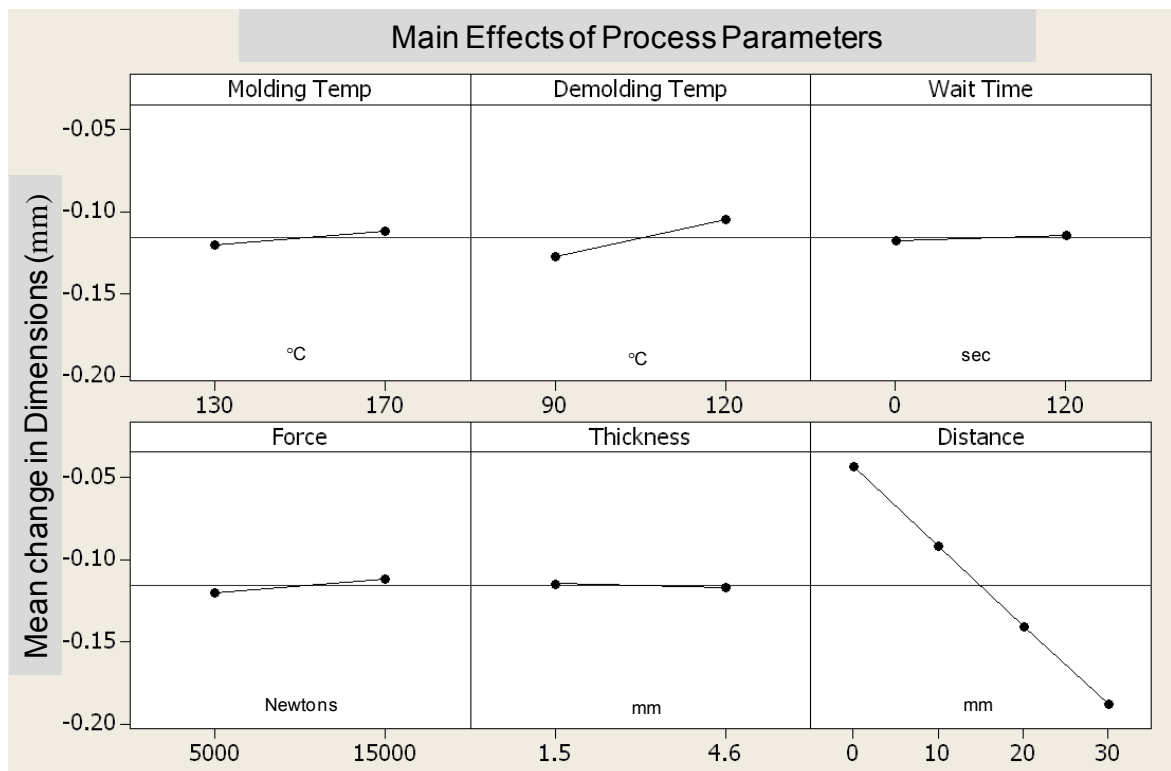


Figure 4.13: This plot shows the influence of the main effects on the global scale. It illustrates how the dimensions change due to the influence of the processing parameters such as Molding Temperature, Demolding temperature, Wait Time and the Force. It also shows the influence of the thickness of the material being embossed and the radial distance of the structures on the mold. Dimensional change in mm is on the y-axis and these changes are seen over lengths of 10, 20 30 and 40 mm from the center of the mold.

Interpreting Figure 4.13 yields an understanding of the dependencies of the molded part dimensions on the hot embossing parameters. It can be concluded that while all the parameters studied have some effect on dimensional variation of the molded structures, location of the structures mold face and the demolding

temperature are the most significant factors. (Effects of cross interactions between the studies parameters are shown in Appendix E).

At any area of the molded part, the deviation from the dimensions of the mold insert was less than 50 μm over a distance of 10 mm. Dimensional change across the diameter of the molded part, over a distance of 80mm, was approximately 400 μm .

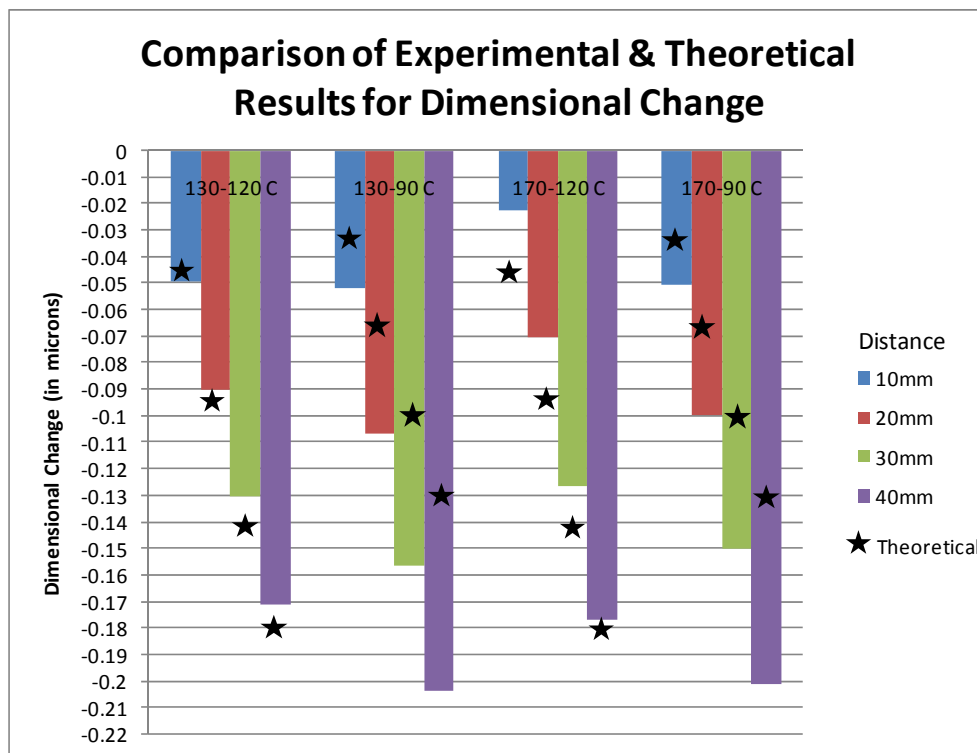


Figure 4.14: This graph shows and a comparison of the theoretical and experimental data for different molding – demolding temperature combinations. The theoretical data points are indicated by the stars and they show similar trends as the experimental data but vary significantly from the experimental data. This is expected since the theoretical model considers only thermal effects and does not account for internal stresses.

Figure 4.14 compares the experimentally measured dimensional changes with the predictions from the theoretical model. The comparison shows a similar trend between the two, though there is some difference in values because the theoretical model considers only the thermal expansion aspect and ignores the effects of internal stresses of the material. The most significant differences are noticed at the lower demolding temperature (90 °C). The theoretical model assumes that after

demolding the polymer will expand only due to thermal effects as it returns to room temperature. However, the experimental results indicate that upon demolding some of the stress induced in the polymer releases and it expands more than what would be expected from a purely thermal phenomenon. In the cases where demolding occurs at much higher temperatures, the theoretical values agree closely with the experimental, indicating that the amount of induced stress is negligible. The information from this DOE study provides the basic mold insert design guidelines and predicts the tolerance requirements for assembly of the molded parts.

4.5. Hot Embossing - A Viable Technology for Mass Production

Molding polymers by hot embossing is known as an effective prototyping method and the advantages and disadvantages of embossing, compared to injection molding are discussed further in Section 5.2. Hot embossing is an ideal process for prototyping and for small scale production since the initial cost is low and time to go from a design to a prototype is short. Typically hot embossing is not considered a viable process for mass fabrication of components primarily due to the long cycle times (typically 10-15 minutes) for each molding run, compared to injection molding (1-2 minutes or less). Thus, in spite of the many advantages of hot embossing as a method of polymer microfabrication, in the context of mass fabrication, injection molding is considered the only viable technology.

An analysis of the possibility and the economic aspects of using hot embossing for mass production were carried out based on basic data from CAMD¹⁴ where hot embossing of microstructures is carried out on the Jenoptik HEX02 machine as a paid service for external customers. The numbers used are approximate and some realistic assumptions have been made based on experience.

Table 4.1 shows the number of molding runs possible in one week assuming that the setup time for a mold is 4 hrs and that each molding run takes 15 minutes. Machine downtime of 8 hrs per week is assumed irrespective of the running time.

¹⁴ Center for Advanced Microstructures and Devices, 6980 Jefferson Hwy, Baton Rouge, Louisiana.
(Website:<http://www.camd.lsu.edu/>)

Each shift equals 8 hours of operating time. From the table, it can be seen that frequently changing mold inserts reduces the productivity significantly.

Based on information in Table 4.1, it can be stated that using a single molding machine and running it full time for 24 hrs a day for 7 days a week, the maximum number of molding runs possible per year = 624 X 52 = 32448. It should be noted that while prototyping a few (10-20) parts, optimization of cycle time does not offer significant benefit, but for larger batches, the cycle time may be reduced significantly by optimizing the process.

	Hrs	Machine Run Time			
		1 Shift	2 Shifts	3 Shifts	3 Shifts, 7Days
Average setup time	4				
Average cycle time per part	0.25				
Down time per week	8				
No. of Runs per week (1 mold)		112	272	432	624
No. of Runs per week (2 molds)		96	256	416	608
No. of Runs per week (3 molds)		80	240	400	592
No. of Runs per week (4 molds)		64	224	384	576
No. of Runs per week (5 molds)		48	208	368	560

Table 4.1 : Number of molding runs possible in a week.

Parts per mold	YIELD					
	100%	95%	90%	80%	70%	50%
2	64,896	61,651	58,406	51,917	45,427	32,448
5	162,240	154,128	146,016	129,792	113,568	81,120
10	324,480	308,256	292,032	259,584	227,136	162,240
15	486,720	462,384	438,048	389,376	340,704	243,360
20	648,960	616,512	584,064	519,168	454,272	324,480
50	1,622,400	1,541,280	1,460,160	1,297,920	1,135,680	811,200
100	3,244,800	3,082,560	2,920,320	2,595,840	2,271,360	1,622,400
1000	32,448,000	30,825,600	29,203,200	25,958,400	22,713,600	16,224,000

Table 4.2 : Production capacity as a function of yield and parts per mold.

Hot embossing is a batch process and each run typically produces more than one part. The number of parts that can be produced in one molding run depends on the surface area taken up by the part – smaller the part, larger the number of parts that can be accommodated on a mold insert of given area.

Table 4.2 shows the peak part production capacity per year as a function of the number of parts on the mold and percentage yield, assuming that molding is run at maximum capacity (32448 runs per year). This shows that not only is hot embossing a versatile manufacturing process well suited for prototype fabrication because of low initial cost, but may also be scaled up to serve as a mass production technology capable of producing parts at a reasonable cost and in higher quantities.

5. Fabrication Processes for 3-D module

The design criteria relevant to the fabrication process for the microfluidic development platform were –

- Short turnaround time suitable for prototyping.
- Overall fabrication process scalable from prototyping to production.
- Low cost.

The sequence of process steps that were used in fabricating the various components of the system were chosen carefully to ensure that these criteria were met. This approach was adopted because the goal of this work was not only to design and build a microfluidics test platform, but to do it in a manner that would make such a device available to users at a low cost and within a reasonable time.

A number of fabrication methods were used to manufacture the components of the complete system which included a combination of micromilling, conventional machining, hot embossing and manual assembly processes. This leads to a higher 'per part' cost but the overhead or setup cost involved is low. Figure 5.1 outlines the sequence of processing steps. Larger components like the structural block and the clamping frame were fabricated by direct milling. Direct micro-milling was also used when on occasion a single polymer microfluidic chip was required so a replication process was not suitable.

Polymer molding in the form of hot embossing was the key technology used to fabricate the microfluidic chips. Some other components of the system platform like the backplane and individual nozzles were also fabricated by hot embossing. Since embossing played a pivotal role in the fabrication, in-depth studies were done on various aspects of the process, starting from mold insert fabrication, all the way to the finishing of molded parts.

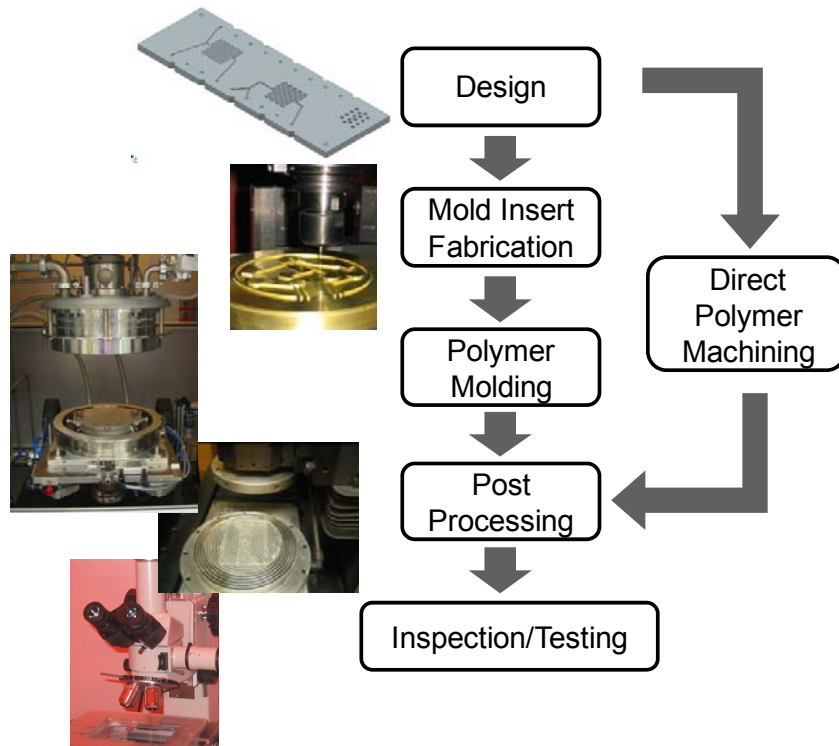


Figure 5.1: Sequence of fabrication steps for components of the microfluidic development platform

5.1. Mold Insert Fabrication

The desired properties of the molded polymer part drive the requirements for the mold insert (molding tool). Mold inserts for micromolding can be fabricated using a number of micromachining technologies. The following criteria are taken into consideration when choosing a mold insert fabrication process-

- Minimum dimension;
- Maximum Aspect ratio;
- Geometric considerations (E.g.- Corner radii, multiple levels);
- Structure strength;
- Surface roughness;
- Turnaround time;
- Cost;

The material of the mold differs based on the technology being used. Silicon can be patterned using a combination of photolithography and dry etching to produce a mold [67]. The very same process can be followed by a metal deposition and electroplating process to transfer the pattern to a nickel shim which can also act as a mold. The LiGA¹⁵ process [68] has also been used to produce high quality nickel and nickel-iron mold inserts [69, 70]. Thick resist lithography using SU-8 followed by electroplating can be used to form a mold [71, 72], however the negative sidewall slope in thick SU-8 layers usually produces geometries that are difficult to demold. On occasion even polymers like PDMS (polydimethylsiloxane) have been used as molds for forming PMMA [21], though this process is not a practical manufacturing process due to the short lifetime of the mold. Table 5.1 shows a qualitative comparison of the different technologies for fabrication of microstructured mold inserts.

<i>Technology</i>	<i>Typical Feature Dimension</i>	<i>Typical Aspect Ratio</i>	<i>Mold insert Materials</i>	<i>Surface Roughness</i>	<i>Typical Structure Strength</i>	<i>Time</i>	<i>Cost</i>
Photolithography + Wet Etching	1 μm to 1mm	1 to 2	Si, Glass	Low-Med	Med-High	Med	Low
Photolithography + Dry Etching	10nm to 500 μm	1 to 20	Si, Glass	Med	Low	Med	High
Photolithography + Electroplating	5 μm to 1mm	1 to 5	Ni, Ni-Fe	Low	Med-High	Slow	Med.
LiGA	10 μm to 1mm	10 to 20	Ni, Ni-Fe	Low	Med-High	Slow	High
Micro-Milling	25 μm to 2mm	1 to 5	Brass Steel Aluminum	High	High	Quick	Med.

Table 5.1: Comparison of mold insert fabrication technologies and their characteristics.

¹⁵ Lithographie, Galvanoformung, Abformung- a microfabrication process used for making high aspect ratio microstructures

As many microfluidic designs do not require very small structures, micromilling of brass discs was chosen as the primary method of mold fabrication. Micromilling can be used to produce molds in various metals. It is by far the most flexible and quickest method which makes it a very attractive technology in spite of the fact that the resolution and surface finish achieved by micromilling is poorer than that achievable by lithography based methods. Dimensions as small as 25 micron wide and aspect ratios of up to four can be achieved by micromilling. Brass is the material of choice for milling the mold because of its easy machinability and good performance in the hot embossing process. Multilevel features and tapered geometries (Figure 5.2) can be fabricated effortlessly by micromilling and combining small structures with large structures on the same mold is also achieved in one single step.

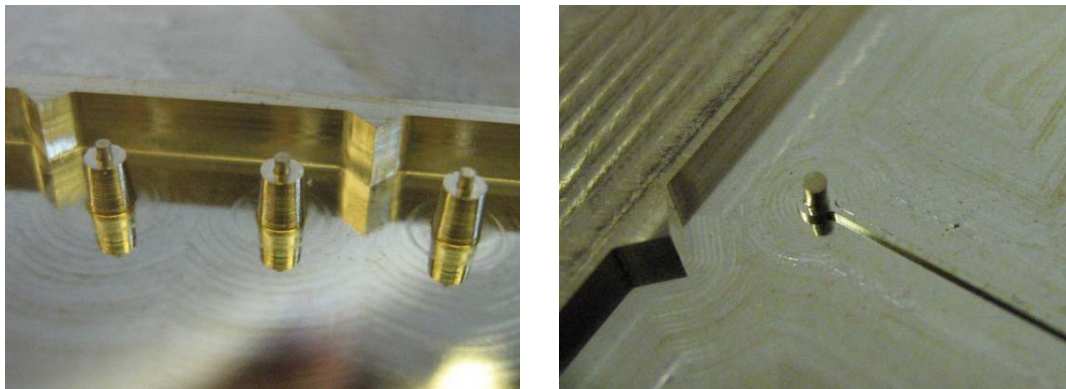


Figure 5.2: Image of regions on a milled brass mold insert with showing tapered and multi-level features

Micromilling of brass blanks was done on the Kern® Micromilling machine [73] (Figure 5.3) using a 40,000 rpm spindle and capable of positional and repetition accuracy with a precision of $\pm 1 \mu\text{m}$ in a space of $\sim 150 \text{ mm}^3$. Milling tools down to 25 μm diameter are available for use with the machine making it possible to mill recessed structures to a minimum of 25 μm in width. The average roughness (Ra) of the structures on a micromilled mold insert ranges from 50 nm to 120 nm.



Figure 5.3: Kern[®] Micromilling Machine used to mill mold inserts in brass. The machine is operated and maintained by Jason Guy as part of the Center for Bio-Modular Multi-scale Systems (CBM²) under Dr. Steven Soper.

The milling process produces burrs on the corners of structures which can typically be polished away with a fine grit polishing paper. However, if the mold insert has more than one level, the burrs cannot be removed by polishing. In such cases, using the mold a few times will remove the burrs. Overall, micromilling is a rapid and inexpensive method of fabricating microstructures mold inserts for prototyping and small scale production. Fabrication time for an average mold insert is 2-6 hrs.

Mold inserts were also fabricated using the LiGA process when extremely small structures were desired or when surface roughness surpassing the capabilities of micromilling was required. Figures 5.4(a-c) show some mold inserts and the polymer parts molded using them.

For rapid prototyping and small scale production of polymer microstructures, hot embossing is a more viable technology. Hot embossing was the primary method of fabrication for polymer components in the course of this work. The Jenoptik Mikrotechnik (Jenoptik Mikrotechnik, Jena, Germany) HEX02 hot embossing machine [54] was used for all the molding activities. Details of the hot embossing process, a methodology for process optimization and a systematic study to evaluate the dimensional variation of molded parts are discussed in Section 4.

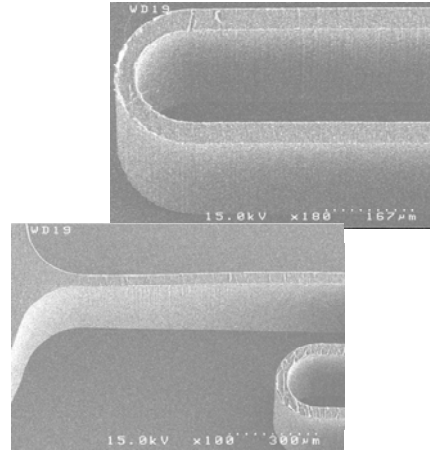
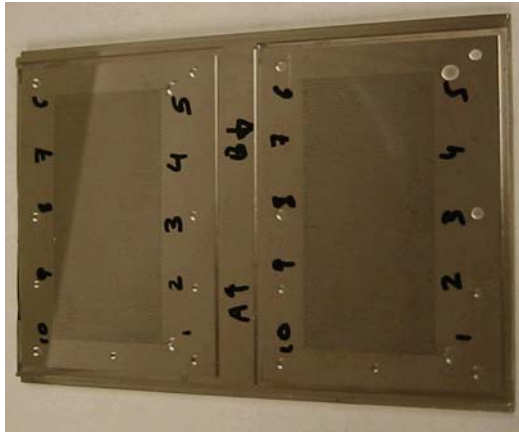


Figure 5.4a: LiGA mold insert (Left) with a winding gas chromatograph channel and the molded PMMA part (Right). Channels/walls are $50\ \mu\text{m}$ wide and $450\ \mu\text{m}$ tall.

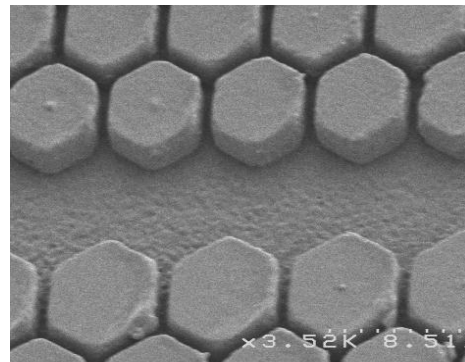
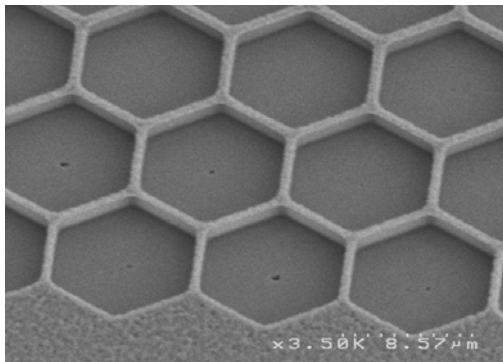


Figure 5.4b: LiGA fabricated mold insert (Left) with $1\ \mu\text{m}$ walled hexagonal structures used to mold honeycomb filter structure (Right) in PMMA.

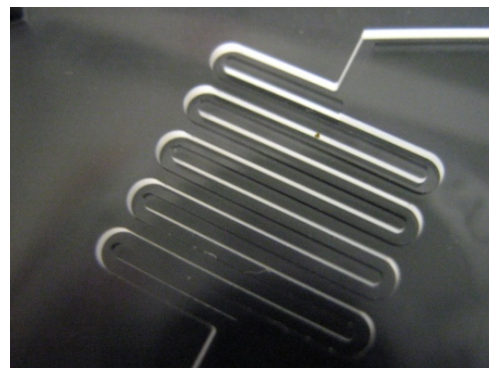
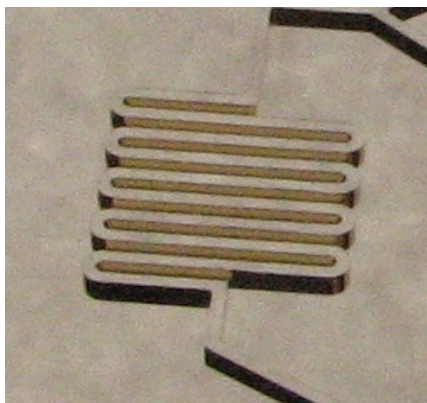


Figure 5.4c: Brass mold insert (Left) with $500\ \mu\text{m} \times 500\ \mu\text{m}$ channel and part molded using it (Right).

5.2. Post Processing of Molded Parts

After replicating polymer parts by hot embossing (details discussed in section 4), they have to undergo a sequence of steps before they are ready for use in the system. The common process all chips undergo is some form of machining and cleaning. Then depending on the functionality, the chips may have electronic pathways laid down, silicon dies flip-chip and wire-bonded, or they may be sealed with a cover-slip or to another chip.

5.2.1. Machining and Cleaning Processes

Molding is a batch process and multiple parts are usually produced during one molding run (Figure 5.5). Separating the components into individual pieces is the first step of post processing. This was done by a combination of intelligent design and the use of conventional cutting tools. Since the format of the microfluidic chip is standardized (Section 3), deep ‘snap-off’ structures were designed into the mold to form the boundary of the chips. It was feasible to separate the chips from the substrate by manually breaking them off.

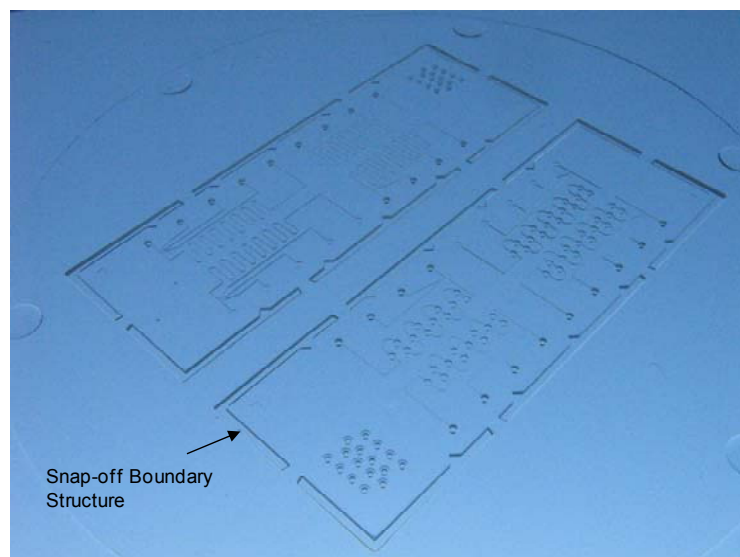


Figure 5.5: Single molded part with two microfluidic chips.

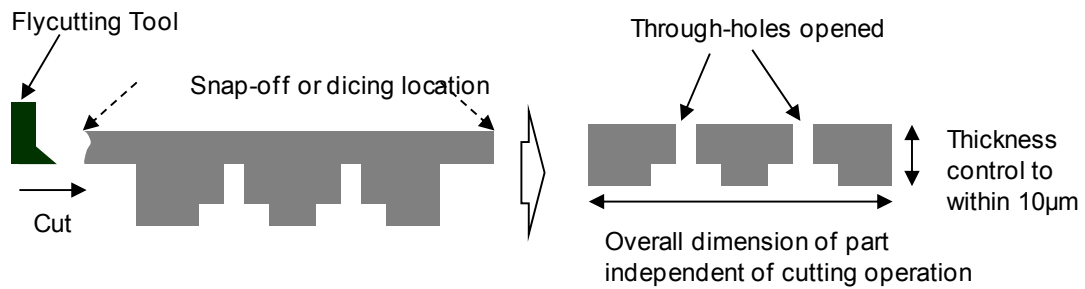


Figure 5.6a: Schematic of flycutting operation used to open through holes and interconnects and to control the final chip thickness.

This was followed by flycutting to remove the residual layer of polymer from the part (Figure 5.6a,b). Flycutting also opens up any interconnects and through holes that were designed into the mold insert. Since the depth of cut during flycutting can be controlled very precisely (better than 5 μm), the final thickness of the machined chip is defined by this step too. Following this, the chips are cleaned by placing them in an ultrasound bath with soap water for 2 minutes, then rinsed in deionized water and finally blow dried.

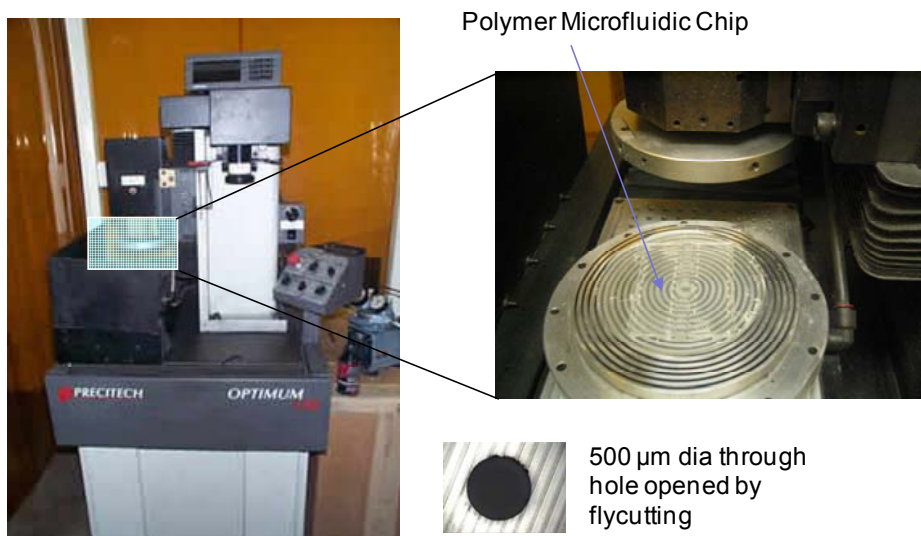


Figure 5.6b: Precitech flycutting machine used to remove excess polymer material from the embossed parts, control the final thickness of the chips and to open interconnect vias.

5.2.2. Electronic Interconnects

Electrical and capacitive fields are commonly used methods of sensing in microfluidics devices [6]. In order to bring fluid in channels into contact with or in very close proximity to an electrical field, conductive wire traces were integrated into the polymer microfluidic chips. A number of well established methods such as lift-off [13], etching and shadow masking [74] were available for this purpose. As the driving design criteria include a quick turnaround time, the methods for electrical interconnection were selected accordingly. The first was 'shadow masking' (Figure 5.7) and the second was 'discrete wire insertion'.

Both methods are simple and effective when only a few wires are required and need to be replaced by more advanced lithography based methods like lift-off or etching when complex wiring layouts with higher precision or smaller line widths are desired.

Shadow masking, as the name implies uses a stencil like structure (Figure 5.7) to mask (cast a shadow on) regions of the substrate. For the shadow mask process, micromilling was used to create a stencil pattern in 1 mm thick sheet of brass (Figure 5.8b). The passive alignment V-grooves that were present on the polymer chips were also used to align the stencil mask to the chip using a specially designed fixture (Figure 5.8a). The whole assembly was placed in an electron beam metal evaporator (Temescal BJD-1800 E-Beam Deposition System). Typical conductive layers consist of 10 nm of Chromium and 100 nm of Gold that are deposited onto the polymer chip through the shadow mask (Figure 5.9a,b).

The main advantage of this method is aligned direct deposition of the conductive pattern onto the molded chips without any complicated chemical processing. Depending on the deposition target, a variety of different metals can be deposited as needed by the application.

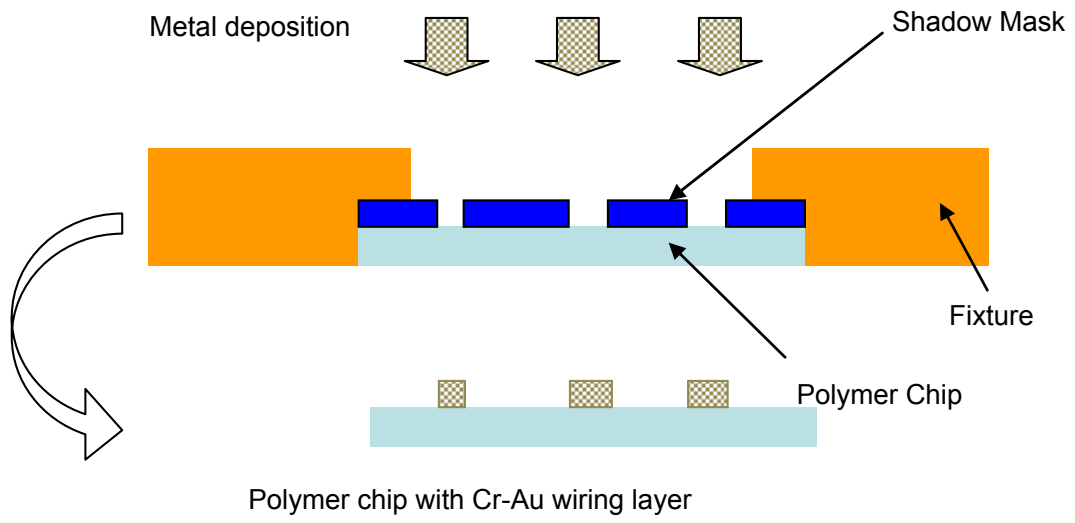


Figure 5.7: Illustrates the metal deposition process using a shadow mask.

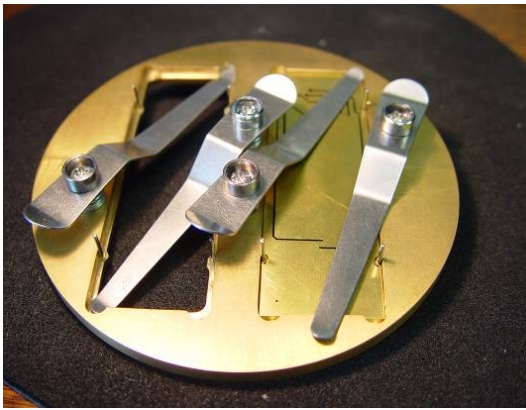


Figure 5.8a: Shadow mask holder.

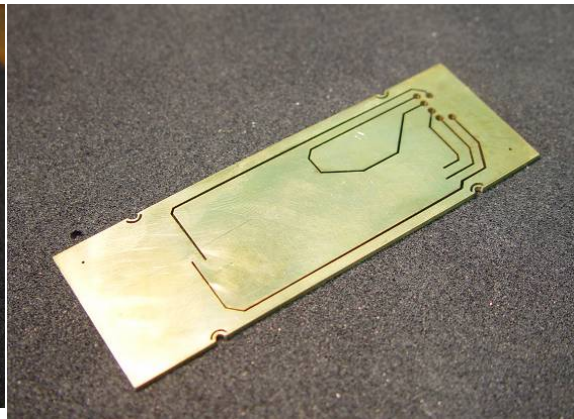


Figure 5.8b: Machined shadow mask.

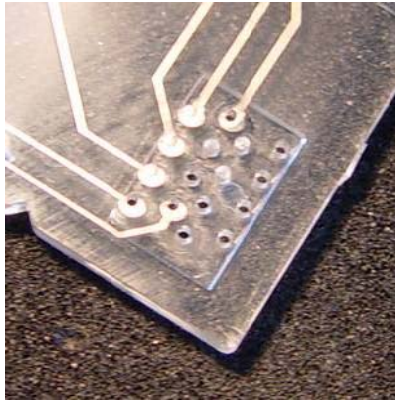


Figure 5.9a: Metal traces at connector site.

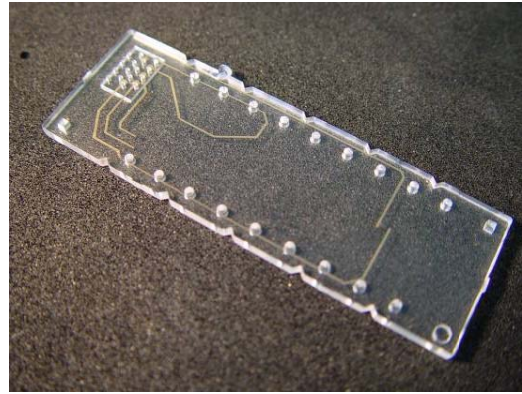


Figure 5.9b: Wire traces on the polymer interconnection chip.

The limitations of the shadow-masking process are that the line widths have to be $\geq 250 \mu\text{m}$ and the design can have only a limited number of wiring lines because removal of too much material weakens the brass shadow mask mechanically and sections of it sag and lose contact with the polymer chip, thus resulting in a poorly formed conductive trace on the polymer after metal deposition.

The second method called 'discrete wire insertion' involves inserting commercially available metal wire into predefined recesses in the polymer chip (Figure 5.10).

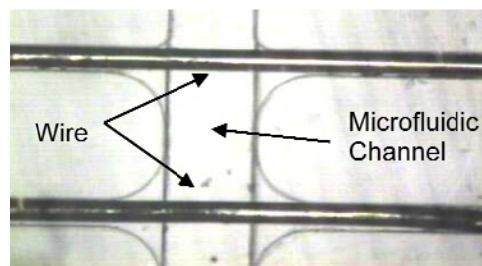
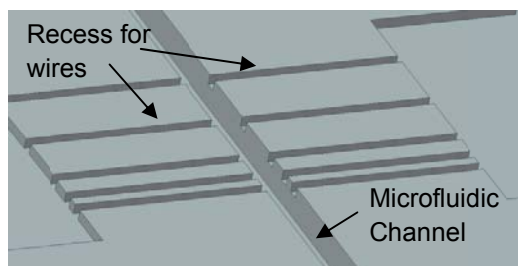


Figure 5.10: Schematic (Left) showing the structure used for discrete wire insertion over a fluidic channel. Image of the actual assembly (Right)

A multilevel mold insert was used to form polymer chips with recesses that are $100 \mu\text{m}$ in depth suitable for $80 \mu\text{m}$ diameter metal wires. These recesses are much shallower than the $500 \mu\text{m}$ deep microfluidic channel across which the wires are placed, hence the fluid can flow unimpeded through the microchannel while making

contact with the metal wires. Adhesive was wicked into the wire recesses to prevent fluid from leaking out.

This method of conductive wiring has the obvious disadvantage of being limited in size to the smallest wires that can be handled with reasonable ease; however, it is an extremely easy method and can be used where wires of specific materials are necessary such as for chemical reference electrodes, heater wires, low resistance copper wires, etc. This wiring method was used in the experimental setup in Section 6.2 in order to carry out conductivity measurements to distinguish between plugs of oil and water.

All wire traces inside the microfluidic chip stack have to be connected to the outside world, allowing the use of a conventional connector. For this, some area on the chip is defined as a connector mounting site. The hole pattern on this site corresponds to a commercially available FH21 series electrical connector fabricated by Hirose® [75]. The component is inserted at the mounting site and electrical conductivity is established with the deposited wire traces using conductive glue available commercially from Creative Materials [76], product number 118-15.

The through holes for the electrical connectors are designed with an expanded recess at the surface of the chip to allow conductive glue to squeeze in and ensure a good electrical contact (Figure 5.11a) with the wire trace. The conductive epoxy was chosen with a curing temperature that is very close to the temperatures for sealing the microfluidic stack (Sealing process is discussed in detail in Section 3.2.2). Hence the sealing and epoxy curing can be carried out in one single step. The chips being sealed are stacked and the conductive epoxy is injected into the electrical port holes. The FH21 electrical connector is then inserted into the port, pushing out the excess epoxy from the holes with its leads. The stack is then clamped in the fixture for sealing. It was found that the temperatures and times required for thermal sealing were always sufficient for fully curing the conductive epoxy. Figure 5.11b shows a 2 layer stack of chips thermally sealed and with a connector installed with conductive glue.

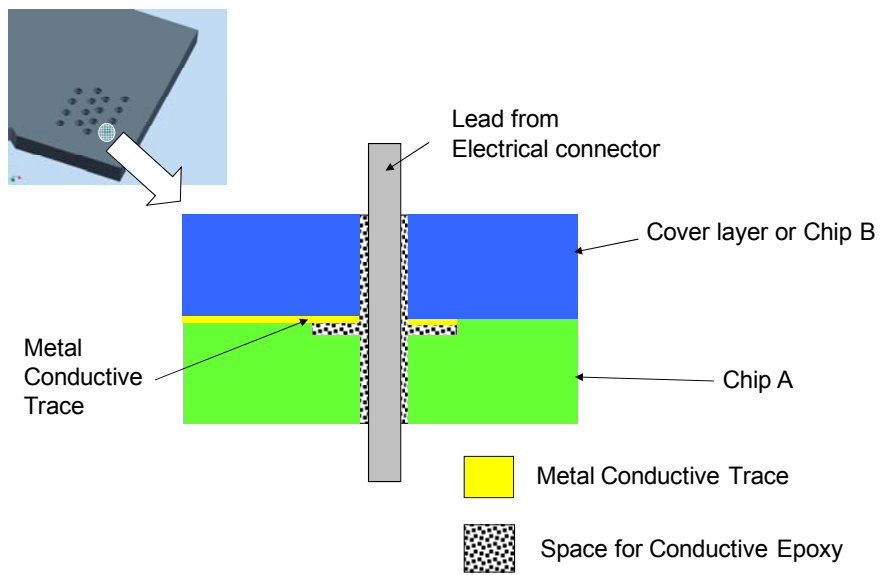


Figure 5.11a: Schematic illustrating the macro interconnection method for electrical wiring

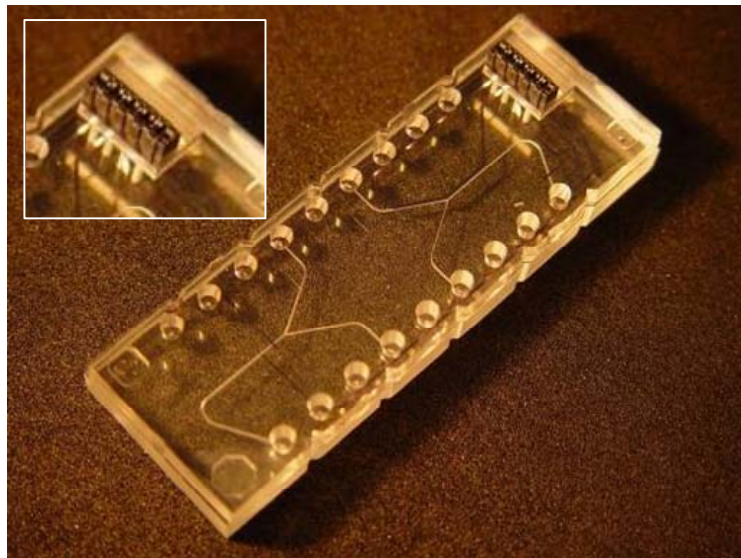


Figure 5.11b: Top view of a sealed chip assembly with microfluidic channels, deposited wiring layers and attached standard electrical connector (Inset).

The conductivity of the wire was measured as shown in Figure 5.12a,b. Two different wire thicknesses were deposited and tested. The measured values are summarized in Table 5.2. It can be seen that the length and thickness of the Au wires are critical factors. Increasing the thickness reduces the resistivity as predicted but not exactly by a factor of two indicating that substrate roughness, thickness uniformity, rough edges, and cracks in the deposited layer are critical properties especially for very thin layers. The average electrical resistivity is $56\Omega/\text{cm}$ for 50nm and $22\ \Omega/\text{cm}$ for the 100 nm thick, 500 μm wide wires. In conclusion, the method was found to be a simple and quick method of fabricating low density electrical/electronic connections into the microfluidic stack.

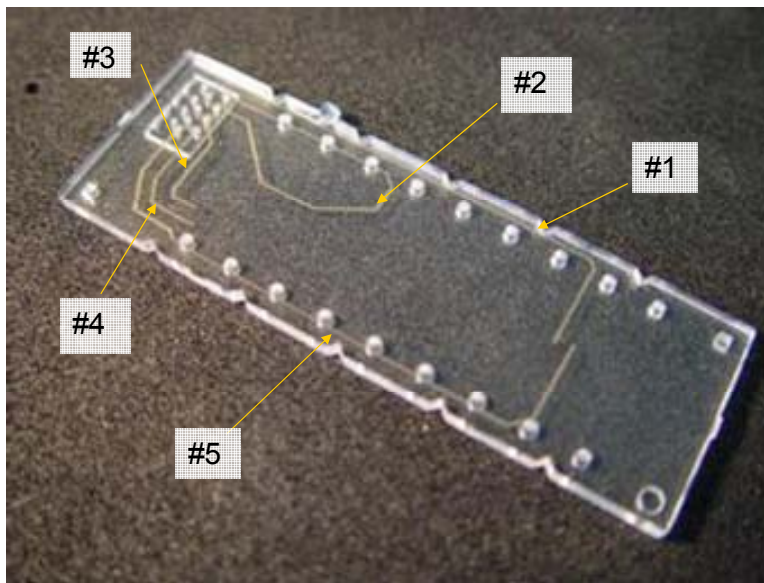


Figure 5.12a: Wire traces deposited onto the polymer surface; the numbers indicated traces of different length measured in Table 5.2.

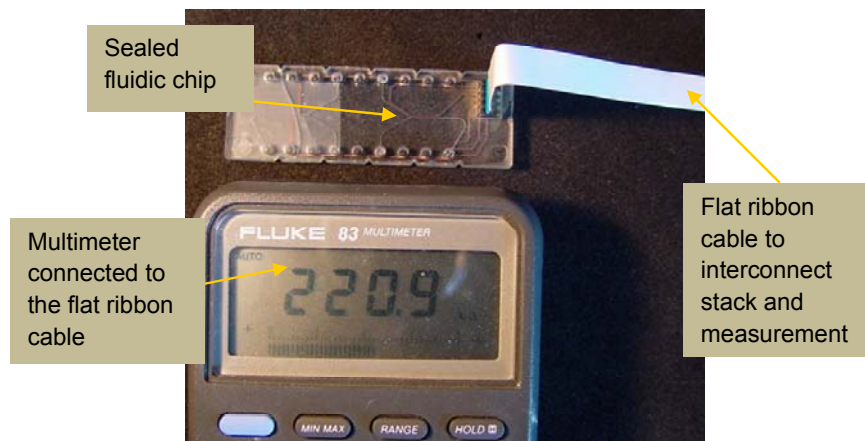


Figure 5.12b: Measurement of the resistance of a deposited electrical pathway through the standard connector and ribbon wiring.

Path #	Path length in cm	Resistivity in Ohm (wire thickness 50 nm)	Resistivity in Ohm (wire thickness 100 nm)
1	6.2	375	150
2	5.5	330	130
3	1.5	75	32
4	1.7	80	35
5	7.2	450	143

Table 5.2: Electrical resistivity of conductive wire deposited onto polymer chips.

5.2.3. Metrology and Inspection

Inspection and testing formed a significant part of the fabrication activities. Table 5.3 briefly summarizes the different kinds of inspection/measurement that were carried out at various stages of the fabrication process, ensuring that high quality functional chips were used in the subsequent experiments.

Fabrication Step	Method(s) of Inspection	Intention
Mold insert Fabrication	<ul style="list-style-type: none"> • Visual inspection under microscope • Surface profiler 	<ul style="list-style-type: none"> • Check integrity of structures • Verify surface roughness
Polymer Molding	<ul style="list-style-type: none"> • Visual inspection under microscope 	<ul style="list-style-type: none"> • Ensure good mold fill and proper molding of microstructures
Flycutting	<ul style="list-style-type: none"> • Visual inspection under microscope • Thickness measurement using micrometer gauge 	<ul style="list-style-type: none"> • Ensure a good surface finish • Check that through holes are open • To verify the final thickness of part is within specifications
Wiring	<ul style="list-style-type: none"> • Conductivity measurement 	<ul style="list-style-type: none"> • Ensure that the conductive traces are functional
Sealing	<ul style="list-style-type: none"> • Cross section microscopy • Flow test using dye 	<ul style="list-style-type: none"> • Evaluate channel deformation due to sealing process • Ensure proper flow and leak free sealing

Table 5.3: Inspection method employed after each fabrication step.

6. Application Demonstrators

The concept of a modular microfluidic stack was developed into a research platform providing standard chip formats with associated design rules and combined with a set of well defined manufacturing steps. This is the pre-requisite to building customer specific platforms in short turnaround times suitable for preliminary investigation and research projects. The following examples demonstrate the widespread use including cell culture for Hansen's disease studies, giant magnetoresistive (GMR) sensor based bio-detection development, optical interrogation of DNA, magnetic separation of paramagnetic microbeads, microreactor for nanoparticles generation and in-situ analysis, a crystal growth test chip for protein crystallography experiments. A variety of confidential commercial customer applications were undertaken, which cannot be discussed in this thesis. All examples will briefly motivate why microfluidic solutions are of interest and will illustrate the particular stack solution developed. It should be noted that for each example several iterations of design were built and that almost all projects are still ongoing.

6.1. Cell Culture Investigation

Cell culture in a microfluidic environment yields the following specific advantages compared to a conventional petri dish culture -

- Cellular interactions, especially, T cell cytotoxicity assays using adherent target cells can be carried out easily inside microchannels without using radio-isotope markers since the actual number of cells before and after the experiment can be counted and compared to the control.
- Lesser number of cells is required to set up an experiment which is important for investigators working with rare cell sub-populations.
- Live adherent (e.g. Macrophages, Dendritic cells) cells can be fluorescently stained / labeled inside the channel requiring much smaller amounts of reagents.
- During in situ live confocal or single-photon microscopy the temperature of the cells have to be maintained at 37 °C. This is much easier to achieve with a microfluidic chip that has a small thermal mass.

A microfluidic cell growth chip was required to study interactions of *Mycobacterium leprae* bacteria, the causative agent of Hansen's disease. The ultimate goal of this study is to observe the interaction of *M. leprae* with its host cell in the first few hours (~6 hours) post infection using confocal microscopy. This type of analysis can be done much better if there are very few cells and bacteria in close association. Moreover, since it is possible to stain the cells within microchannels without detaching them (which is required if the cells are cultured in plates or dishes) there should be very little background staining (which is increased due to membrane distortions while detaching the cells). The first step towards this effort was to verify survival of the mycobacterium in a microfluidic environment for the maximum duration of the experiment (~12 hrs).

This application required the simplest configuration of the modular microfluidic stack consisting of a standard interconnect chip and a 'microfluidic cell culture chip' bonded together. The initial design for a microfluidic cell culture chip included 4 channels with square cross sections 50 μm , 75 μm , 100 μm and 150 μm (Figure 6.1). However, in initial biological experiments, it was found that even with the largest cross sectional channel (150 μm x 150 μm), the cells perished due to the lack of sufficient media. Hence in the next generation design, the chip was fabricated with a single micro channel (Figure 6.1) with an approximate fluidic volume of 350 μl . This design was based on the known fact that 1.0 ml of media is required to sustain 10^6 healthy cells for ~72 hr in a stationary culture.

The cells flourished in this microchannel setup but it was seen that gaseous waste produced by the cells was being trapped in the fluidic channel as it was sealed airtight (Figure 6.2). Research is in progress for design improvements to allow the removal of the gaseous materials while retaining the aqueous media and the cells. But these initial results have indicated the viability of growing rare population cells in a microfluidic device for experimental studies of small cell populations.

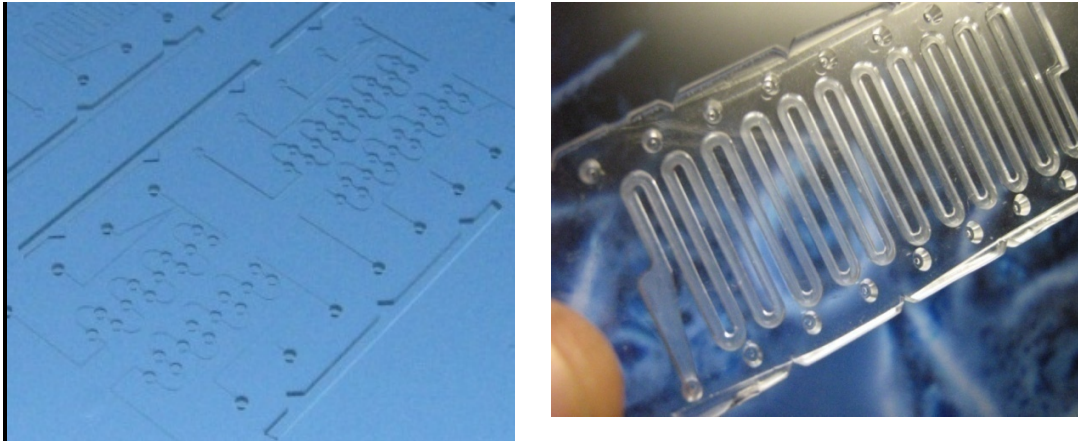


Figure 6.1: First generation chip design for cell culture (Left), second generation chip design (Right) with single serpentine channel.

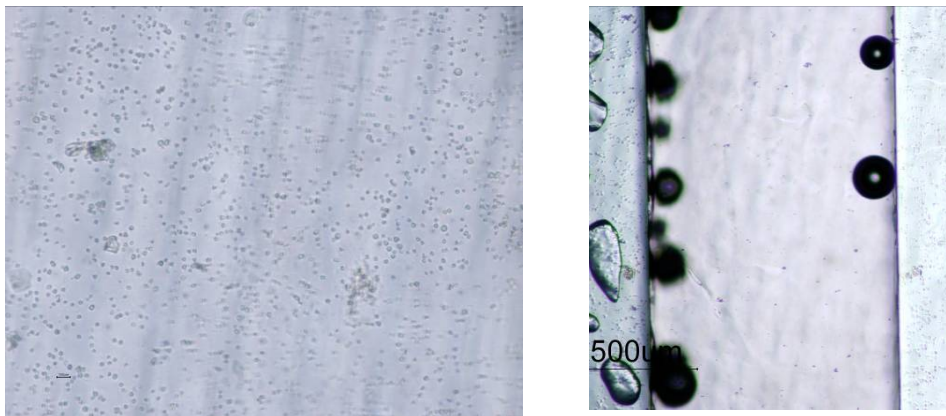


Figure 6.2: Mycobacterium leprae bacteria cells growing in a microchannel (left). Gaseous by products accumulating along the channel sidewalls(right)

Conclusion -Though the initial experiments were not successful, it was possible to quickly adjust the designs and continue the tests without delay. Interaction with customer proved important and the close and dynamic interaction across different scientific disciplines stimulated more ideas and new improved designs to offer working microfluidic solutions to cell biologists.

6.2. Protein Crystallization Platform

Protein crystal structure analysis using X-rays diffraction (also called Protein Crystallography or PX) is the single most important technique in structural biology which allows macromolecules (proteins and nucleic acids) to be visualized on the atomic scale [77]. The resulting structural information, when combined with the results of traditional biochemical experiments, can elucidate the functioning of enzymes (which are all macromolecules) and help design macromolecules fulfilling specific functions, e.g. drug design and enhancement. In recent years PX has moved from a field of basic research to a technique with important practical and commercial applications, the most important one of which is drug design.

To be able to analyze protein structure, macromolecules have to be provided as small crystals. Vapor diffusion [78] is the commonly used method of growing these macromolecular crystals due to the relative ease of setting up trials manually and adaptability to automation. The method is not without drawbacks, as the drops frequently form a skin of denatured protein where their surface is exposed to air which can inhibit crystal growth and recovery of crystals from the drop. The experiments are also very sensitive to temperature changes because the small drop changes temperature much faster than the larger reservoir. This causes a transient disequilibrium which can ruin a successful trial and makes it difficult to recover crystals not grown at room temperature.

An alternate method for growing crystals is by free-interface diffusion in which a small volume of the macromolecule solution and the precipitant solution are placed in contact allowing the precipitant to diffuse into the macromolecule solution. For this method to be effective the mixing must be by diffusion rather than by convection. These experiments are typically done in small capillaries. A microfluidics based experimental bench will offer the advantages of automation and economic parallel screening of modified mixtures while retaining the advantages of free-interface diffusion.

The desired experimental approach is to place plugs of macromolecules and precipitant in contact and isolate them with plugs of a non miscible fluid like oil (Figure 6.3). A microfluidic stack solution consisting of two chip layers has been fabricated as illustrated in Figure 6.4. The first chip consists of a junction structure where the alternate plugs of macromolecule solution and oil are generated. This mixture is then pushed into the second chip layer which consists of a serpentine storage channel. After filling with many plugs of slightly different mixtures the storage chip can be disconnected from the plug forming chip and placed in an environment where temperature and pressure may be varied to screen for ideal crystal growth conditions.

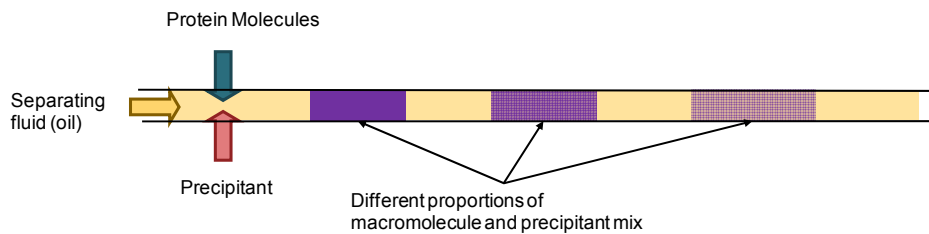


Figure 6.3: Schematic of desired fluid injection protocol in microchannel for protein crystallography experiments. Plugs of aqueous protein-precipitant mix are separated by plugs of oil.

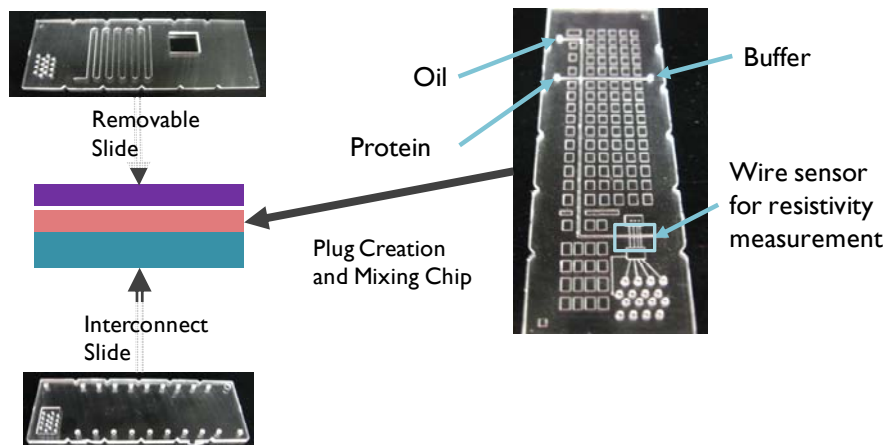


Figure 6.4: Arrangement of the protein crystallization experimental setup with a three layer chip stack forming the complete system. The first layer for interconnection, second for creating the aqueous-oil plugs and the third for storing the protein-precipitant mixtures

Controlled volumes of liquid are pumped into the first chip via synchronized syringe pumps to create the precipitant-macromolecule plugs, separated by plugs of oil. A means of measurement has to be incorporated into the plug forming chip in order to measure and control the plug volumes. This is an important feature for future process automation. This is achieved by using conductive wires running across the microfluidic channel to carry out a resistive measurement of the fluid.

This aqueous plug formation as well as the monitoring mechanism was successfully tested. Initial data was acquired using an USB-based analog-digital converter and data acquisition system (USB-1208FS, Measurement Computing¹⁶) and is illustrated in Figure 6.5. The results show that simple resistivity measurement allows plug formation analysis. The data also shows that further improvement in controlling the motion of the synchronized syringe pumps is needed before uniform plugs are formed throughout the run.

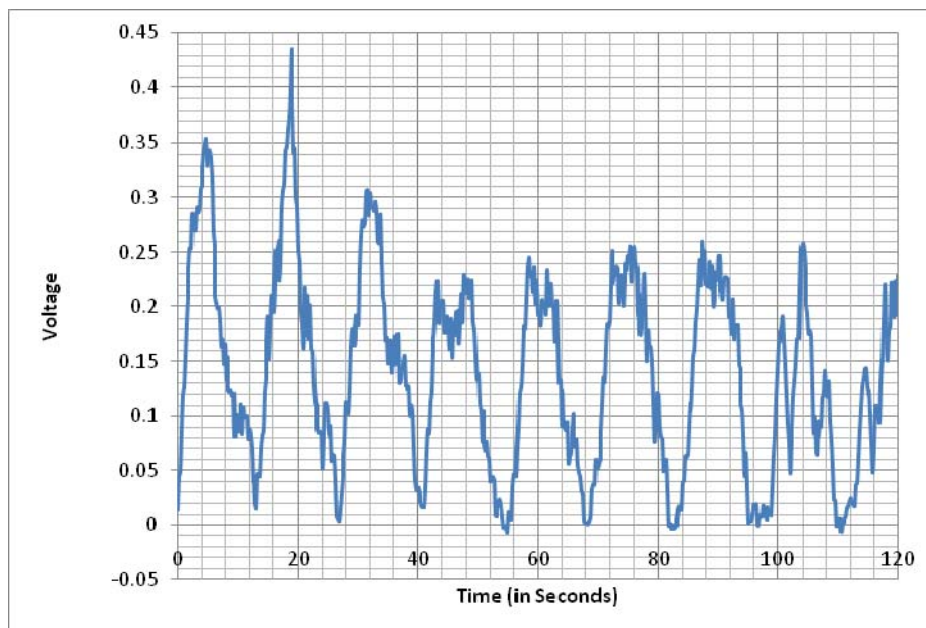


Figure 6.5: Voltage waveform measured by electrodes across the microfluidic channel. The peaks indicate the passage of an aqueous plug and the valleys indicate the passage of an oil plug. The data was acquired using as USB based analog to digital converter.

¹⁶ <http://www.measurementcomputing.com/>

Conclusion – This two layer stack consisting of a mixing and storage chip demonstrates an attractive solution to allow parallel screening of crystal forming mixtures. Another upgrade on the pumping hardware and control unit is needed before optimized performance (SIP) is realized.

6.3. Giant Magneto-Resistive Sensor (GMR) based Bio-Detection

The microfluidic development platform was used to assist in 3 different aspects of a larger development effort geared towards developing a sensing system for airborne biological threats. The methodology for detection is illustrated in Figure 6.6.

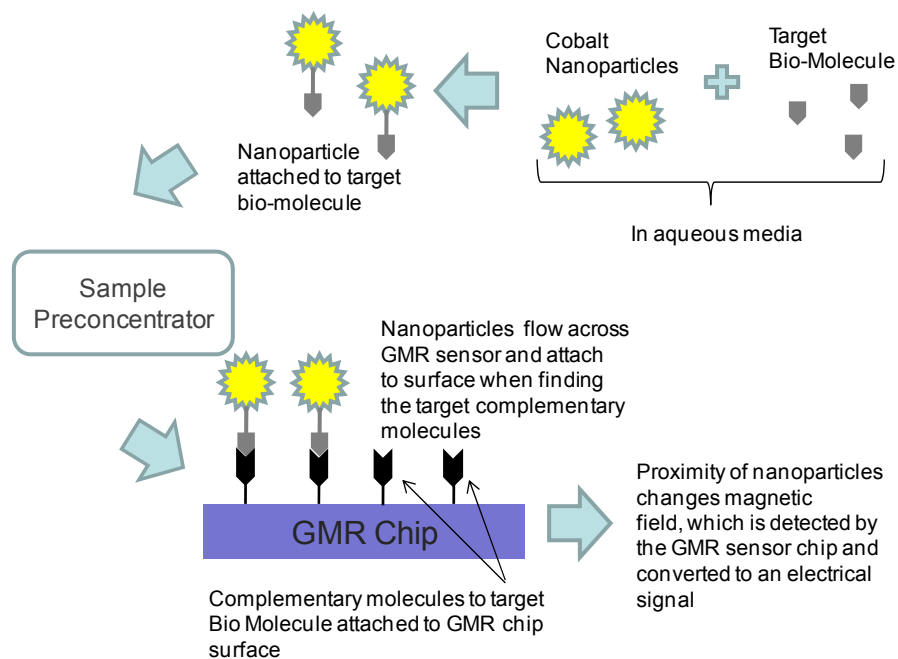


Figure 6.6: Schematic illustrating the working of the GMR based bio-detection device.

A sample containing the biological target molecule is mixed with functionalized magnetic cobalt nanoparticles that are suspended in aqueous media. Once attached to the nanoparticles, the sample concentration can be increased by using a magnetic preconcentrator. The concentrated sample volume is then passed through a microfluidic channel structured on the surface of a silicon based GMR chip. The GMR chip surface is prepared with complementary molecules to allow selective

binding of the target molecules. The molecule binding brings the magnetic nanoparticles close to the GMR surface causing a change in the GMR resistivity and provides a detectable electrical signal. While the principle is simple, its realization is challenging and requires design and research in multiple science and engineering disciplines including –

- silicon microfabrication and electronic packaging to fabricate the GMR sensor board;
- a magnetic preconcentration unit ;
- a microfluidic channel system to bring the fluid in contact with the GMR sensor;
- a fluidic handling system;
- nanotechnology to fabricate the cobalt beads ;
- a bio-protocol to bind the sample/target molecules to the beads and GMR surface;
- an electronic control and signal processing unit;

Each aspect requires a specific module as a research task, as illustrated in Figure 6.7, which then have to be combined to achieve the overall sensor function.

The microfluidic development platform was used to carry out focused research and development on 3 different aspects of the overall development effort –

1. Surface chemistry screening for complement binding on the GMR chip surface.
2. Pre-Concentration of magnetic particles.
3. Real-time X-ray analysis of nanoparticles production chemistry.

The details of these tasks are explained in more detail in the following sections.

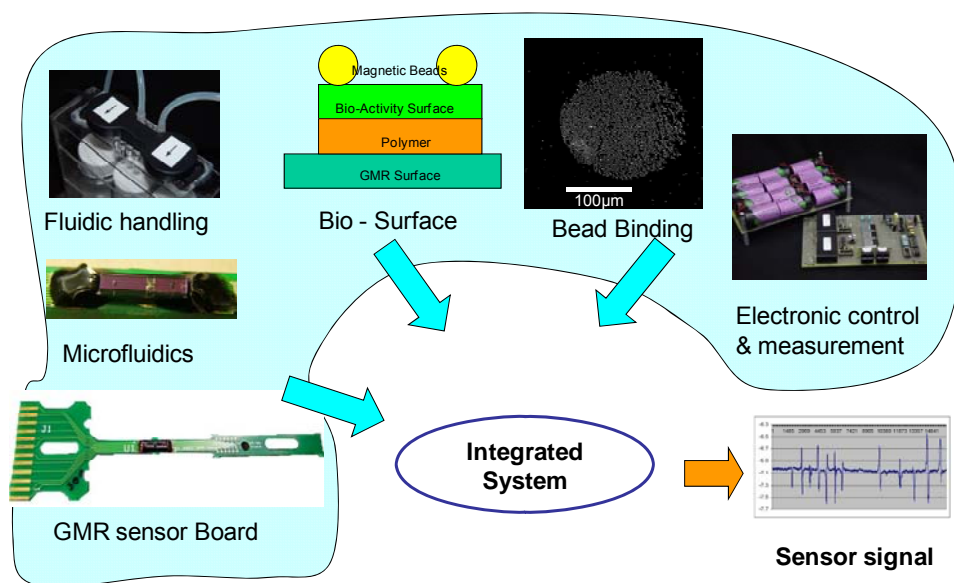


Figure 6.7: Schematic illustrating the various modules of the GMR based sensor system being developed.

Surface Chemistry Screening

As part of the GMR based detection device development effort, appropriate biological molecules had to be attached to the surface of the GMR sensor chip. One way of applying molecules is through microspotting on a specially prepared surface which requires systematic screening studies of bio-binding chemistry to develop the appropriate bio-protocol. Since GMR chips are expensive, the screening experiments were carried out using dummy silicon chips with a silicon nitride surface, identical to that of the actual GMR chips. It was also desired that the screening experiments be run in a microfluidic environment similar to the final application. To accomplish this, a polymer microfluidic chip was fabricated with cavities for the dummy silicon chips and connected microfluidic channels that allow controlled flow of different liquids over the surface of the inserted silicon chips shown in Figure 6.8a. The polymer chip was designed to accommodate 12 silicon chips. A temporary clamping method was used to seal the microfluidic chip and form a closed pathway for the reagents. After completion of the fluidic experiment the lid can be removed allowing a close up qualitative optical inspection of the reaction results as shown in Figure 6.8b where Streptavidin coated paramagnetic beads are bound to a biotinylated surface. Aspects such as uniform coverage and low background binding

in the regions outside of the spotted bioactive area can easily be inspected and provide immediate feedback to the biologist.

A more quantitative method uses fluorescence labeled target molecules. In this experiment, the silicon dies were first pre-processed using dip chemistry and by covalently coating with protein conjugate using a sequence of aminopropyltriethoxysilane, gluteraldehyde, and strepavidin – horse radish peroxidase (S-HRP) treatment.



Figure 6.8a: Microfluidic chip with silicon die inserts for biological screening experiments.

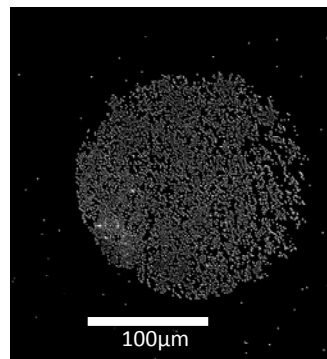


Figure. 6.8b: Brightfield image of Dynal M-280 2.8 μm Strepavidin coated paramagnetic beads bound to a biotinylated surface.

After completing the surface treatment the chip surface was temporarily sealed and a chemiluminescent material (Pico Supersignal, Pierce Biotechnology, Inc.) was then flowed through the microfluidic channels to interact with the silicon die surfaces. In order to determine the detection limit GMR chips with 1:10 serial dilutions of the Strepavidin – Horse Radish Peroxidase protein conjugate were placed in different chambers and the chemiluminescent signal produced by the interaction with the Pico Supersignal was captured using an X-ray film placed directly on top of the microfluidic stack. After development the film was scanned into digital format. Then the mean was calculated for relevant regions with SCION software (public domain from NIH) and results are shown in Figure 6.9.

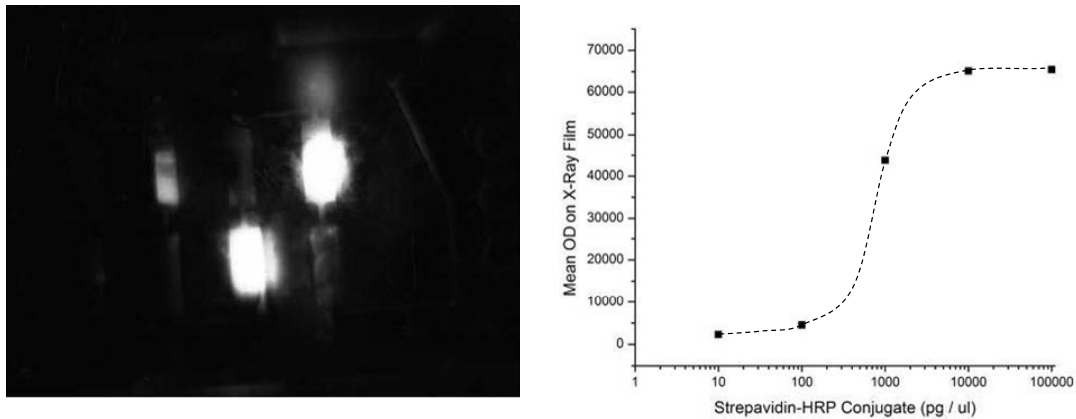


Figure 6.9. Image to the left shows light intensity for different conjugate concentrations while the graph to the right illustrates the results of a quantitative analysis of the signal.

Conclusion – The resultant graph shows that the biochemical system exhibits a low signal below a Streptavidin-HRP concentration of 100 pg/ μ l and signal saturation beyond a concentration of 10000 pg/ μ l. Open access to the chip surfaces allowed the biologist to prepare a biological surface using existing lab equipment and enabled him to optimize the bio-protocol, in a format that was similar to the final microfluidic application setup. An experimental setup that was identical to the final application is crucial for easy transfer of experimental results into a developed MEMS system.

Magnetic Separation

A major challenge for any biological sensor using microtechnology solutions is to reduce the real world sample volume (on the order of milliliters) to a volume on the order of nanoliters without losing any of the target molecules. As the GMR sensor uses magnetic particles to label the sample molecules, using magnetic fields to manipulate the microbeads inside a microfluidic channel is a reasonable approach for sample preconcentration that has also been explored by others [19, 79].

In order to develop the case specific layout for magnetic preconcentration, a microfluidic chip layer was fabricated with microfluidic splitter structures and cavities for introducing permanent or electromagnets (Figure 6.10). The modular microfluidic stack was temporarily sealed using a gasket layer and experiments were carried out

to observe the manipulation of a continuous flow of particle loaded fluid as a function of magnetic field strength.

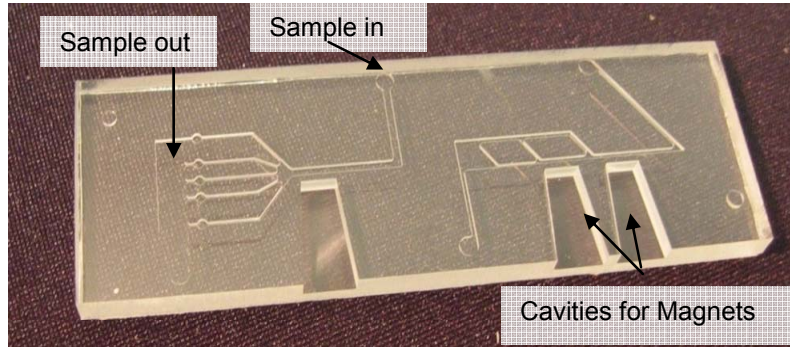


Figure 6.10: A microfluidic chip for experiments on separation of magnetic microbeads under the influence of a magnetic field produced by a permanent magnet or electromagnet.

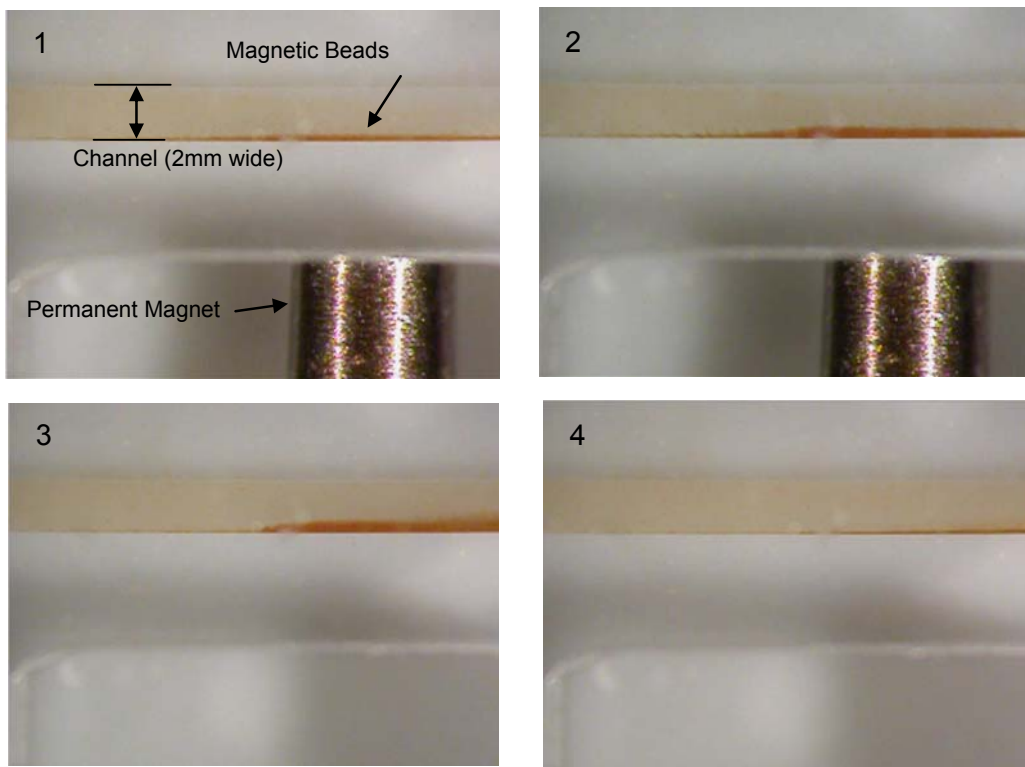


Figure 6.11: Beads being captured and released in a microfluidic channel using a permanent magnet.

Figure 6.11 shows a close up view of the fluidic channel on the microfluidic chip. By introducing a permanent magnet into the cavity adjacent to the channel while the

fluid is passing by, the magnetic beads agglomerate along the channel wall. As the magnet is removed, the beads disperse and flow away down the channel.

While this first experiment demonstrates the feasibility of magnetically manipulating the flow of magnetic beads by permanent magnets, it is required for the actual application that the manipulation be turned on and off easily using electromagnets. Magnetic fields can be generated by wire traces deposited adjacent to one segment of a Y-branch diverter in a channel, a concept that was illustrated by Pekas et al[80]. The wire is deposited by metal evaporation as described in Section 5.3.2. The assembled microfluidic chip stack is shown in Figure 6.12. The inset picture is a close up showing the gold wire trace running parallel to one branch of the channel designed to direct the magnetic particles into it.

Conclusion - The flexible adjustments offered to the demands of a diverse group of users (biologists, electrical engineers) demonstrate the opportunities of the stack platform but also illustrates the need to continuously expand and improve its capabilities.

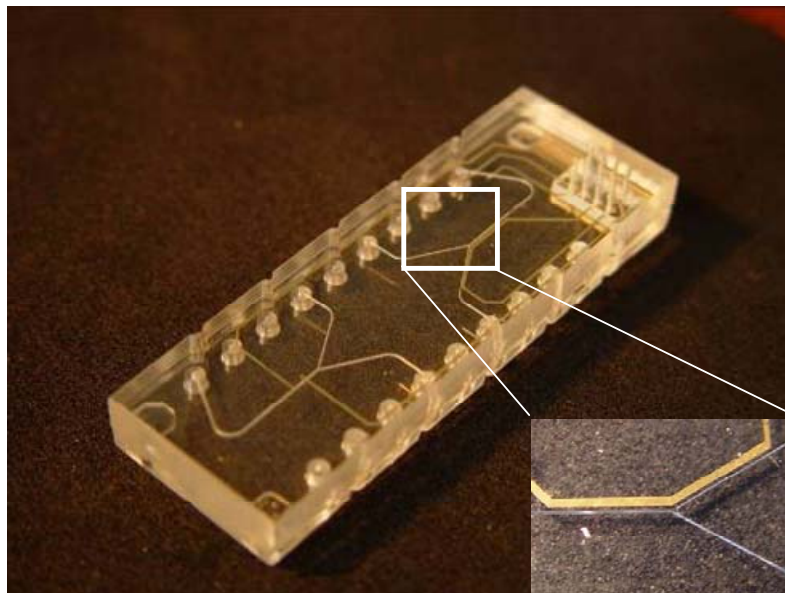


Figure 6.12: Assembled and sealed microfluidic stack with wire traces for magnetic guiding and conductive sensing of microbeads.

6.4. Nanoparticle Reactor for X-Ray Analysis

Polymer based microfluidic reactors are a promising technology for wet chemical synthesis of nanoparticles. A group at CAMD has been involved in the synthesis of magnetic cobalt nanoparticles due to its unique properties and applications in high-density magnetic recording media, nanobiotechnology, catalysis and sensors [81-83]. These cobalt nanoparticles are also used as labels in the microreactor system for the GMR project (Section 6.3). Wet-chemical synthesis is one promising approach for industrial applications as it provides good control over the reaction conditions and because of its intrinsic scale-up potential by parallel processing using many identical reactors.

It was recently demonstrated that microreactors offer a better control on reaction kinetics parameters than the conventional “flask” technique due to efficient heat and mass transfer and they have been successfully utilized for size control synthesis of nanoparticles [28, 84, 85]. A continuous flow microreactor was being used for the synthesis of cobalt nanoparticles from a cobalt acetate tetrahydrate (1.0 g, 4.0 mmol) and sodium dodecyl sulfate (SDS) (10.0 g) and a reducing agent (an aqueous solution of NaBH_4 (0.4 g, 10 mmol) in 10 mL of water).

Once produced, the nanoparticles are typically characterized by Transmission Electron Microscopy and X-ray absorption spectroscopy technique to analyze structural and electronic changes in the system. Initial studies showed that precursor and reaction conditions effect the properties of the particles and that in-situ measurements while the reaction process is taking place will yield a better understanding of the process and valuable structural-dynamic information about the reaction path of nanoparticle synthesis [86].

To make this possible, a microfluidic stack was designed with the nanoparticle reactor as one of the layers of the stack. The stack was then placed in the path of an X-ray beam (CAMD, X-ray Micro-Probe Beamline) in order to carry out real time analysis of the nanoparticles as they are formed. The designed microfluidic structure included a junction of two flow paths followed by a serpentine section for mixing. The

chip (Figure 6.13) consists of two such reactor structures, one with channel dimensions $200\ \mu\text{m} \times 200\ \mu\text{m}$ and the other $500\ \mu\text{m} \times 500\ \mu\text{m}$. An interconnect chip with fluidic ports was sealed to the reactor chip to form the microfluidic stack. Tubes were fitted into the fluid ports and sealed permanently using hot melt glue. This method of interconnection was used because the stack had to be placed in an X-ray chamber surrounded by electrical circuitry and the possibility of accidental leaks had to be avoided.

As the two components, cobalt acetate tetrahydrate and sodium dodecyl sulfate, meet at the junction of the microreactor and start flowing down the mixer section, nanoparticles synthesis takes place. By looking at different positions along the mixer path one can collect information corresponding to different times after the reaction started.

The micro fluidic reactor was fixed on the positioning stage of the Kirkpatrick-Baez focusing system of x-ray microprobe double crystal monochromator beamline (Figure 6.14b). A schematic drawing of the experimental set-up for obtaining in-situ X-ray Absorption Near Edge Structure (XANES) data is shown in Figure 6.14a. XANES data of Co nanoparticles were collected at two positions of the microchannel: at the very beginning (starting point of the reaction) and at the end of the channel, corresponding to the end of the reaction time. Thus by analyzing the reaction at different spatial positions along the length of the channel time resolution of the reaction process is achieved.

The XANES spectra are displayed in the Figure 6.15 along with the spectrum of a Co foil used as reference. Pre-edge shoulder (A), as a characteristic feature of 3d transition metals which is assigned to symmetry-forbidden transitions of 1s core electrons to 3d empty states can be used as an indicator for the pure metallic phase present in the sample. The intensity of the 1s-3d transition (height of pre-edge shoulder) has been increased from the “start” of the reaction until the “end”, indicating a continuous growth of the synthesized nanoparticles.

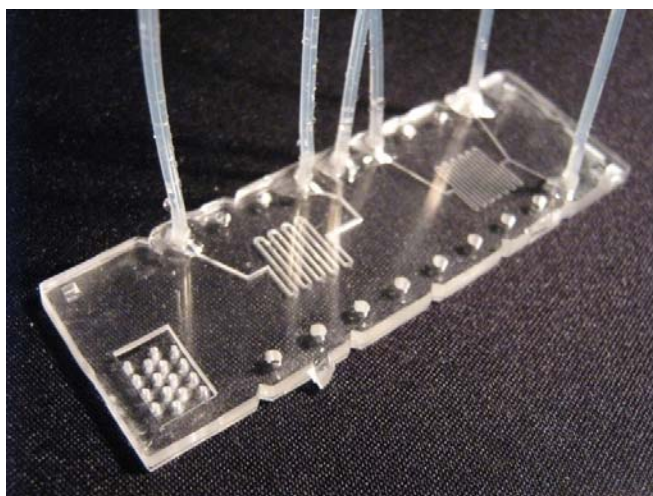


Figure 6.13: Real time X-ray spectroscopy chip for nanoparticles synthesis.

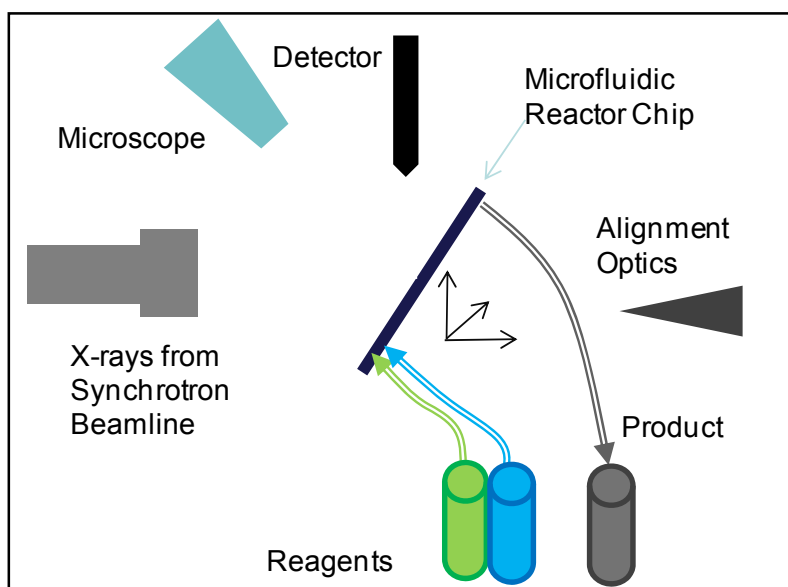


Figure 6.14a: Schematic illustrating the experimental setup used during XANES analysis of nanoparticles reaction.

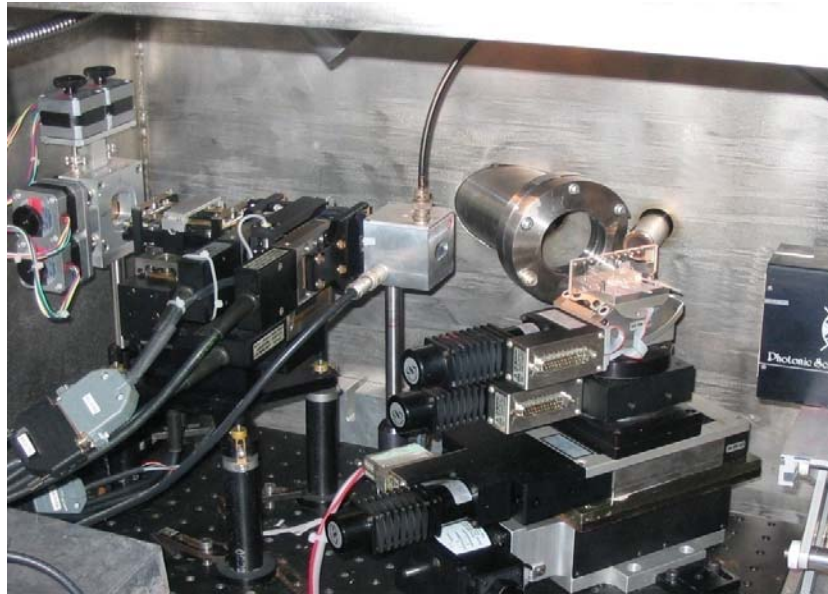


Figure 6.14b: Image of experimental setup of microfluidic reactor inside X-ray chamber.

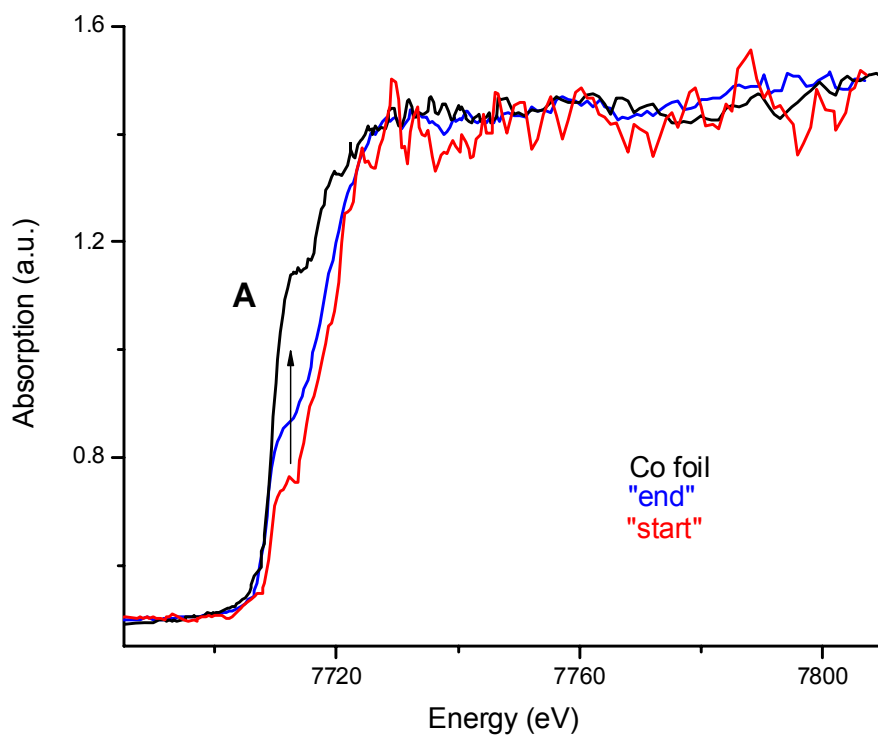


Figure 6.15: In situ Co K-edge XANES spectra of Co nanoparticles formed at the beginning of the microreactor (red) and at the end (blue) in comparison with Co foil (black).

Conclusion - The initial results demonstrate that the formation of Co nanoparticles can be analyzed with XANES as the spectrum taken near the mixing point is somewhat different from the one taken later (at the end of the 100mm long mixing channel, after 50 seconds of reaction time). Though the quality of the spectra needs further improvement these initial results clearly show the potential of using microtechnology solutions for time resolved in-situ investigations of chemical reactions by translating time into position in the reactor and benefiting from the controlled flow conditions within microfluidic channels.

6.5. Embedded Optical Waveguide for Fluorescence Excitation

Fluorescence detection is a commonly used optical detection method for biological samples [6]. In microfluidic chips, the molecules being interrogated by fluorescence are confined in channels, either free floating or bound to the channel floor and walls. Conventional waveguides and optical fibers [87] have been used in the past to deliver light to a certain point in a fluidic channel generating fluorescence excitation at that specific location [88]. However, the intention here was to replace the local excitation with an extended region excitation, activating all the fluorescent probes contained along the length of a microfluidic channel. Such a waveguide can be combined with an array of fluorescence probes to enhance the detection in a multitude of applications. For example, integrating it with a polymerase chain reaction (PCR) device will provide real-time information about the reaction taking place or a zipcode assay could be microspotted along the length of the channel and illuminated simultaneously using a single light source allowing parallel screening.

The idea to combine optic and fluidic functions was a 'leaky' waveguide embedded into the channel floor serving the function of delivering light to the fluorescent probes that are attached to the floor of the fluidic channel above it (Figure 6.16). The polymer chips were fabricated employing a single step double sided embossing process (Figure 6.17b). In order to confine light to the bottom region of the waveguide and also minimize stray light interfering with the measurement, the channel was shaped as shown in Figure 6.17a

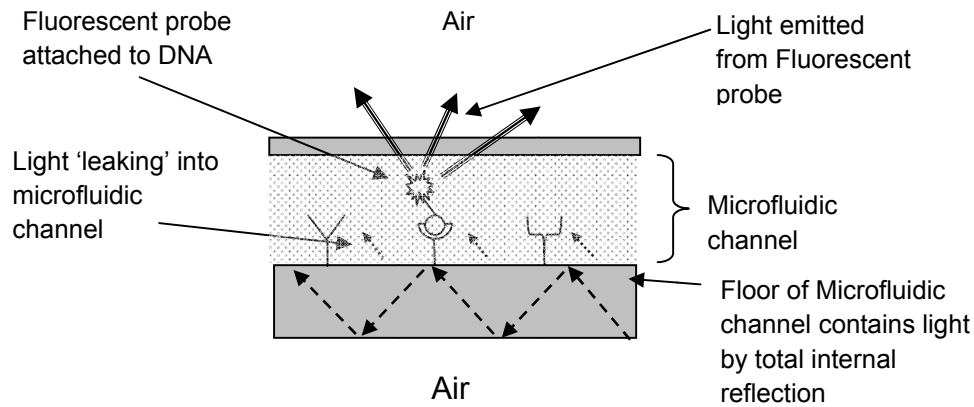


Figure 6.16: Schematic of a cross section along the length of a channel on the fluidic-optic chip.

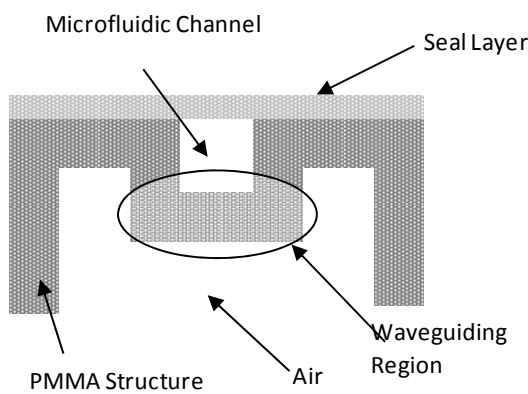


Figure 6.17a: Schematic cross section of chip.

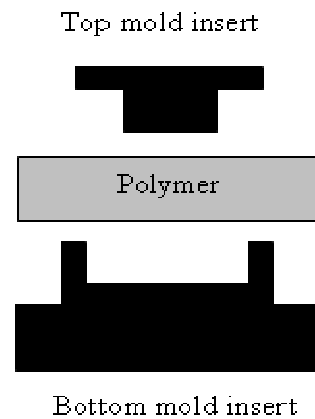


Figure 6.17b: Schematic of double-sided hot embossing used to fabricate microfluidic chip with integrated waveguide.

A typical waveguide consists of a high refractive index core enclosed in a low refractive index cladding material. In this opto-fluidic chip, PMMA forming the floor of the microfluidic channel also acts as the core of the waveguide. Air on the bottom and the sides and aqueous fluid in the fluidic channel on the top, shown schematically in Figure 6.17a, act as the low refractive index cladding material [$\eta_{\text{pmma}}(1.49) > \eta_{\text{fluid}}(1.33) > \eta_{\text{air}}(1.00)$]. Thus this structure confines light in the

waveguiding region and also forms the bottom of the fluidic channel. The molded microfluidic chip is shown in Figure 6.18a and a cross section of the chip is shown in Figure 6.18b.

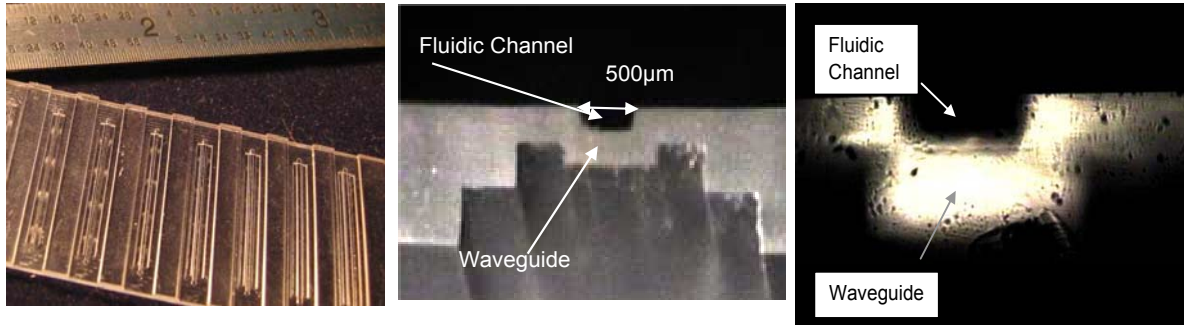


Figure 6.18a: Image of molded polymer chip with multiple embedded waveguides.

Figure 6.18b: Image of the cross section of a single fluidic channel and waveguide.

Figure 6.18c: Optical microscope image of light emanating from the waveguide.

The microscope image in Figure 6.18c shows the cross sectional profile of light confined in the waveguide structure. It can be seen that most of the light is confined to the waveguide core region. The performance of the waveguide chip was tested on an optical bench setup (Fig 6.19a,b) by coupling light into it and measuring fluorescence intensity along its length. A 635nm wavelength, 2mW laser diode was used as the light source. A multi-mode fiber was used to deliver light to the chip from the laser source. Light was passed through a band pass filter (625nm-645nm, Omega Optical, Brattleboro, VT), and was then projected into the waveguide using a microscope objective. The light was coupled through the edge face into the waveguide. The microchannel on the chip was filled with a 5 ng/μl ΦX174/HaeIII DNA digest intercalated by a TOPRO3 dye. Fluorescence emission was collected using a 4X microscope objective and Zoom 6000 microscopy tube (Navitar, NY) adjustable from 0.7X to 4.5X, and detected by a Cascade 1K Photometrics CCD camera (Roper Scientific, NJ). A band pass filter (570nm-610nm, Omega Optical) was used to isolate the emitted fluorescence light from the background and excitation wavelengths.

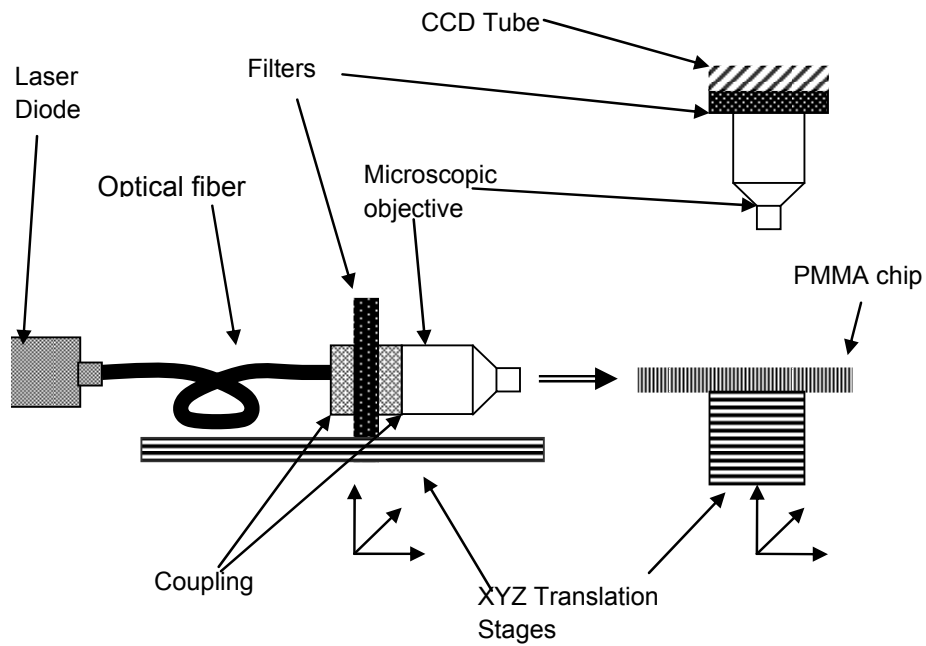


Figure 6.19a: Schematic of the experimental setup for measuring fluorescence intensity.

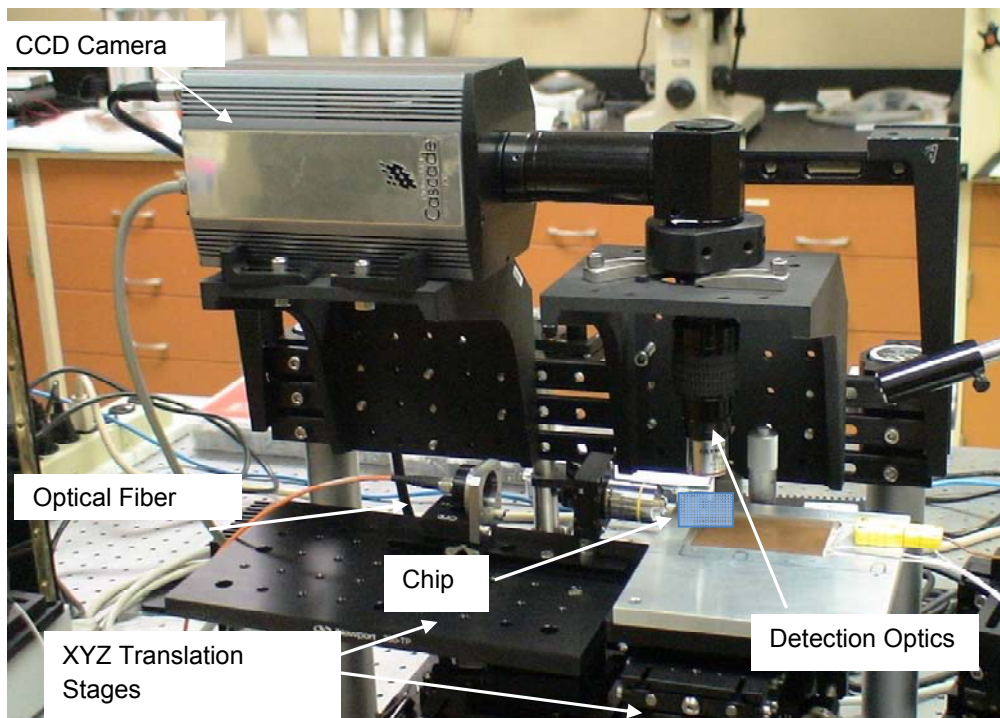


Figure 6.19b: Optical bench setup used for fluorescence intensity measurements.

Using this experimental setup, fluorescence intensities of labeled DNA was detected at different positions along the length of the channel. It can be seen from the results plotted in Figure 6.20 that the fluorescence intensity attenuates as we move away from the point where light is coupled into the waveguide. These losses are due to absorption of light in the material (PMMA), as well as scattering from the surrounding interfaces that are not perfectly smooth and defect free. However, the losses are less than 20% over the 20 mm distance, indicating an acceptable uniformity. The inset picture in Figure 6.20 shows a fluorescence image as dye in the microchannel channel is excited by light from the waveguide under it.

In subsequent experiments, the channels were microspotted with fluorescent markers which were excited through the embedded waveguide. Figure 6.21 shows the resultant fluorescence from the markers in the channel.

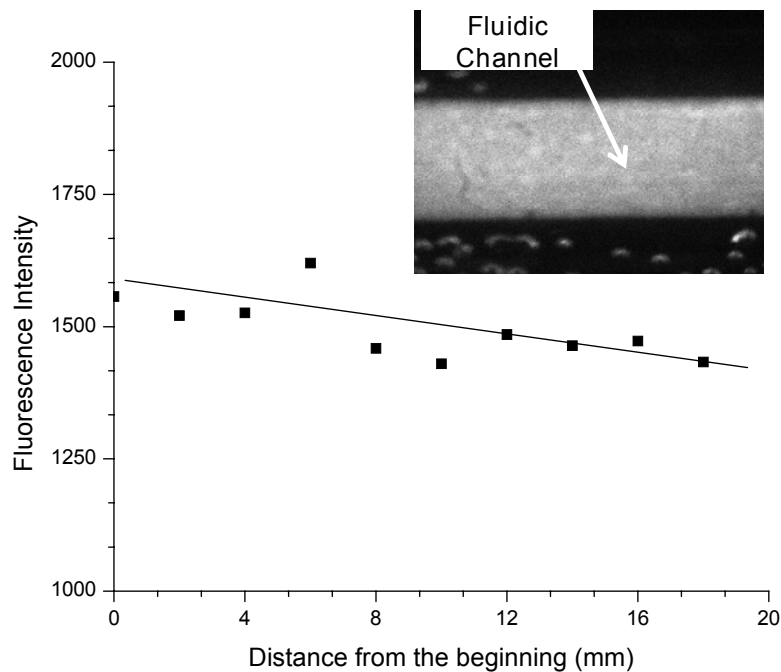
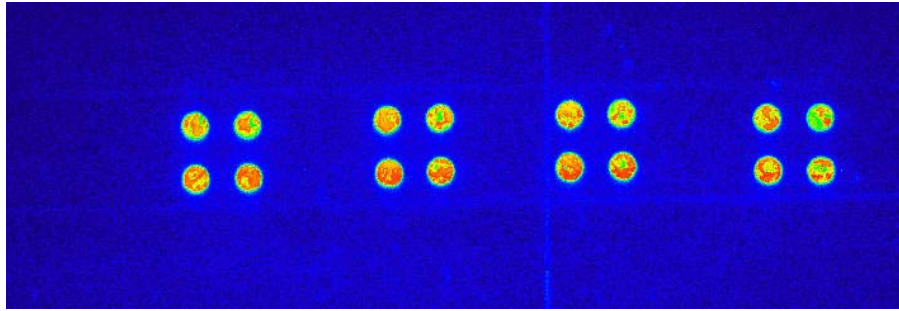


Figure 6.20: Fluorescence intensity measured at different distances from the beginning of waveguide. Inset - Fluorescence image of DNA labeled with a TOPRO3 dye in a microfluidic channel with an incidence laser at the side surface of PMMA waveguide.



0

65535

Figure 6.21: Analysis of Alexa Fluor 660-labeled oligonucleotide marker (1 μM) dispensed in a 500- μm wide channel with spot size of 150 μm , center to center spacing of 300 μm . The waveguide-embedded channel was irradiated by oxygen plasma for 2 min, activated by EDC, incubated at 37°C for 1 h. The excess probes were washed with 0.1% SDS, and detected by the evanescent fluorescence microscopy with prism coupling laser into the waveguide.

Conclusion- In order to meet the application requirement of combining optical and fluidic function, an improved fabrication process was developed providing more advanced quasi 3-D patterning ability of polymer sheets. By using the floor of the fluidic channel as optical waveguide, very compact, highly functional opto fluidic chips can be built with a simple fabrication process. Light is currently launched from the side into the waveguide but new designs will include more sophisticated coupling optics. E.g. - 45° mirror that will allow light to be launched from either top or bottom in full agreement with the vertical stack concept.

The polymer microfluidic stack was effectively used as a platform for developing various experiments and application prototypes in a very short time. This was possible due to the established standard designs in combination with well understood fabrication processes. Projects utilizing this infrastructure are in various stages of progress and constant improvements are being made to the initial designs, supporting the use of MEMS solutions in life science applications.

7. Conclusion

The overall goal of this thesis was achieved by designing, fabricating and testing a microfluidic development platform and successfully using the system in a number of different biological applications. The platform consists of three principle units – the Modular Microfluidic Chip Block (MMC) consisting of a vertical stack of individual microfluidic chips, an Interconnect Block (ICB) providing a mechanical alignment support frame for the MMC and convenient macro-micro as well as micro-micro interconnect features, and a Supplies and Instrument Block (SIB) which will be flexibly configured according to the application and customer needs. It typically consists of standard laboratory and electronic equipment to which the platform is interconnected.

Individual chips with a footprint of 1" x 3" are forming the MMC Block made from polymer materials using a rapid prototyping fabrication approach combining micromilling and hot embossing. This approach best suits the typical user requirements of fast turnaround time, easily changed designs, and moderate fabrication costs for typically less than 20 chips. In the course of this thesis a methodology was developed using sensor information available from the Jenoptik HEX2 hot embossing machine that allows process optimization for different designs, mold inserts as well as a wide variety of thermoplastic materials including PMMA, PC, PS, COC, PP, and others with only a few tests. A design of experiment (DOE) was conducted to understand structure tolerances as a function of critical process parameters and provide design guidelines for the chip layout. The study revealed that demolding temperature is the most critical process parameter for maintain tight dimensional control.

In order to meet the requirement of a flexible and easy to reconfigure MMC stack a passive alignment approach based on elastic averaging was implemented utilizing the outside perimeter of the molded chips in combination with a mechanical frame embedded in the ICB. Overlay accuracy ranging from better than 100 μ m down to

20 μm is possible when considering the design guidelines from the DOE study. This will allow the transfer of fluids through vias of similar dimensions from one chip to the other with only minor disturbance of the flow. Another critical aspect is sealing of fluidic chips. Within the scope of this research two different methods suitable for temporary and permanent sealing have been established and employed regularly. The temporary solution uses cast silicone gaskets, typically a few hundred μm thick, and suitable for sealing of larger structures down to 500 μm . For tight seals of smaller structures (down to 50 μm) thermal bonding was successfully applied using a dedicated press designed and built as part of this research. A variety of post-processing steps are employed to finish the molded chips, for example opening of through-holes by fly-cutting or micro-drilling, and adding conductive pattern by metal deposition through a shadow mask.

The ICB is designed as structural block with interface features to the macro world, a microfluidic backplane, and the mechanical clamping frame needed for passive alignment. Macrofluidic ports enable the 'plug&play' interconnect of syringe pumps but can be replaced with other customer-defined fluid connector such as Luer fittings. The fluidic backplane is a user-specific fluid routing chip that connects any outside reservoir with a user-defined microchannel.

The potential of the microfluidic development platform was verified in a number of experiments. A cell culture chip for Hansen's disease studies was built and initial studies demonstrated that cells can survive for the study time of up to 10 hours. In-situ optical monitoring with an optical microscope also showed that cell waste is the main reason for cell death and needs to be avoided in future experiments. Another project focused on using a giant magnetoresistive (GMR) sensor as bio-detector required a number of modules for investigations of bio-surface functionalization, bio-protocol studies, magnetic field supported pre-concentration, and wet-chemical synthesis of magnetic nanoparticles. A variety of modules have been constructed helping to optimize the different functional aspects of the sensor system. Another project required the development of an opto-fluidic chip which combines in one chip both, optical and fluidic function. This chip was successfully used to generate

fluorescent signals from spot arrays embedded in a fluidic channel and allowing parallel screening for different biological targets in one fluidic device. Two last examples deal with microfluidic structures for wet-chemical reactions. Both designs allow systematic studies of reaction parameters and how they impact the properties of the final product – magnetic nanoparticles and protein crystals. They also provide a platform that allows in-situ analysis using synchrotron radiation based spectroscopy methods, X-ray Absorption Near-Edge Spectroscopy (XANES) and Protein Crystallography (PX), respectively.

In conclusion, the current and future potential of the microfluidic development platform has been shown and has already sparked many new projects. Through the close interaction with users and their needs it became obvious that this platform remains a 'work in progress' requiring continuous research and development efforts in all aspects from design to fabrication and application. The existing solution provides both a reliable and useful solution for existing research projects as well as an open forum to incorporate new ideas and challenges accelerating the use of MEMS solution for multi-domain microfluidic applications.

References

1. *Market analysis for microsystems II 2002-2005, A NEXUS Task Force Report.* 2002, NEXUS.
2. Reyes, D.R., D. Lossifidis, P.-A. Auroux, and A. Manz, *Micro total analysis systems. 1. Introduction, theory, and technology.* Analytical Chemistry, 2002. **74**(12): p. 2623-2636.
3. Wang, H.-Y., A.K. Bhunia, and C. Lu, *A microfluidic flow-through device for high throughput electrical lysis of bacterial cells based on continuous dc voltage.* Biosensors and Bioelectronics, 2006. **22**(5): p. 582-588.
4. Soper, S.A., D.C. Williams, Y. Xu, S.J. Lassiter, Y. Zhang, S.M. Ford, and R.C. Bruch, *Sanger DNA-sequencing reactions performed in a solid-phase nanoreactor directly coupled to capillary gel electrophoresis.* Anal Chem, 1998. **70**(19): p. 4036-43.
5. Jacobson, S.C., R. Hergenroder, L.B. Koutny, and J.M. Ramsey, *High-Speed Separations on a Microchip.* Analytical Chemistry, 1994. **66**(7): p. 1114-1118.
6. Mogensen, K.B., H. Klank, and J.P. Kutter, *Recent developments in detection for microfluidic systems.* Electrophoresis, 2004. **25**(21-22): p. 3498-3512.
7. Schomburg, W.K., J. Fahrenberg, D. Maas, and R. Rapp, *Active valves and pumps for microfluidics.* Journal of Micromechanics and Microengineering, 1993. **3**(4): p. 216-218.
8. Xia, F., S. Tadigadapa, and Q.M. Zhang, *Electroactive polymer based microfluidic pump.* Sensors and Actuators A: Physical, 2006. **125**(2): p. 346-352.
9. Andersson, H. and A. van den Berg, *Microfluidic devices for cellomics: a review.* Sensors and Actuators B-Chemical, 2003. **92**(3): p. 315-325.
10. *Website for Accu-Chek* <http://www.accu-chek.com/>. [cited 2007 January 5th].
11. *Website for Abbot Point of Care, manufacturers of the I-Stat device* <http://www.abbottpointofcare.com/istat/>. [cited 2007 January 5th].
12. *Website for Affymetrix, Manufacturers of the GeneChip® Instrument System -* <http://www.affymetrix.com/>. [cited 2007 January 5th].
13. Madou, M.J., *Fundamentals of microfabrication.* 1997: CRC Press.
14. Mock, T., L. Curilla, B. Holroyd, and R.W. Yatscoff, *Clinical evaluation of the i-STAT analyzer.* Clinical Biochemistry, 1995. **28**(3): p. 336-336.

15. Terry, S.C., J.H. Jerman, and J.B. Angell, *Gas Chromatographic Air Analyzer Fabricated on a Silicon Wafer*. IEEE Transactions on Electron Devices, 1979. **ED-26**(12): p. 1880-1886.
16. Esashi, M., S. Shoji, and A. Nakano. *Normally close microvalve and micropump fabricated on a silicon wafer*. 1989. Salt Lake City, UT, USA: Publ by IEEE, Piscataway, NJ, USA.
17. Shoji, S., M. Esashi, and T. Matsuo, *Prototype miniature Blood Gas Analyzer Fabricated on a Silicon Wafer*. Sensors and Actuators, 1986. **14**(2): p. 101-107.
18. Woolley, A.T. and R.A. Mathies, *Ultra-High-Speed DNA-Sequencing Using Capillary Electrophoresis Chips*. Analytical Chemistry, 1995. **67**(20): p. 3676-3680.
19. Choi, J.W., K.W. Oh, J.H. Thomas, W.R. Heineman, H.B. Halsall, J.H. Nevin, A.J. Helmicki, H.T. Henderson, and C.H. Ahn, *An integrated microfluidic biochemical detection system for protein analysis with magnetic bead-based sampling capabilities*. Lab on a Chip, 2002. **2**(1): p. 27-30.
20. Schiff, H., C. David, M. Gabriel, J. Gobrecht, L.J. Heyderman, W. Kaiser, S. Koppel, and L. Scandella, *Nanoreplication in polymers using hot embossing and injection molding*. Microelectronic Engineering, 2000. **53**(1-4): p. 171-174.
21. Narasimhan, J. and I. Papautsky, *Polymer embossing tools for rapid prototyping of plastic microfluidic devices*. Journal of Micromechanics and Microengineering, 2004. **14**(1): p. 96-103.
22. Truckenmuller, R., Z. Rummler, T. Schaller, and K. Schomburg, *Low-cost thermoforming of micro fluidic analysis chips*. Journal of Micromechanics and Microengineering, 2002. **12**(4): p. 375-379.
23. Kricka, L.J., P. Fortina, N.J. Panaro, P. Wilding, G. Alonso-Amigo, and H. Becker, *Fabrication of plastic microchips by hot embossing*. Lab on a Chip, 2002. **2**(1): p. 1-4.
24. Gray, B.L., D. Jaeggi, N.J. Mourlas, B.P. van Driehuisen, K.R. Williams, N.I. Maluf, and G.T.A. Kovacs, *Novel interconnection technologies for integrated microfluidic systems*. Sensors and Actuators a-Physical, 1999. **77**(1): p. 57-65.
25. Jo, B.-H., L.M. Van Lerberghe, K.M. Motsegood, and D.J. Beebe, *Three-dimensional micro-channel fabrication in polydimethylsiloxane (PDMS) elastomer*. Journal of Microelectromechanical Systems, 2000. **9**(1): p. 76-81.

26. Chiou, C.H. and G.B. Lee, *A micromachined DNA manipulation platform for the stretching and rotation of a single DNA molecule*. Journal of Micromechanics and Microengineering, 2005. **15**(1): p. 109-117.
27. Giselbrecht, S., T. Gietzelt, E. Gottwald, C. Trautmann, R. Truckenmuller, K.F. Weibezahn, and A. Welle, *3D tissue culture substrates produced by microthermoforming of pre-processed polymer films*. Biomedical Microdevices, 2006. **8**(3): p. 191-199.
28. Song, Y., C.S.S.R. Kumar, and J. Hormes, *Synthesis of palladium nanoparticles using a continuous flow polymeric micro reactor*. Journal of Nanoscience and Nanotechnology, 2004. **4**(7): p. 788-793.
29. Kim, J.-H., J.-S. Kim, H. Choi, S.-M. Lee, B.-H. Jun, K.-N. Yu, E. Kuk, Y.-K. Kim, D.H. Jeong, M.-H. Cho, and Y.-S. Lee, *Nanoparticle probes with surface enhanced Raman spectroscopic tags for cellular cancer targeting*. Analytical Chemistry, 2006. **78**(19): p. 6967-6973.
30. Fu, Q. and J. Liu, *Integrated single-walled carbon nanotube/microfluidic devices for the study of the sensing mechanism of nanotube sensors*. Journal of Physical Chemistry B, 2005. **109**(28): p. 13406-13408.
31. Tummala, R., *Fundamentals of Microsystems Packaging*. 1 ed. 2001: McGraw-Hill Publishing.
32. Gravesen, P., J. Branebjerg, and O.S. Jensen, *Microfluidics-a review*. Journal of Micromechanics and Microengineering, 1993. **3**: p. 168-182.
33. Erickson, D. and D. Li, *Integrated microfluidic devices*. Analytica Chimica Acta, 2004. **507**(1): p. 11.
34. Han, K.-H. and A.B. Frazier, *Reliability aspects of packaging and integration technology for microfluidic systems*. IEEE Transactions on Device and Materials Reliability, 2005. **5**(3): p. 452-457.
35. Christensen, A.M., D.A. Chang-Yen, and B.K. Gale, *Characterization of interconnects used in PDMS microfluidic systems*. Journal of Micromechanics and Microengineering, 2005. **15**(5): p. 928-934.
36. Puntambekar, A. and C.H. Ahn, *Self-aligning microfluidic interconnects for glass- and plastic-based microfluidic systems*. Journal of Micromechanics and Microengineering, 2002. **12**(1): p. 35-40.
37. Yang, Z. and R. Maeda, *Socket with built-in valves for the interconnection of microfluidic chips to macro constituents*. Journal of Chromatography A, 2003. **1013**(1-2): p. 29-33.

38. Fredrickson, C.K. and Z.H. Fan, *Macro-to-micro interfaces for microfluidic devices*. *Lab on a Chip*, 2004. **4**: p. 526-533.
39. Madou, M., J. Zoval, G. Jia, H. Kido, J. Kim, and N. Kim, *Lab on a CD*. *Annual Review of Biomedical Engineering*, 2006. **8**: p. 601-628.
40. Slocum, A.H., Weber, A.C., *Precision passive Mechanical Alignment of wafers*. *Journal of Microelectromechanical systems*, 2003. **12**(6): p. 826-834.
41. Slocum, A.H., *Precision Machine Design*. 1992: Prentice Hall: Englewood Cliffs, NJ.
42. Jones, R.V., *Some uses of elasticity in instrument design*. *Journal of Scientific instruments*, 1962. **39**: p. 193-203.
43. Larsen, E.R. *Adapting project management principles and tools for research and development*. 2004. Austin, TX, United States: American Institute of Chemical Engineers, New York, NY 10016-5991, United States.
44. Conigliaro, J.P. *Hybrid methodologies for small scale engineering*. 2001.
45. MacDermott, C.P. and A.V. Shenoy, *Selecting Thermoplastics for Engineering Applications*. 2nd ed. 1997: Marcel Dekker.
46. Buser, R.A. *Active Lab-on-chip with a disposable fluidic system*. in *7th International conference on Miniaturized Chemical and Biochemical Analysis Systems*. 2003. California.
47. Rosato, D., *Plastics Processing Data Handbook*. 1997: Springer-Verlag.
48. Sperling, L.H., *Introduction to Physical Polymer Science*. 2005: Wiley Interscience.
49. Harper, C.A., *Handbook of Plastics, Elastomers, & Composites*. 4th ed: McGraw Hill.
50. Liu, R.H., J. Yang, R. Lenigk, J. Bonanno, and P. Grodzinski, *Self-Contained, Fully Integrated Biochip for Sample Preparation, Polymerase Chain Reaction Amplification, and DNA Microarray Detection*. *Analytical Chemistry*, 2004. **76**(7): p. 1824-1831.
51. B. K. Lee, D.S.K., T. H. Kwon, *Replication of microlens arrays by injection molding*. *Microsystem Technologies*, 2004. **10**: p. 531-535.

52. Edwards, T.L., S.K. Mohanty, R.K. Edwards, C.L. Thomas, and A.B. Frazier, *Rapid micromold tooling for injection molding microfluidic components*. Sensors and Materials, 2002. **14**(3): p. 167-178.
53. Worgull, M. and M. Heckeke, *New aspects of simulation in hot embossing*. Microsystem Technologies, 2004. **10**(5): p. 432-437.
54. Website for Jenoptik Mikrotechnik <http://www.jo-mikrotechnik.com/>. [cited 2007 January 15th].
55. Rotting, O., W. Ropke, H. Becker, and C. Gartner, *Polymer microfabrication technologies*. Microsystem Technologies, 2002. **8**(1): p. 32-36.
56. Heckeke, M. and K. Schomburg, *Review on micro molding of thermoplastic polymers*. Journal of Micromechanics and Microengineering, 2004. **14**.
57. Schiff, H., L.J. Heyderman, M.A.D. Maur, and J. Gobrecht, *Pattern formation in hot embossing of thin polymer films*. Nanotechnology, 2001. **12**(2): p. 173-177.
58. Datta, P. and J. Goettert, *Method for polymer hot embossing process development*. Microsystem Technologies, 2006: p. 1-6.
59. Lee, G.B., S.H. Chen, G.R. Huang, W.C. Sung, and Y.H. Lin, *Microfabricated plastic chips by hot embossing methods and their applications for DNA separation and detection*. Sensors and Actuators B-Chemical, 2001. **75**(1-2): p. 142-148.
60. Juang, Y.J., L.J. Lee, and K.W. Koelling, *Hot embossing in microfabrication. Part I: Experimental*. Polymer Engineering and Science, 2002. **42**(3): p. 539-550.
61. Juang, Y.J., L.J. Lee, and K.W. Koelling, *Hot embossing in microfabrication. Part II: Rheological characterization and process analysis*. Polymer Engineering and Science, 2002. **42**(3): p. 551-566.
62. Amid, P.K., A.G. Shulman, I.L. Lichtenstein, and M. Hakakha, *Biomaterials for abdominal wall hernia surgery and principles of their applications*. Langenbeck's Archives of Surgery, 1994. **379**(3): p. 168-171.
63. Hupert, M.L., M.A. Witek, Y. Wang, M.W. Mitchell, Y. Liu, Y. Bejat, D.E. Nikitopoulos, J. Goettert, M.C. Murphy, and S.A. Soper. *Polymer-based microfluidic devices for biomedical applications*. 2003. San Jose, CA, United States: The International Society for Optical Engineering.
64. Worgull, M., M. Heckeke, and W.K. Schomburg, *Large-scale hot embossing*. Microsystem Technologies-Micro- and Nanosystems-Information Storage and Processing Systems, 2005. **12**(1-2): p. 110-115.

65. Website for Minitab Statistical Software - (<http://www.minitab.com/>). [cited 2007 January 15th].
66. Website for Metronics, makers of Quadra Check software - <http://www.metronics.com/>. [cited 2007 January 5th].
67. Nilsson, D., S. Jensen, and A. Menon, *Fabrication of silicon molds for polymer optics*. Journal of Micromechanics and Microengineering, 2003. **13**: p. S57-S61.
68. Menz, W., W. Bacher, M. Harmening, and A. Michel. *The LIGA technique--A novel concept for microstructures and the combination with Si-technologies by injection molding*. 1991. Nara, Jpn: Publ by IEEE, Piscataway, NJ, USA.
69. Bacher, W., K. Bade, B. Matthis, M. Saumer, and R. Schwarz, *Fabrication of LIGA mold inserts*. Microsystem Technologies, 1998. **4**(3): p. 117-119.
70. Aristone, F., P. Datta, Y. Desta, A.M. Espindola, and J. Goettert, *Molded multilevel modular micro-fluidic devices*. Proceedings of SPIE - The International Society for Optical Engineering, 2003. **4982**.
71. Lorenz, H., M. Despont, P. Vettiger, and P. Renaud, *Fabrication of photoplastic high-aspect ratio microparts and micromolds using SU-8 UV resist*. Microsystem Technologies, 1998. **4**(3): p. 143-146.
72. Chien, R.-D., *Hot embossing of microfluidic platform*. International Communications in Heat and Mass Transfer, 2006. **33**(5): p. 645-653.
73. Website for KERN Micromilling machine - <http://www.kern-microtechnic.com/2-Machines-Micro.html>. [cited 2007 January 15th].
74. Tixier, A., Y. Mita, J.P. Gouy, and H. Fujita, *Silicon shadow mask for deposition on isolated areas*. Journal of Micromechanics and Microengineering, 2000. **10**(2): p. 157-162.
75. Website for Hirose USA (<http://www.hiroseusa.com/>). [cited 2007 February 5th].
76. Website for Creative Materials (<http://www.creativematerials.com/>) [cited 2007 February 5th].
77. Smyth, M.S. and J.H. Martin, *X Ray Crystallography*. Journal of Clinical Pathology: Molecular Pathology, 2000. **53**(1): p. 8-14.
78. McPherson, A., *Preparation and Analysis of Protein Crystals*. 1982: Robert E Krieger Publishing Co.

79. Choi, J.W., C.H. Ahn, and H.T. Henderson. *Planar bio/magnetic bead separator with microfluidic channel*. 1998. Santa Clara, CA, USA: SPIE, Bellingham, WA, USA.
80. Pekas, N., M. Granger, M. Tondra, A. Popple, and M.D. Porter, *Magnetic particle diverter in an integrated microfluidic format*. *Journal of Magnetism and Magnetic Materials*, 2005. **293**(1): p. 584-588.
81. Liu, Y.Q., S.A. Majetich, R.D. Tilton, D.S. Sholl, and G.V. Lowry, *TCE dechlorination rates, pathways, and efficiency of nanoscale iron particles with different properties*. *Environmental Science & Technology*, 2005. **39**(5): p. 1338-1345.
82. Farrell, D., Y. Cheng, R.W. McCallum, M. Sachan, and S.A. Majetich, *Magnetic interactions of iron nanoparticles in arrays and dilute dispersions*. *Journal of Physical Chemistry B*, 2005. **109**(28): p. 13409-13419.
83. Lisiecki, I., *Size, shape, and structural control of metallic nanocrystals*. *Journal of Physical Chemistry B*, 2005. **109**(25): p. 12231-12244.
84. Song, Y., C.S.S.R. Kumar, and J. Hormes, *Fabrication of an SU-8 based microfluidic reactor on a PEEK substrate sealed by a 'flexible semi-solid transfer'(FST) process*. *Journal of Micromechanics and Microengineering*, 2004. **14**(7): p. 932-940.
85. Fletcher, P.D.I., S.J. Haswell, E. Pombo-Villar, B.H. Warrington, P. Watts, S.Y.F. Wong, and X.L. Zhang, *Micro reactors: principles and applications in organic synthesis*. *Tetrahedron*, 2002. **58**(24): p. 4735-4757.
86. Zinoveva, S., P. Datta, R.D. Lewis, R. Desilva, C. Kumar, and J. Hormes. *Time Resolved Observation of Wet-Chemical Synthesis of Nanoparticles by Spatially-Resolved X-ray Spectroscopy*. in *Conference on Synchrotron Radiation Instrumentation (SRI)*. 2007. Baton Rouge.
87. Lin, C.-H. and G.-B. Lee, *Micromachined flow cytometers with embedded etched optic fibers for optical detection*. *Journal of Micromechanics and Microengineering*, 2003. **13**(3): p. 447-453.
88. McMullin, J.N., H. Qiao, S. Goel, C.L. Ren, and D. Li, *Integrated optical measurement of microfluid velocity*. *Journal of Micromechanics and Microengineering*, 2005. **15**(10): p. 1810-1816.

Appendix A

Passive Alignment using elastic averaging

The elastic averaging process is based on using multiple contact points between two bodies to effectively over constrain them. A four legged chair is a simple example of elastic averaging. Theoretically, only 3 points can make contact with a plane, so a chair with four legs resting on the floor has only 3 legs touching the floor. But when a person sits on the chair, the load causes the chair to deform elastically and bring all four legs in contact with the floor, forming a stable structure. As a load is applied, the elasticity of the bodies or members in contact allows the local errors to average out. The same concept is applied to precision alignment of the layers of the microfluidic stack.

An approximate model consisting of closed form solutions and finite element analysis based on the process illustrated in a thesis by Patrick Willoughby¹ was used to predict the alignment accuracy.

The steps of the process are as follows –

1. Construct model of flexible elements in contact
2. Determine sensitivity of dimensional parameters to tolerances
3. Create stiffness equations
4. Map cross coupling effects of the contact points
5. Form local stiffness matrix and combine to generate global stiffness matrix
6. Calculate overall offset/alignment accuracy based on global stiffness for perturbations at the contact sites

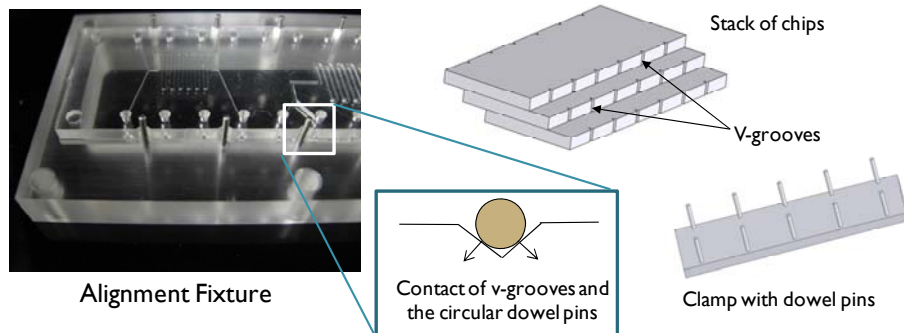


Figure A1: Elastic averaging based alignment using dowel pins and V-grooves used to align the chips in microfluidic stack

Step 1: Construct model

The first step involves simplifying the model into a number of springs. Each contact is modeled as two spring in series (Figure A2). One of the springs denotes the geometric stiffness of the contact member and the other would denote the stiffness due to Hertzian contact stress.

¹ PhD thesis - Willoughby, P., "*Elastically Averaged Precision Alignment*, in *Mechanical Engineering*". 2005, Massachusetts Institute of Technology: Boston. p. 158.

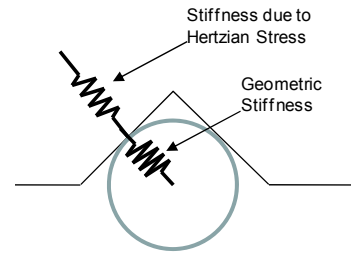
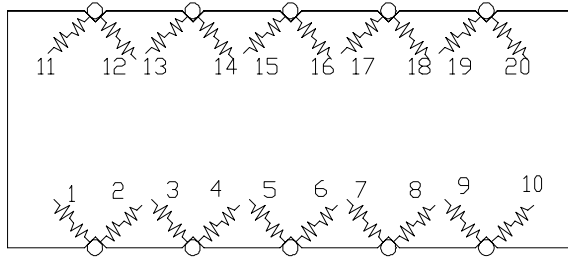


Figure A2: Model of the microfluidic slide(left) illustrated with springs at each point of contact with the alignment pins. The springs represent Geometric stiffness of the dowel pins and the stiffness due to the Hertzian contact (right)

Step 2: Create stiffness equations

The dowel pins can be approximated as cantilevered beams (Figure A3)

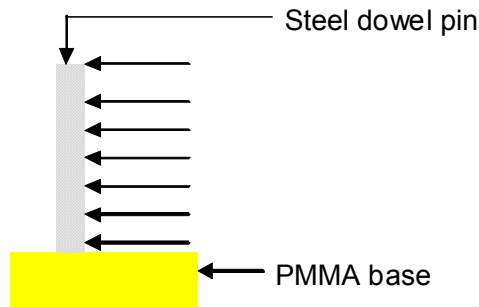


Figure A3. Schematic representation of a steel dowel pin in a PMMA base which can be modeled as a uniformly loaded cantilever beam.

For a uniformly loaded beam,

$$\delta = -\frac{wl^4}{8EI}$$

Where,

δ = deflection at the end of the beam.

w = uniformly distributed load along the length.

l = length of the beam.

E = Young's modulus of material of the dowel pin.

I = Moment of inertia of the beam.

$$stiffness = \frac{F}{\delta} = \frac{wl}{\frac{wl^4}{8EI}} = \frac{8EI}{l^3}$$

Therefore stiffness (due to geometry) of a uniformly loaded cantilever beam

$$k_{geom} = \frac{8EI}{l^3}$$

Stiffness due to Hertzian contact is given by -

$$k_{hertz} = \frac{P \times \text{Height of beam}}{\lambda [P^2 (\eta_1 + \eta_2)^2 (B + A)]^{1/3}}$$

Where,

$$\eta_1 = \frac{1 - \nu_1^2}{E_1}, \eta_2 = \frac{1 - \nu_2^2}{E_2}$$

ν_1, ν_2 = Poisson's ratio of steel and PMMA
 E_1, E_2 = Young's modulus for steel and PMMA

$$B + A = \frac{1}{2} \left[\frac{1}{R_1} + \frac{1}{R_1} + \frac{1}{R_2} + \frac{1}{R_2} \right] = \frac{1}{2} \left[\frac{1}{.5} + \frac{1}{.5} + 0 \right] = 2$$

and

λ is a geometric ratio, the value of which is obtained from Figure 11.6 of the book "Mechanical Analysis and Design 2nd edition"-Burr and Chetam. Pg 681

$$f_1 = k_1 \times x_1$$

Load per unit length of the contacts.

$$P = \frac{f_1}{l}$$

l = length of beam in contact

Total Stiffness k_{total} is given by

$$\frac{1}{k_{total}} = \frac{1}{k_{geom}} + \frac{1}{k_{hertz}}$$

Step 3: Create stiffness matrices

$$f_1 = K_1 \times x_1$$

$$f_2 = K_2 \times x_2$$

Where K_n is the stiffness and x_n is displacement in the direction of f_n . In Matrix form, we get-

$$\begin{bmatrix} f_1 \\ f_2 \end{bmatrix} = \begin{bmatrix} K_1 & 0 \\ 0 & K_2 \end{bmatrix} \begin{bmatrix} x_1 \\ x_2 \end{bmatrix} \text{----- (1)}$$

Resolving the individual forces into global co-ordinates (Figure A4) we get –

$$F_x = f_2 \cos \theta - f_1 \sin \theta$$

$$F_y = f_2 \sin \theta + f_1 \cos \theta$$

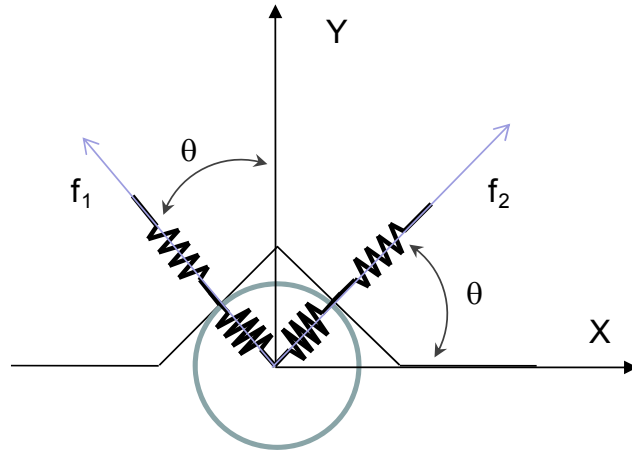


Figure A4: Schematic illustrating the direction of actual forces f_1 and f_2 exerted by a contact and their resolution into global co-ordinates

Where F_x is the sum of forces in the X direction and F_y is the sum of forces in the Y direction and f_n represents the force exerted at the contact

Representing the total forces in matrix form

$$\begin{bmatrix} F_x \\ F_y \end{bmatrix} = \begin{bmatrix} -\sin \theta & \cos \theta \\ \cos \theta & \sin \theta \end{bmatrix} \begin{bmatrix} f_1 \\ f_2 \end{bmatrix} \text{----- (2)}$$

Similarly transforming the displacements x_n along global coordinates, we get

$$\begin{bmatrix} \Delta X \\ \Delta Y \end{bmatrix} = \begin{bmatrix} -\sin \theta & \cos \theta \\ \cos \theta & \sin \theta \end{bmatrix} \begin{bmatrix} x_1 \\ x_2 \end{bmatrix} \text{----- (3)}$$

Combining Eqns 1, 2, and 3 we get –

$$\begin{bmatrix} F_x \\ F_y \end{bmatrix} = \begin{bmatrix} K_1 \sin^2 \theta + K_2 \cos^2 \theta & -K_1 \sin \theta \cos \theta + K_2 \sin \theta \cos \theta \\ -K_1 \sin \theta \cos \theta + K_2 \sin \theta \cos \theta & K_1 \cos^2 \theta + K_2 \sin^2 \theta \end{bmatrix} \begin{bmatrix} \Delta X \\ \Delta Y \end{bmatrix}$$

F_n

k_n

d_n

This equation represents the forces and displacements at one contact. Using this relationship, a complete matrix representing all the contacts may be formed as follows

$$\begin{bmatrix} F_1 \\ F_2 \\ F_3 \\ \vdots \end{bmatrix} = \begin{bmatrix} k_1 & 0 & 0 & \vdots \\ 0 & k_2 & 0 & \vdots \\ 0 & 0 & k_3 & \vdots \\ \dots & \dots & \dots & \ddots \end{bmatrix} \begin{bmatrix} d_1 \\ d_2 \\ d_3 \\ \vdots \end{bmatrix}$$

In elastic averaging the points of contact do not behave as isolated entities but have a cross coupling effect on each other. The extent of the coupling effect may be evaluated

experimentally or by finite element methods. Including these cross-coupling effects in the above equation we get

$$\begin{bmatrix} F_1 \\ F_2 \\ F_3 \\ \vdots \end{bmatrix} = \begin{bmatrix} k_1 & k_{12} & k_{13} & \vdots \\ k_{12} & k_2 & k_{23} & \vdots \\ k_{13} & k_{23} & k_3 & \vdots \\ \dots & \dots & \dots & \ddots \end{bmatrix} \begin{bmatrix} d_1 \\ d_2 \\ d_3 \\ \vdots \end{bmatrix}$$

where the off diagonal terms in the stiffness matrix are the cross-coupling terms.

Using these individual forces (F_n), the cumulative moment about the center may be calculated for the whole body using the following equation

$$\begin{bmatrix} \text{force_equilibrium_equation} \\ \text{moment_equilibrium_equation} \\ \text{geometric_constraints} \end{bmatrix} [\text{vectors_of_displacement}] = \begin{bmatrix} \text{force} \\ \text{moment} \\ \text{zeros} \end{bmatrix}$$

where the *force_equilibrium_equations* denote the sum total of the individual stiffnesses at each point and the *moment_equilibrium_equations* denote the product of the sum total of the individual stiffnesses with the distances from the center. This mathematical model may now be used to simulate the alignment accuracy by inputting random perturbations at the points of contact.

Appendix B

Calculation of Alignment Accuracy

To verify the alignment accuracy between two aligned chips, differential measurement of alignment markers (Figure B1) was used.

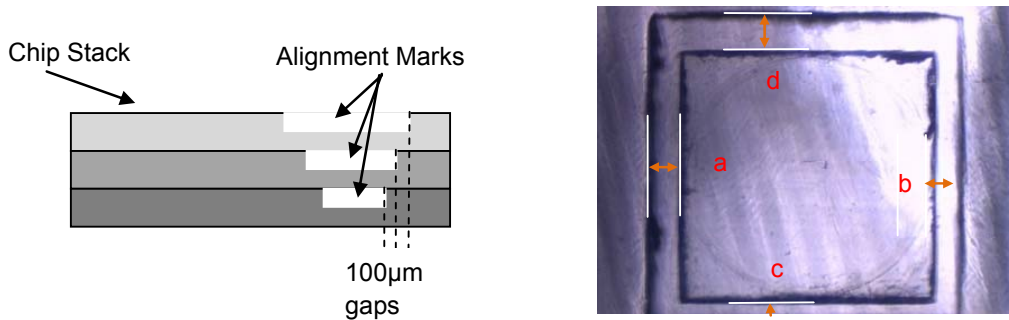


Figure B1: Schematic illustrating the arrangement of alignment markers (Left). Top view of alignment markers from 2 aligned chips. Concentricity of squares is indication of good alignment.

Thus displacement of alignment marker on one chip relative to the other in x and y directions are denoted by x_n and y_n respectively where $n=1$ for the left bottom alignment markers and $n=2$ for the right top alignment markers (Figure B2).

$$x_n = a - b$$

$$y_n = c - d$$

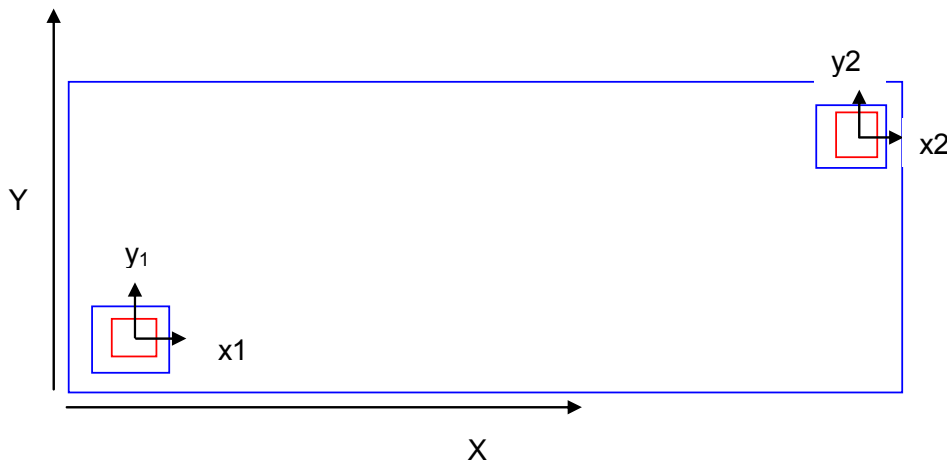


Figure B2: Illustration of overlaid alignment markers and the coordinate system used for calculations. Blue squares indicate alignment markers on the first chip and red squares indicate alignment markers on second chip. Displacement of the second chip(red) is calculated with respect to the first chip(blue).

This denoting the displacements at marker position 1 as vectors x_1 and y_1 and marker position 2 as vectors x_2 and y_2 , the offsets can be illustrated geometrically (Figure B3).

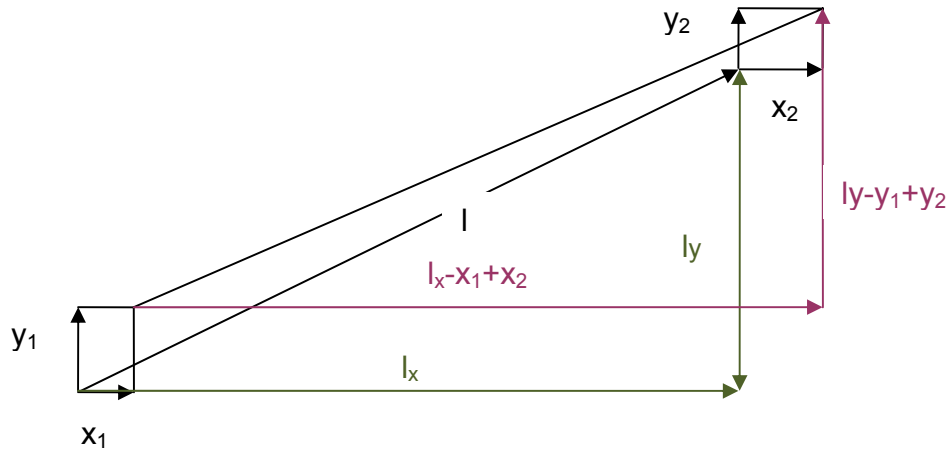


Figure B3: Geometric evaluation of displacement and angle between Chip1 and Chip 2

Angle between of red chip and blue chip is given by

$$r = \tan^{-1} \frac{m_2 - m_1}{1 - m_2 m_1}$$

where

$$m_1 = \frac{l_y - y_1 + y_2}{l_x - x_1 + x_2}$$

And

$$m_2 = \frac{l_y}{l_x}$$

Relative displacement of center of chips in X direction is given by –

$$\Delta x = \frac{(x_1 + x_2)}{2}$$

Relative displacement of center of chips in Y direction is given by –

$$\Delta y = \frac{(y_1 + y_2)}{2}$$

Appendix C

Experimental and simulation details for soft gasket sealing layer between two microfluidic chips

Elastomeric materials such as silicone were used as gaskets between two layers of microfluidic chips. Cast silicone was the chosen material for the gasket fabrication because of ease of fabrication. In order to determine the effective deformation and to preclude the possibility of through holes being blocked when the gasket is compressed, finite element analysis (FEA) was carried out. In order to acquire material data for the silicone being used, compression testing experiments were carried out.

For viscoelastic materials like rubber, the tensile modulus in compression is also dependent on the shape of the material and secondly, specific information regarding cast silicone material that was used for gasket fabrication was not readily available, so the compressive modulus for different gasket materials was evaluated experimentally. A pressure vs deflection graph was generated for the different candidates for the gasket material (Figure: C1) and as can be seen the behavior of the material is linear for smaller deflections (<200 μm) and becomes progressively non linear for higher deflections. In the case of gaskets, the deflection will be limited to low ranges of deflection. To evaluate the modulus, the values from the linear region were used and the slope of the line was measured (Figure C2). Experimental data from the compression tests was compared with results from the FEA and was found in close agreement (Figure C3).

The compression modulus evaluated from the experiments was used to simulate the compression of a cast silicone gasket using ANSYS to predict the closure of through holes as a function of compression. The results are shown in Section 3.2.3.

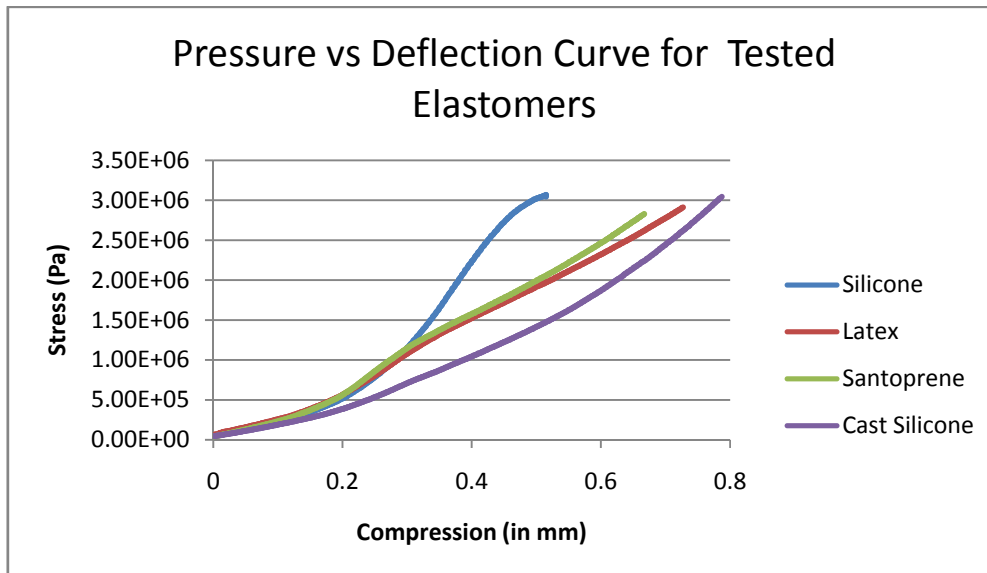


Figure C1: Results from compression testing of various elastomeric materials

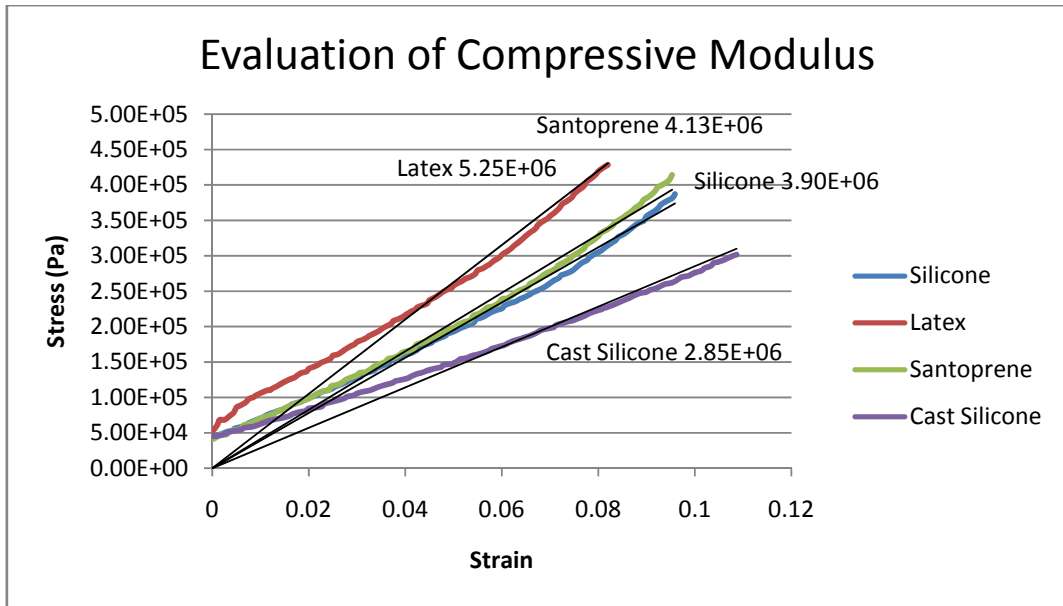


Figure C2: Evaluating the compressive modulus of different elastomeric materials for small amounts of compression, calculated by measuring the slope of the linear region from the pressure-deflection graph in Figure C1.

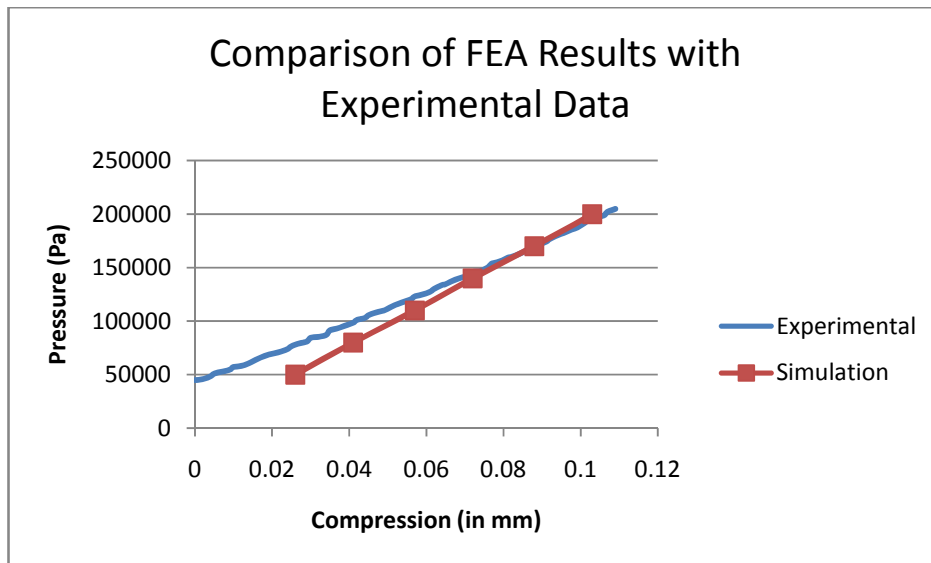


Figure C3: Plot shows a comparison between the results from the experiment and finite element simulation using ANSYS for compression of cast silicone used for forming gaskets. The difference between the experimental data and simulation results is attributed to approximation of initial conditions during the experiment.

Appendix D

Evaluation of clamping force applied via screw torque

Load can be applied to a plate by the application of torque on a bolt attached to it. This method was used while sealing layers of the microfluidic stack thermally. The relationship between the load and the torque is derived as follows.

The clamping force of a bolt is given by² –

$$F = \frac{T}{K \times d} \quad , \text{where}$$

F = Clamping Force,

T = Torque

d = nominal diameter of screw thread

and

$$K = \frac{1}{2d} \left(\frac{P}{\pi} + \mu_s d_2 \sec \alpha + \mu_w D_w \right) \quad , \text{where}$$

P = is the screw thread pitch

μ_s = coefficient of friction between threads

d_2 = pitch diameter of thread

μ_w = coefficient of friction between bearing surfaces

D_w = equivalent diameter of the bearing surfaces

α = thread half angle

While the clamping force can be calculated theoretically using the above formulae, the dependence of the result on multiple variables makes this an inherently inaccurate method of evaluating the force. Among the methods of bolt preloading, the use of a torque wrench typically yields $\pm 25\%$ accuracy. Hence evaluating accurate values for a clamping force based on theory is unreliable when applied to the specific cases in the system and manufacturing process.

² Erik Oberg et al, 27th Edition Machinery's Handbook, Industrial Press Inc, 2004

Appendix E

Interactional Effects of Hot Embossing Parameters

An interaction plot (Figure E1) was created to get a better understanding about the interactions of the different variables of the molding process that were studied for this effect on dimensional stability.

Changes in dimensions over a constant length of 10mm at different radial distances from the center (0, 10, 20 and 30mm) were plotted. While the differences observed are very close to the range of measurement error, the large number of measurements effectively shows significant trends in the effects plots. It allows interpretation of the influence of combined factors on dimensional variation. For example, the interaction between Force and Thickness (A) indicates that for the lesser thickness (1.5 mm) change in force does not have a significant effect whereas for the thicker material (4.5 mm) a change in force results in significant change in dimensions.

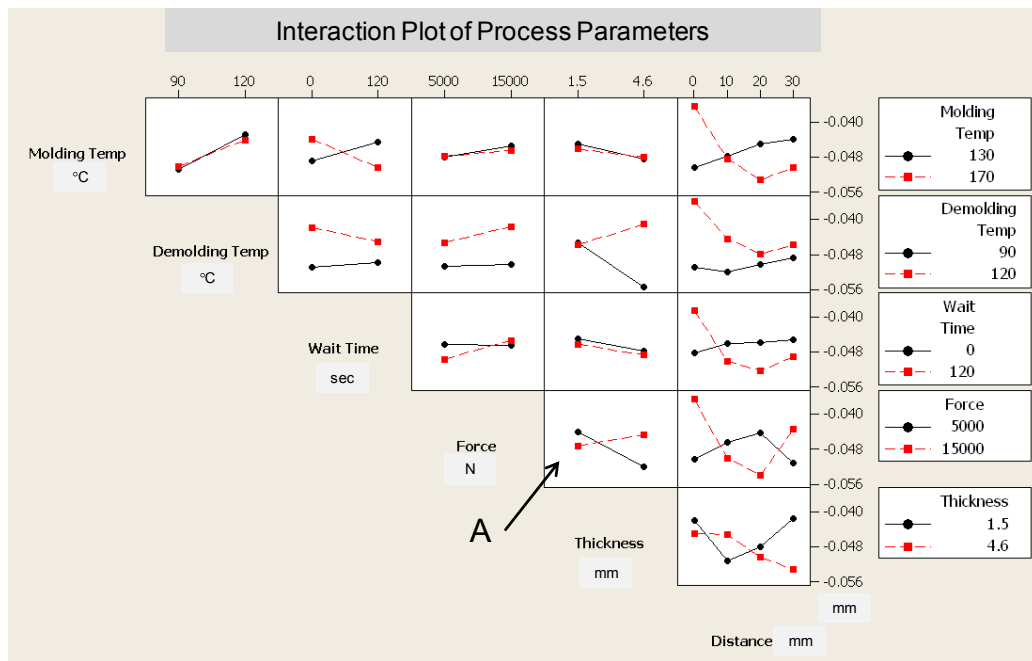


Figure E1: Interaction plots for the various factors are shown in this graph.